Composite Silica-Based Films as Platforms for Electrochemical Sensors

Oksana Tananaiko, Alain Walcarius

Composite silica-based films as platforms for electrochemical sensors

Oksana TANANAIKO,[1,*] Alain WALCARIUS[2,*]

[1] *Department of Analytical Chemistry, National Taras Shevchenko University of Kyiv, Volodymyrska Str., 64, Kyiv, Ukraine, 01601*

[2] *Université de Lorraine, CNRS, LCPME, 54000 Nancy, France*

** Corresponding authors: otananaiko@gmail.com (Tel.: +380 (44) 239 34 44; +380 (67) 892 34 82), alain.walcarius@univ-lorraine.fr (Tel.: +33 (3) 72 74 73 75)*

Abstract

Sol-gel-derived silica thin films generated onto electrode surfaces in the form of organic-inorganic hybrid coatings or other composite layers have found tremendous interest for being used as platforms for the development of electrochemical sensors and biosensors. After a brief description of the strategies applied to prepare such materials, and their interest as electrode modifier, this review will summarize the major advances made so far with composite silica-based films in electroanalysis. It will primarily focus on electrochemical sensors involving both non-ordered composite films and vertically oriented mesoporous membranes, the biosensors exploiting the concept of sol-gel bioencapsulation on electrode, the spectroelectrochemical sensors, and some others.

Key words: thin films, sol-gel materials, composites, mesoporous silica, modified electrodes, electrodeposition, sensors, biosensors.

Table of contents

1. Introduction

The progress in the development of affordable and reliable methods for the analysis of the complex objects or real media, while avoiding the need for time consuming sampling procedures or expensive apparatus, requires special attention to chemical and biochemical sensors. The development of sensors is accompanied by the synthesis of recognition elements on the surface of transducers for sensitive and selective detection of the target analyte. They must possess a long-term stability, satisfactory reproducibility and sensitivity of the analytical signal. Significant advances in chemical/biochemical sensors have occurred in recent two decades due to the ever-growing emergence of various kinds of thin films that can be engineered onto transducer surfaces, especially electrodes.[1, 2] A particular attention is paid to composite films in which the dimension of the layer ranges between few nanometers to micrometers. They are built by mixing two or more dissimilar components and, as a result, a new material with improved properties and structure is formed. The properties of the composite films depend not only on the individual components used but also on the morphology and the interfacial characteristics.[3] When two or more constituents are combined, the properties of a traditional coating can be refined to address specific requirements.[4] Composite films associating distinct materials are likely to provide synergetic or complementary behaviours. This may lead to unique physical, chemical, optical, mechanical, magnetic or electrical properties that are unavailable or less marked from just one component. Such multicomponent materials have attracted more attention as sensitive elements of electrochemical sensors. Various composites are examined for the construction of the recognition elements of many electrochemical sensors, including organic and inorganic polymers, as well as macromolecules mixed or doped with metals or metal oxide (nano)particles and (or) with carbon nanomaterials.[3, 4, 5] The precise attention is paid to polymeric materials combined with biomolecules and nanoparticles of different nature.[1,

[2, 6] Among them, thin films based on silica and sol-gel materials are of big interest, notably because they can be easily combined and (or) functionalized with different kind of organic and inorganic substances.

In spite of its insulating nature and although not redox-active, silica has found interest in electrochemistry in general and in electroanalytical chemistry in particular. Major advances made during the last century have been largely reviewed.[7-11] At that time, the investigations were mainly based of bulky silica-based materials (most often as powders dispersed into a conductive matrix such as carbon paste electrodes) or deposited as thick films (most often with a polymeric binder to maintain the silica particles more durably onto the electrode surface). In the past two decades, more and more works have been devoted to the exploitation of thin layers made of a continuous silica film uniformly deposited onto a solid electrode support, thanks to the versatility of the sol-gel process,[11-14] including those exhibiting an ordered structure at the nanoscale.[14-16] These materials are attractive as they bring additional properties compared to the traditional electrochemical interfaces, such as their ability to recognize target analytes (enabling their accumulation prior to detection), their host properties for various biocatalysts and/or electrocatalysts, their permselective behaviour, or their ability to ensure fast mass transport of guest species (as a result of their rigid three-dimensional framework).[14, 17] They can be easily manufactured in the form of organic-inorganic hybrids or as nanocomposite materials by implementing the numerous possibilities offered by the sol-gel process.[17-20] Silica-based organic-inorganic nanocomposites have a long history and are usually classified into two categories depending on whether the organic and inorganic components are interacting via weak bonds (class I) or are linked by covalent or iono-covalent chemical bonds (class II).[21] The interest of the first category relies on the ability to entrap redox proteins or enzymes, nanocarbons or metal nanoparticles catalysts, electrochemiluminescence reagents, or electroactive polymers,

which remain accessible to external reagents or target analytes owing to the rigid three-dimensional and porous inorganic network.[14, 16, 20, 22] This is essential for the proper functioning of electrochemical sensors and biosensors. The second category is also very attractive in this field as the rich chemistry of organosilane reagents enables the covalent bonding of various organo-functional groups that can be exploited for the selective preconcentration and/or electrocatalytic sensing of target species, or for the attachment of suitable mediators necessary in electrochemical biosensors, for instance. From that point of view, the advent of the ordered mesoporous silica materials (that can be also prepared in thin film configuration[23]) has opened new avenues. They enable very fast molecular transport (leading to enhanced electrochemical signals[24]), they can be functionalized by a large number of organo-functional groups that remain highly accessible owing to the regular and widely open porous structure, making them particularly interesting in electrochemistry and sensing.[16, 25] Moreover, combining the sol-gel process with interfacial surfactant templating allows a preferential vertical orientation of the nanochannels with respect to the underlying electrode support, including in a chemically modified form,[26] being especially promising for analytical purposes.[27]

In this review, we will cover the main advances made in the past two decades in the development of electrochemical sensors and biosensors manufactured from continuous sol-gel-derived silica-based composite (or doped) thin films. We will first describe briefly the strategies applied to generate these composite layers onto solid electrode surfaces and then discuss their use in designing electrochemical sensors and biosensors made of composite and/or biocomposite films integrating silica along with molecular reagents, biomolecules, organo-functional groups, polymers, surfactants, molecular imprints, inorganic nanoparticles or other nanomaterials.

2. Strategies for confining silica-based materials to electrode surfaces

Silica is an electronic insulator and its use in electrochemistry requires the establishment of a close contact to an electrically conducting material. A straightforward way is to disperse silica-based nanoparticles in carbon paste electrodes or in the carbon ink used to fabricate screen-printed electrodes,[10] or to deposit them onto a solid electrode surface usually together with a polymer binder to ensure the mechanical strength of the resulting composite, as for other inorganic particles-based thick films.[28] In order to avoid unwanted matrix effects, the above approaches were rapidly supplanted by strategies directed to the one-step generation of continuous silica-based thin films onto electrode surfaces by exploiting the versatility of the sol-gel process.[11-16, 29] The main deposition procedures are illustrated in Figure 1A. A sol solution is prepared from silica precursors (*i.e.*, tetraalkoxysilane species, $Si(OR)_4$, usually in hydro-alcoholic medium) that are hydrolyzed (Eq. 1) to form a stable sol, the aging of which being likely to induce the formation of a gel upon condensation (Eq. 2) in the presence of a suitable catalyst.[30]

$$Si(OR)_4 + 4H_2O \overset{H^+}{\Longrightarrow} Si(OH)_4 + 4ROH \quad (1)$$

$$2Si(OH)_4 \overset{OH^-}{\Longrightarrow} (OH)_3Si - O - Si(OH)_3 + H_2O \quad (2)$$

For film preparation, the polycondensation of the hydrolyzed precursors is usually induced by solvent evaporation (thus concentrating the silica precursors and favouring therefore their condensation without the need for a catalyst). This can basically be achieved by dropping an aliquot of the sol solution onto a solid surface and letting it evaporate, but more controlled methods are dip-coating or spin-coating where the sol-gel film is obtained by gravitational or centrifugal draining associated to fast drying.[31] In doing so, one can tailor the deposition process to form thin films of different thickness and structure by varying the

sol composition (especially the precursors' concentration) and controlling the evaporation rate. The film gel is then dried/cured to complete the formation of the silica network. Such coating can be formed on any type of flat supports, including electrode surfaces and in multi-layer configurations.[29] An alternative in sol-gel thin-film design on electrode is via an indirect electrodeposition method.[32, 33] In this case, a pH increase is induced at the electrode/solution interface by applying a suitable negative potential to the electrode (reducing water into OH^- species), acting as a catalyst for the condensation of the silica precursors. Again, the film thickness can be controlled by adjusting the synthesis conditions (sol composition, applied potential and duration of the electrodeposition). An advantage of the electrodeposition method over the evaporation-based ones is the possibility of getting uniform deposits on electrodes with complex geometries such as macroporous metals,[34] metal nanofibers,[35] or carbon micro- and nanomaterials.[36, 37]

The above dip-coating, spin-coating and electrodeposition methods can be easily extended to the production of silica-based composite thin films, as illustrated in Figure 1B. At first, the addition of an organo-trialkoxysilane (R'-$Si(OR)_3$, with R' being a selected organo-functional group) into the starting sol leads to its co-condensation with $Si(OR)_4$ and the formation of an organic-inorganic hybrid network of organo-silica bearing the organic functions R' attached in a covalent way to the inorganic structure (see part (a) in Fig. 1B). The amount of incorporated organic groups can be tuned by varying the R'-$Si(OR)_3$/$Si(OR)_4$ molar ratio in the precursors solution, and multi-functionalized composite films can be obtained by adding one or more R'-$Si(OR)_3$ reagents in the medium.[17-20] Electrodeposition can be also implemented to generate such organically-modified deposits.[38] Other types of composite layers are obtained by exploiting the hosting properties of porous silica, and especially the versatility of the sol-gel process to enable the direct entrapment of biomolecules, nano-objects or even polymeric materials in the course of film formation, by

simply dispersing these additives in the starting sol solution (see illustrations in part (b) of Fig. 1B). As a matter of fact, thanks to the room temperature processing of the method, sol-gel bioencapsulation is becoming an elegant way to confine biomolecules in a rigid three-dimensional matrix while keeping their biological activity,[39] including as thin films onto an electrode surfaces for applications in the biosensors field.[7, 22] Silica-based biocomposite thin films can be also produced electrochemically, as pioneered for redox proteins bioencapsulation by two independent groups in 2007,[40, 41] and later on also for much bigger biological agents such as bacteria, leading to artificial biofilms.[42] Otherwise, several other nano-objects have been entrapped into silica films during their sol-gel processing. With respect to their attractiveness for the development of electrochemical sensors, they encompass primarily noble metal or metal oxide nanoparticles and carbon particles, giving birth respectively to metal- and carbon-ceramic composite electrodes,[9, 20, 43] which can be also prepared as thin films but mainly by electrochemically assisted deposition (EAD).[44-48] These modifiers are exploited in particular for their electrocatalytic properties and/or as an effective means of imparting electrical conductivity to the silica-based composite layer. Co-encapsulation of biomolecules and metal nanoparticles or carbon nanomaterials is also documented for bioelectrocatalytic sensing.[49, 50] Finally, interpenetrated organic polymer-silica composite films can be produced by either polymer doping or polymer grafting during sol-gel deposition, as well as polymerization of organic polymers within pre-formed silicate films,[14, 43] or indirectly electrodeposited via interfacial pH change by EAD.[51] Combining electropolymerization and sol-gel electrodeposition is also possible, leading to the formation of conductive polymer-silica hybrid thin films.[52]

Of particular interest are the regularly ordered and widely open silica mesostructures that are formed by the template route because they offer incomparable permeation properties when deposited as thin films on electrodes,[24, 53-55] and better

accessibility to the active sites when prepared in the form of organic-inorganic hybrids as compared to their non-organized analogs,[56, 57] which is of outstanding importance in the development of electrochemical sensors.[16] They are usually prepared by evaporation induced self-assembly (EISA) from a sol solution containing the silica precursors and surfactant molecules, which is deposited onto a solid support by dip-coating, leading to the self-assembly of silica-surfactant micelles upon evaporation and their deposition as lyotropic liquid crystalline mesophases onto the support surface.[58, 59] EISA is a versatile and controllable soft-templating method to prepare mesoporous thin films, but it suffers from some limitations when attempting to control the alignment of the mesochannels with respect to the underlying support (especially in a vertical orientation), which requires alternative approaches.[23] And this is important as a vertical orientation of mesopores should be the best configuration to ensure fast transport through the membrane for reagents/analytes to reach the electrode surface, promoting high sensitivity for electrochemical detection.[27] The two main methods likely to reach this goal, and applied so far to manufacture electrochemical sensors, are presented in Figure 2. The first one is the so-called electrochemically assisted self-assembly (EASA) discovered in 2007,[26, 60, 61] involving an electrochemically induced vertical growth of silica walls around cationic surfactant hemi-micelles concomitantly formed on the electrode surface biased at a suitable negative potential (see part (a) in Fig. 2A). Such a combination of electrochemical interfacial surfactant templating and electrochemical modulation of the sol-gel process constitutes an easy, fast (few seconds) and versatile way to get highly ordered mesoporous silica films made of a hexagonal packing of mesopores (see part (b_1) in Fig. 2A) with vertical orientation (see part (b_2) in Fig. 2A), as also confirmed by grazing-incidence X-ray diffraction (see part (c) in Fig. 2A). The obtained films cover uniformly the electrode surface with typical thicknesses around 80 nm (see part (d) in Fig. 2A) and they can be prepared in

multilayer configuration while maintaining the mesopore interconnection between each layer (see part (e) in Fig. 2A). Thicker films (μm scale) can be obtained by using an alternative current-assisted deposition method.[62] They can be functionalized with a variety of organo-functional groups by combining the EASA method with click chemistry,[63, 64] and if attaching redox-active groups to the mesopore walls (such as ferrocene as illustrated in part (f) of Fig. 2A), they remain electrochemically accessible in spite of the insulating nature of the silica membrane thanks to effective electron hopping between adjacent ferrocene moieties.[65] They can also serve to grow conducting polymer nanofilaments or to immobilize other redox-active components.[26] The second approach is the Stöber solution growth method (Fig. 2B) proposed in 2012.[66] The growth mechanism involves a gradual transformation of silicate–cationic surfactant composites from spherical to cylindrical micelles with the assistance of ammonia hydrogen bonding and controlled silica condensation (see part (a) in Fig. 2B). The driving force is the slow hydrolysis (hour scale) of tetraethoxysilane (TEOS) molecules in an ammonia and ethanol solution, at a concentration low enough to enable their preferential deposition at the junction between the spherical micelles and the substrate, favouring the formation of parallel mesochannels growing perpendicularly to the substrate in the form of films with uniform thickness (see parts (b) and (c) in Fig. 2B) and a high level of ordering (see parts (d) and (e) in Fig. 2B). The method is basically applied to deposition only onto hydrophilic substrates but also onto pre-formed mesoporous supports as porous alumina.[67] The films can be detached from the surface and, thanks to the monodisperse diameter of mesochannels at few nanometres, the resulting free-standing membranes can be applied to molecular separation, for instance.[68] For both methods (EASA and Stöber growth), the film porosity is revealed by removing the surfactant template by solvent extraction or calcination, the latter being evidently restricted to non-functionalized materials. These films are characterized by both charge and size

selectivities at the molecular level,[69, 70] making them unique permselective membranes on electrode surfaces.[26, 27]

3. Electrochemical sensors designed from composite silica films

Hereafter, we will distinguish the electrochemical sensors made of non-ordered silica materials (*i.e.*, 'classical' sol-gel-derived silica-based composites) in section 3.1, while considering the specific case of ordered silica films (*i.e.*, as obtained using surfactant templates) in section 3.2.

3.1. Composite films based on non-ordered silica

Non-ordered silica films are widely used in electrochemistry as electrode modifiers in spite of their insulating properties.[8, 10, 14] To improve their ionic or electronic conductivity, organic or inorganic conductive/electroactive additives or nanomaterials are often used in the construction of silica-based electrochemical sensors.[71-75] The open structure of silica films ensures proper access of the analyte to the functional groups at the electrode/film/solution interphase and makes possible an effective accumulation of trace amounts of the analyte, which contributes to enhanced sensitivity of the determination. The selection of appropriate analytical reagents or functional groups attached to – or encapsulated in – silica films can lead to selective extraction and preconcentration of the target analyte from complex mixtures on the surface of such modified electrodes. The incorporation of redox-active species such as charge transfer mediators into the silica matrix allows to increase significantly both sensitivity and selectivity of the sensors due to their electrocatalytic properties helping at improving the determination of the target analytes.[76-80] A great diversity of modification has opened wide prospects for obtaining sensitive

elements of electrochemical sensors based on sol-gel modified electrodes in recent decades. Sol-gel-derived silica films are prepared on electrode surfaces as specified in Section 2, and most of the obtained sensors[71-82] are operating in voltammetry, amperometry, electrochemiluminescence or electrochemical impedance spectroscopy, in static conditions or in flow analysis modes.[79] The various types of electrochemical sensors based on non-ordered silica composite films are presented hereafter, depending on whether they consist of silica films comprising polyelectrolytes or organic reagents, silica-nanomaterials composites, or silica-based molecularly imprinted polymers (MIPs). The analytical characteristics of the two first categories are presented in Table 1 whereas the data relative to MIPs-based sensors are gathered in Table 2.

3.1.1. Non-ordered silica films containing polyelectrolytes and organic reagents

The incorporation of organic polyelectrolytes in silica-modified electrodes may contribute to improve their conductivity (*i.e.*, for conducting polymers) or to accumulate analytes or reject interferences via electrostatic interactions (*i.e.*, for charged polymers), with possible enhancement of selectivity and sensitivity for the developed sensors. For example, trace amounts of Mo(VI) in vitamins was achieved using a pyrolytic graphite electrode modified with a SiO_2-polydimethyldiallylammonium chloride film and an anionic azo dye lumogalion adsorbed on the film surface.[75] The best conductivity and mass transfer properties were exhibited by the composite film obtained in the presence of non-ionic surfactant Tween 20. The electrode can be regenerated and reused for 5 times. Improved stability was also reported when using a Nafion layer over a functionalized silica film applied to the detection of heavy metal ions.[71] Poly(vitamin B1) electropolymerized onto a nanocomposite silica (SBA-15) incorporating V_2O_5 and CeO_2 contributed to enhance both

the conductivity and the stability of the modified electrode applied to the determination of nitrophenol derivatives in the environment, demonstrating a lifetime as long as 30 days.[81]

Organic reagents can be also accommodated to silica films either by soft binding (adsorption) or by covalent attachment, this latter approach leading generally to more durable immobilization. Anionic redox mediators (hexacyanoferrate) were immobilized by electrostatic interaction on protonated amine-functionalized silica film on a gold electrode, and demonstrated good stability when applied to the determination of nitrite ions in water by flow injection analysis.[82] Another example is the determination of ascorbic acid in human plasma using a composite material made of manganese porphyrin mediator entrapped in a silica film generated on carbon electrode by the laser ablation deposition technique.[72] Voltammetric sensors for Cd^{2+}, Pb^{2+} and Cu^{2+}, were developed by coating glassy carbon electrodes with a composite of thiol self-assembled monolayers on mesoporous silica supports (to accumulate the metal ions) and Nafion layer (to enhance plasticity). They enabled detecting 0.5 ppb of Pb^{2+} and 2.5 ppb of Cd^{2+} in river water, groundwater, and seawater with a minimum preconcentration.[71]

3.1.2. Non-ordered silica films and nanomaterials

As reported in Table 1, several nano-objects can be used as additives in silica films on electrodes, such as metal nanoparticles, carbon nanomaterials, or metal oxides.

Metal nanoparticles, especially those based on noble metals, are attractive modifiers of silica films because they enable considerable improvement of their conductivity and electrocatalytic properties.[83, 84] They contribute to increase the sensitivity and selectivity of silica-based electrochemical sensors due to enhancing the electroactive surface area of the modified electrodes and electron mediating properties between the analyte and the electrode surface. Examples are available for silica films bearing nanoparticles of gold

(AuNP),[76, 79, 85, 86] silver (AgNP),[80, 87] or lead (PbNP).[88] Most often, organically modified silica (ORMOSIL) is used as the host matrix with chelating groups that are likely to stabilize durably the metal nanoparticles on the electrode surface.[76, 79, 80, 86, 88] AgNP demonstrated electrocatalytic activity towards nitrite ions,[80] and enabled selective cyanide sensing in electroplating wastewater samples.[87] The presence of PbNP improved the response of a thiol-functionalized silica film electrode for ultrasensitive silver sensing, reaching a detection limit down to 1.2 pM of Ag(I) after 90 s of accumulation.[88] AuNPs were most often exploited for their electrocatalytic properties (*e.g.*, for H_2O_2 detection[85]), sometimes associated in a synergetic way to other species (*e.g.*, mediators), as exemplified for a glassy carbon electrode modified with a mesoporous silica film containing rhodium(II) phosphomolybdate and AuNPs as sensitive element of a flow amperometric sensor for bromate ion and methionine.[79] The electrode demonstrated stable response in flow-injection amperometric mode for more than 100 measurements per day.

Carbon-based nanomaterials can also help at increasing the electronic conductivity of the film and improving its electrocatalytic features, as pointed out for single and multi-walled carbon nanotubes,[78, 89] graphene oxides,[76, 86, 90] or other nano-carbons.[73] They were mostly exploited for the determination of biologically relevant molecules such as dopamine, acetaminophen (paracetamol) or uric acid (Table 1), sometimes associated to metal nanoparticles (AuNP) or metal oxides (Fe_2O_3).[73, 86] A particular family is that of humidity sensors based on impedance or resistance measurements that are proportional to air humidity. This is the case of mesoporous silica-carbon nanotubes composites,[89] or mixed silica-titanium composite film obtained from titanium(IV) n-butoxide and polydimethylsiloxane deposited in the presence of a Ce-dopant onto silver palladium planar electrodes,[91] to name but a few.

3.1.3. Molecularly imprinted silica-based films

The development of silica films with imprinted target analyte is a prospective way to obtain a new type of highly specific molecularly imprinted polymer (MIP) mimicking the molecular recognition of organic molecules by biological molecules.[92-95] Such films called "molecularly imprinted silica" (MIS) are widely used as sensitive elements of electrochemical sensors (Table 2). Typical MIPs can be obtained by polymerization involving either non-covalent imprinting (which can be realised by physical, hydrophobic, van der Waals forces, hydrogen bond or electrostatic interactions between the analyte molecule and the polymer network) or imprinting via reversible covalent attachment.[92] For MIS materials, the most common strategies include non-covalent entrapment.[96] MIS films are fabricated using the sol-gel technique and the overall procedure involves successive steps: (1) the preparation of a sol containing the suitable silica and organosilica precursors and the target probe molecule (called "template"), (2) the physical entrapment of the template during gelation (cross-linking) of the sol, and (3) the removal of the template from the dry silica matrix. The functionalized organosilica precursors (*i.e.*, mainly phenyl-, methyl- or vinyl-trialkoxysilane reagents, but also aminopropyltriethoxysilane) are selected for their possible interactions with the target molecule, whereas the tetraalkoxysilane acts as network former, to get the final ORMOSIL. The template molecules are generally small and have a rigid planar structure, which is important for leaving clear imprints in the silica matrix. After synthesis, the template molecule is removed from the porous MIS film via soaking in aqueous buffer or organic solvent. Various routes for coating MIS onto electrode surfaces can be followed (Fig. 3A).[96] The most straightforward ones are based on the physical deposition of the sol by spin-coating or drop casting, for which gelation is induced by evaporation with concomitant MIS formation.[97-100] They are convenient for film formation on flat electrode supports. Sometimes, they are combined with strategies to ensure

durable chemical attachment of the MIS to the electrode, which implies the use of an organosilane acting as a molecular glue between the silica film and the electrode surface.[101-103] Electro-assisted deposition (EAD) is also a powerful mean to generate MIS films of controlled thickness,[74] and is particularly suited to the preparation of uniform MIS deposits on heterogeneous electrode surfaces (*i.e.*, made of carbon nanotubes assemblies of graphene oxide layers).[104-107]

MIS films can offer several advantages compared to organic polymer-based MIP materials. Silica films are easy to obtain by the sol-gel process, quite rapidly and at room temperature, avoiding any thermal or chemical decomposition of the imprinted molecules. They are mechanically stable due to their three-dimensional rigid structure made of a high level of cross-linking, which is also favourable to a rather fast mass transport of the target analyte inside the film, which can lead to faster response time compared to classical MIPs. A comparative study between a MIS and a MIP specific to the iprodione fungicide has revealed better performance for the MIS, including faster permeation and more specific recognition (with imprinting factor of MIS 2.5 times higher than that of the acrylate-based MIP), but also a lower binding capacity of MIS relative to the MIP material.[108] Note that the open structure of the ORMOSIL is a positive point for getting quite fast response time but it can also result in non-specific binding, requiring to find the best compromise between a sufficient porosity of the film (to ensure fast diffusion processes) and imprinted cavities selective enough for the target analyte.

Several examples of electrochemical detection with MIS-coated electrodes are reported in Table 2, which can be distinguished on whether they are made of ORMOSIL alone or containing additives such as nanomaterials or organics.

One of the first electrochemical sensors developed on the basis of MIS film was applied to the detection of dopamine (DA) by cyclic voltammetry.[97] In contrast to non-imprinted films, the DA-imprinted MIS have a satisfactory affinity for dopamine compared to structurally similar molecules such as serotonin, epinephrine, or dihydroxynaphthalene. In another work, MIS films imprinted with tyramine and dopamine also demonstrated good selectivity, with interference levels not exceeding 5%.[98] A methyl parathion-templated MIS thin film electrodeposited onto a glassy carbon electrode was successfully used for the detection of methyl parathion in pears, exhibiting fast and sensitive response; thanks to effective "π–π" interactions and hydrogen bonding in the imprinted cavities, very good selectivity was achieved in the presence of interfering substances such as α-hydroxyl-4-nitrophenyl-dimethyl-phosphonate, *p*-nitrophenol and nitrobenzene, except for parathion (giving a signal of about 50% relative to that of methyl parathion).[109] Chlorogenic acid determination in hot drinks was achieved using a gold electrode pre-treated with mercaptopropyltriethoxysilane (MPTMS) and covered with a MIS film made of TEOS, phenyltriethoxysilane (PTEOS) and 3-aminopropyltrimethoxysilane (APTMS).[102] MPTMS served as molecular glue between Au surface and MIS while phenyl and amino groups helped with the probe recognition via electrostatic, hydrogen bonding and "π–π" interactions (Fig. 3B). Polyelectrolytes can be also added to the MIS in order to induce positive or negative charges that are likely to affect the probe binding process, as reported for the voltammetric sensing of purine bases (adenine and guanine) in hydrolysed solutions of DNA.[99] Finally, it is also possible to perform chiral electrochemical recognition using very thin MIS films on ITO electrode, as pointed out for the distinction of enantiomer pairs (respectively (R)- and (S)-N,N′- dimethylferrocenylethylamine and D- and L-3,4-dihydroxyphenylalanine).[110] In this work, the modified electrode was not directly applied to quantitative determinations but, taking into account the attractiveness of electrochemical

chiral analysis,[111] the elaboration of chiral MIS for electrochemical sensing could be a versatile and rather simple way to achieve this goal by avoiding the need to elaborate very sophisticated multicomponent systems.[112]

On the other hand, nanomaterials possessing electrocatalytic activity towards the target analytes can be successfully associated to MIS, forming sensitive nanocomposite layers on the electrode surface. Examples are available for graphene oxide (GO),[100] multi-walled carbon nanotubes (MWCNT),[74, 101, 103, 104, 106, 107, 113] and noble metal nanoparticles.[105, 114] As for other types of silica-based composite film sensors (section 3.1.2), the introduction of such nanomaterials into the MIS contributes to enhancing the electron transfer rates, the electroactive surface area of the electrode and thus the sensitivity of the electrochemical sensing, the selectivity of the detection originating again from the imprinted cavities in the film. Several sensors with good analytical performance have been reported. Paracetamol was determined in tablets and human urine using a phenyl-functionalized MIS comprising GO deposited on glassy carbon electrode (GCE).[100] A very stable and sensitive electrochemical sensor for benzylpenicillin in blood plasma was constructed on carbon electrode modified with multiwalled carbon nanotubes (MWNTs) decorated with Fe_3O_4, doped with chitosan and covered with MIS film; the sensor exhibited good selectivity for benzylpenicillin in the presence of streptomycin, clindamycin, oxacillin and erythromycin, or 100-fold excess of ascorbic acid, dopamine and uric acid.[104] A layer-by-layer construction method was applied to develop a sensitive and selective electrochemical sensor for the determination of L-phenylalanine in blood plasma and other physiological fluids.[106] It is based on aniline electropolymerization on a carbon electrode to get a polyaniline (PANI) layer, its subsequent coverage with β-cyclodextrin (β-CD) incorporated MWNT, and final covering with MIS film obtained by EAD (Fig. 3C) Selectivity factors towards the stereoisomer D-phenylalanine was 0.23, and it was even

much better (ranging between 0.09 and 0.12) for L-proline, DL-methionine, L-histidine, and L-norleucine, confirming a good selectivity for L-phenylalanine.[106] A composite film made of TEOS–CTAB-based MIS combined with L-histidine-functionalized MWCNT and poly(dimethylsiloxane) on GCE was applied to the ultrasensitive (pM range) detection of tetracycline in pharmaceutical capsules, human serum and tap water, with good selectivity over anthracyclines.[113] Other examples involving MWCNTs and MIS nanocomposite films have been described the determination of thymidine in tablets,[107] naloxone in urine,[74,] or L-histidine in human blood serum,[101] always with good selectivity over structurally-related compounds. GCE modified with MWCNTs/vinyl-functionalized MIS film was reported to be a good sensor for caffeine in coffee and energy drinks, with quite fast response time (maximum response after 15 min incubation time), yet with few non-specific binding of some analogues (xanthine, theophylline, theobromine) but they did not interfere with caffeine determination as they appeared at different potential values.[103] Finally, gold nanoparticles (AuNPs) can also contribute to improving the response of MIS-based electrochemical sensors. For example, a composite film made of chitosan and phenyl-functionalized MIS encapsulating *p*-nitrophenol and AuNPs was electrogenerated in one step on GCE and the resulting electrode applied for the selective detection of *p*-nitrophenol, with 6-fold enhancement of the voltammetric signal compared to *m*-nitrophenol, *o*-nitrophenol and 2,3-difluoro-*o*-nitrophenol (Fig. 3D).[114] A sensor for bisphenol A combining both MWCNTs and AuNPs with an amino-functionalized MIS thin film obtained by EAD was also described, exhibiting a particularly good selectivity (only 15% of the signal corresponding to 3 µM bisphenol A was observed in solutions containing phenol, 1,4-dihydroxybenzene or 4-*tert*-butylphenol at the much higher concentration of 3 mM).[105]

3.2. Composite films based on ordered mesoporous silica

With rare exceptions,[115-120] most electrochemical sensors involving ordered mesoporous silica films on electrodes are based on the use of vertically aligned nanochannel membranes prepared either by EASA[121-157] or Stöber growth,[158-180] or even both these methods[181, 182] (Table 3). They will be noted as vertically-oriented mesoporous silica film (VMSF) hereafter. Several kinds of composite films can be distinguished: (1) those made of the mesoporous silica film filled with the organic template used for its synthesis (mainly surfactants[25-27, 33, 137] but also coordination polymers[183]), mainly deposited on flat electrode surfaces as indium-tin oxide (ITO)[163, 164, 173, 175, 177, 178] or electrodeposited as nanocomposite films around reduced graphene oxide;[125] (2) those made of surfactant-extracted mesoporous silica electrodeposited as nanocomposite films around various kinds of nanocarbons (reduced graphene oxide, three-dimensional graphene, carbon nanotubes or graphene-carbon nanotube assemblies);[121, 123-125, 128, 130, 138, 140, 146, 149, 153, 155, 156] (3) a wide range of chemically modified mesoporous silica films that can be basically divided further in two categories depending on whether they contain organo-functional groups (either weakly immobilized[126, 129, 139, 145, 162, 165, 166, 169, 171, 172, 176, 179, 180] or strongly attached via covalent bonds[116, 118-120, 122, 126, 127, 131, 133, 134, 136, 137, 143, 147, 150-152, 157, 160, 161, 174]) or serve as hosts for nano-objects (such as polymers[140, 141, 158] or nanoparticles[159, 167, 168, 170, 181, 182]); and (4) other composites made of ordered silica films combined with other nanomaterials (such as clays,[117, 132, 135] for instance). An illustrative summary of the various sensing applications of composite electrodes made of VMSF materials, respectively with filled pores, open pores and functionalized pores, is given in Figure 4. The main analytical/sensing schemes are based on permselectivity, preconcentration electroanalysis, direct or indirect detection, electrocatalysis and apta- or immunosensing. VMSF films with filled pores can be used for hydrophobicity-based preconcentration and anti-fouling selective detection, or even for mediated electrocatalytic detection when the template is electroactive. VMSF films

with open pores of nanometric dimensions are characterized by size and charge selectivity at the molecular scale,[26, 27] which can be exploited in permselective sensing involving preconcentration/rejection associated to electrochemical detection or for enhanced electrochemiluminescence sensing due to the accumulation of the cationic probes. Finally, the various ways to modify VMSF films lead to a series of reactive surfaces (with anchoring ligands, metal nanoparticles, conductive polymers, redox-active moieties, or diagnostic reagents such as aptamers-antibodies, for instance), which are likely to be exploited in several electrochemical sensing applications. They encompass selective preconcentration and detection, direct and mediated electrocatalysis, indirect amperometric detection or signal transduction of hybridization events. They are briefly described and discussed hereafter by type of composite materials, based on the data provided for various analytes and electrode configurations in Table 3.

3.2.1. Ordered silica films with surfactant in the nanochannels

Such composite films on ITO electrodes have been exploited for the extraction and subsequent electrochemical determination of lipophilic analytes (drugs, pesticides, explosives) in real media without pre-treatment thanks to their anti-(bio)fouling properties. The small molecules are accumulated in the surfactant phase and electrochemically detected whereas ionic species and large molecules (*i.e.*, larger than the nanochannels diameter) are excluded from reaching the underlying ITO surface. Examples are available for the analysis of chloramphenicol in human whole blood[163] or in milk and honey samples,[164] antioxidants (retinol, Trolox) in fruit juices,[177] nitroaromatic explosives and pesticides in water samples or foodstuffs,[175] halonitrobenzene derivatives in lake water and soil dispersion,[173] or the tetramethylbenzidine (TMB) substrate.[178] The depletion of TMB catalyzed by G4zymes can be also used to detect biomarkers (ATP, thrombin, DNA) in

complex biological samples.[178] The calibration curves were most often characterized by two linear ranges, being more sensitive at low concentration due to more effective preconcentration.[163, 173, 175] The effectiveness of the analyte accumulation into the film is demonstrated by much larger sensitivity than on bare ITO electrodes.[163, 164] All neutral species are in principle likely to be dissolved in the surfactant phase but only the lipophilic ones are efficiently extracted and thus preconcentrated, as pointed out for a mixture of dihydroxybenzene isomers (*e.g.*, the more hydrophobic catechol is much more effectively accumulated via hydrophobic interactions than the rather hydrophilic hydroquinone).[125] Note that, in turn, hydroquinone can be accumulated via hydrogen bonding to the silica surface (*i.e.*, after removal of the surfactant), but this falls under the next section 3.2.2.

A special case is that of mesoporous silica film prepared from an electroactive structure-directing agent (such as the coordination polymer made of iron triazole complexes $Fe(Htrz)_3$[183]), which can be used itself as a redox mediator for the electrocatalytic detection of the analyte, as demonstrated for hydrogen peroxide sensing.[141]

3.2.2. Surfactant-free ordered silica films electrodeposited onto nanocarbons

After the surfactant has been removed, the resulting widely open mesoporous films with vertically aligned nanochannels enable very fast mass transport from the solution to the electrode surface,[24, 54, 60] being attractive to impart high sensitivity to the electrochemical detection of target analytes.[16, 27, 184] Selectivity can be also induced by the film as only analytes smaller than the mesopore aperture are likely to cross the film, the larger ones being excluded (*i.e.*, size selectivity),[70] while cationic species are preferably accumulated (and anions repelled) due to electrostatic attractions (repulsions) by the negatively charged silanolate groups present on the silica surface (*i.e.*, charge selectivity).[69] Note that charge selectivity can be tuned by adjusting pH and/or ionic strength of the

medium, by modifying the surface charge of the material (turning silanolate into protonated silanol groups, for instance) or by changing the thickness of the electrical double layer in the nanochannels.[26, 27, 185] An important point for application is the good adhesion of the film to the electrode surface, in a mechanically stable form after the surfactant removal. This is intrinsically the case of silica films on ITO electrodes (thanks to their surface hydroxyl groups),[61] but it may require the use of a "molecular glue" for other supports, such as electrografted aminopropyltriethoxysilane on carbon electrode[186] or chemisorbed mercaptopropyltrimethoxysilane on a gold electrode.[187] Another strategy is the electrochemical activation of carbon supports to generate surface-active groups likely to ensure the durable attachment of EASA-produced mesoporous silica films.[188] This has been largely applied to the electro-assisted deposition of VMSF around nanocarbon supports and the use of the resulting nanocomposite films for electrochemical sensing.[121, 123-125, 128, 130, 138, 142, 147, 149, 153, 155, 156]

Many examples are given in Table 3 for the determination of various analytes, including drugs or pharmaceuticals,[128, 130, 138, 146] neurotransmitters[121, 164] or other biologically relevant molecules,[121, 153, 156, 164] pesticides,[124, 142, 144, 148, 149, 155] and hydroquinone derivatives.[123, 125] In many cases, the analytical procedure clearly involves the accumulation of the analyte in the film prior to its electrochemical detection on the electrode substrate (*i.e.*, by electrostatic binding of cations[121, 128, 130, 142, 146, 148, 149, 153, 164] or the formation of hydrogen bonds[123, 125, 153, 155] or both,[156] or via electro-oligomerization[144]), but in some cases it is difficult to make a real distinction between a possible preconcentration in the film and a direct electrocatalytic detection on the nanocarbon surface, both being expected to enhance the voltammetric signals. Also, synergetic effects and electrocatalytic behaviour are sometimes claimed[124, 142, 149] but rarely demonstrated by both a signal enhancement and a noticeable decrease in the

overpotentials.[121, 146, 155] As above (section 3.2.1), the calibration curves may show two distinct linear ranges, with higher sensitivity at lower concentration due to more effective preconcentration ability (as demonstrated, for example, for paraquat detection[148, 149] showing unambiguous adsorption behaviour at low concentration and an adsorption-diffusion regime in more concentrated solutions,[148] enabling efficient trace analysis in the nM range). Again, the anti-fouling and anti-interference features of the VMSF can be exploited for the analysis of real media, as exemplified for biologically relevant molecules in human serum,[121, 156] or drugs in whole blood or urine samples.[130, 138, 146] In these cases, the mesoporous silica film acts as a real molecular filter enabling the small analytes to reach the electrode surface and being detected without (bio)fouling because bigger molecules cannot cross such physical barrier (as explicitly pointed out for propranolol detection in the presence of haemoglobin,[189] for instance). Of related interest is the label-free electrochemical detection of protein kinase activity and inhibition in the presence of a redox probe in solution, by distinguishing between the large currents observed in case of peptide cleavage and the hampered diffusion of the redox probe through the film in the absence of cleavage (due to the adsorption of the phosphorylated peptide).[190] Finally, one has to mention that only few stability data are available (Table 3), which might be an issue for VMSF made of silica gel-based walls. Actually, the operational stability in aqueous solutions is limited to few measurements (typically five[146, 155]) and rather short times (10-30 min[123, 138, 153]), suggesting to consider their utilization primarily as components of single-use sensors.

3.2.3. Ordered silica films doped with analytical reagents

The accumulation ability of VMSF, notably towards cationic species, can be exploited to dope such films with suitable analytical reagents that are usually used in

solution, with the idea to concentrate them close to the electrode surface. This has been basically developed for enhancing the electrochemiluminescence (ECL) of $Ru(bpy)_3^{2+}$ on ITO electrodes modified with VMSF. The concept was first reported from a model system involving the use of tri-*n*-propylamine (TPrA) as the coreactant and a dilute solution of $Ru(bpy)_3^{2+}$ (9 µM).[180] Thanks to strong electrostatic attraction, $Ru(bpy)_3^{2+}$ cations are accumulated onto the silica walls and both these species and TPrA molecules are diffusing very fast in the oriented nanochannels, contributing to ECL signals larger by *ca.* two orders of magnitude for the film electrode as compared to bare ITO, as demonstrated for the detection of not only TPrA but also atropine and nicotine[180] (notably in commercial products for nicotine[172]). It was then extended to the analysis of aromatic explosives[179] or dopamine[165] with a smartphone-based ECL system involving VMSF on disposable screen-printed carbon electrodes or ITO electrodes. Further researches were devoted to build ECL devices based on VMSF generated onto other supports such as paper µchips[171] or polyethyleneterephthalate coated with indium-tin oxide[129] as flexible composite electrodes for the electrochemical sensing of drugs or antibiotics in biological samples. To avoid possible reagent leaching in the external solution, a second VMSF layer bearing positively charged groups can be overcoated onto the $Ru(bpy)_3^{2+}$-loaded one, the effectiveness of the approach being demonstrated by multiple successive cyclic voltammetry (CV) or ECL experiments (no noticeable signal change after 24 cycles, compared to the intensity drops by 31% and 48% respectively observed for CV and ECL measurements).[127] Most systems were based on VMSF generated by the Stöber growth method, except one example (lidocaine sensing in serum[145]) confirming that the EASA-based films can be also useful for manufacturing ECL devices. The other silica-based ECL sensors are presented in section 5.1. Finally, one has to mention that $Ru(bpy)_3^{2+}$-loaded VMSF on ITO electrode have been

applied as electrocatalytic sensors for the mediated detection of guanine in beer and pharmaceuticals.[139]

3.2.4. Ordered silica films bearing covalently attached organo-functional groups

A good way to circumvent the problems associated to the loosely bound reagents in VMSF is the use of covalently functionalized films.

A first category includes VMSF with organic groups grafted only on top of the silica membrane (*i.e.*, not inside the nanochannels). They are prepared either by coating or by grafting the film prior to surfactant extraction. For example, VMSF covered with polydimethylsiloxane on top facilitates greatly the transport of small hydrophobic molecules through the film while acting as a barrier for the hydrophilic ones (flux differences by *ca.* 3-4 orders of magnitude),[174] enabling the electrochemical sensing of non-polar molecules such as bisphenol A in wine[160] or paraoxon in milk.[174] A second example encompasses the geno-, immuno- or aptasensors made of VMSF functionalized respectively with a gene/DNA strand, an antibody, or an aptamer, covalently grafted on top of the oriented mesoporous silica membrane, and operating with a redox probe in solution.[126, 131, 136, 143, 150-152, 161] Upon hybridization with the complementary strand (DNA/antigen/aptamer) acting as the analyte, there is less space available for the redox probe to cross the so-functionalized membrane and to reach the electrode surface (see illustration in extreme right of Fig. 4), leading to a lower electrochemical signal. This current decrease is proportional to the analyte (DNA, antigen, or aptamer) concentration in solution, constituting therefore the signal transduction of the recognition event. This electroanalytical scheme has been applied to the genosensing of DNA,[136] the immunosensing of tumor antigen CA15-3,[126] C-reactive protein,[131] or prostate specific antigen (PSA),[150, A151] and the aptasensing of cardiac troponin I,[161] insulin,[143] or PSA,[152] their corresponding analytical performance

being given in Table 3. Otherwise, DNAzyme attached on top of VMSF can be activated by copper and ascorbic acid species and its molecular switching is likely to control the diffusion of a redox probe from the solution to the underlying electrode surface, this system acting thus as a molecular gate for the indirect detection of those analytes.[122] Of related interest is the grafting of i-motif DNA moieties whose changes in confirmation around physiological pH is likely to regulate the diffusion of a redox probe through the film, resulting in a pH-dependent amperometric response that has been applied for pH monitoring in brain microdialysates.[176]

A second category is made of organic ligands or other preconcentration agents covalently attached onto the internal surface of the nanochannels. The interest of the ordered mesoporous silica supports in this case is the possibility of having hybrid materials carrying a high density of organo-functional groups easily and quickly accessible for the species in solution,[191, 192] much better than the non-ordered analogous silica-based adsorbents,[193] which helps provide sensitive electrochemical detection when used as electrode modifiers.[16, 25] Glassy carbon or gold electrodes coated with VMSF bearing organic ligands such as amine,[133] thiol[116, 119] or 5-mercapto-1-methyl-tetrazole,[118] can be applied to the preconcentration of metal ions (Ag^{+}, Cu^{2+}, Hg^{2+}) and their detection by anodic stripping voltammetry. When protonated, the amine groups become cationic and are likely to accumulate analytes that are negatively charged at physiological pH, such as tryptophan or uric acid, which are then electrochemically detected on the underlying electrode surface.[120, 157] Effective preconcentration by electrostatic attraction is also achieved with VMSF functionalized by quaternary ammonium groups, as pointed out for the selective detection of ascorbic acid in the presence of dopamine, the opposite selectivity being obtained on non-modified VMSF electrode.[137]

A third category is that of VMSF functionalized with electroactive moieties. Combining EASA with click chemistry has proven to be an effective method to get oriented mesoporous silica films with redox-active groups covalently attached to the mesopore walls, such as metallocenes,[63-65] iron polypyridine complexes[194, 195] or tetrazine derivatives,[196] while keeping their electrochemical activity and/or their photophysical properties. In such an electrically insulating film, the overall charge transfer mechanism involves an electron hopping between adjacent redox species (electron transfer), most often combined to mass transport implying the electrolyte ions (to maintain charge balance). The interplay between both processes is influenced by the density of redox-active groups in the material as well as the nature and concentration of electrolyte ions in solution.[65] From the electrochemical sensing point of view, only ferrocene functionalized VMSF has been exploited so far. The first conceptual application is the indirect amperometric detection of non-electroactive anions that act as charge compensating species during the oxidation of ferrocene into ferricinum, the measured currents being proportional to the concentration of these anions and the signal is made of both faradic and capacitive contributions as one needs to operate in electrolyte-free medium.[147] The detection of several anions in mixture is also possible by using the sensor at the output of an ion chromatograph. A second application is based on the mediator properties of the ferrocene groups, which can be exploited for the electrocatalytic detection of cysteine and glutathione with a marked selectivity for the former thiolated compounds most probably because of the confined space of mesopore channels.[134] Electrocatalysis with mediators immobilized in non-ordered silica films has been otherwise reported for biosensing applications (see section 4), but to date not yet with VMSF probably due to the difficulty to accommodate redox proteins or enzymes in mesopores of so small diameters.[197]

3.2.5. Ordered silica films as hosts for nano-objects

VMSF can be used as host for metallic nano-objects generated electrochemically by reduction of metal precursors (*i.e.*, $PtCl_6^{2-}$ or $AuCl_4^-$) at the bottom of the nanochannels. Sometimes, the VMSF material was functionalized beforehand with ammonium moieties to induce a positive charge likely to accumulate the precursor anions.[159, 170] Supported Pt nanostructures/nanoparticles[182] and Au nanoparticles[170] have been obtained and exploited for their conductive and/or electrocatalytic properties, for the electrochemical sensing of hydrogen peroxide[170, 182] or ascorbic acid,[159] for instance. NiO(OH) nanostructures were also electrodeposited in VMSF and applied to the non-enzymatic detection of glucose,[167] but surprisingly in 0.1 M NaOH, a medium in which the silica film is not expected to survive (dissolution occurs in strong alkaline medium[198]). A last example is the nano-confinement by electrophoresis of small graphene quantum dots in VMSF and their use for signal amplification in the electrochemical sensing of heavy metal ions in contaminated seafood samples or soil leaching solutions, and dopamine in serum samples.[181]

Otherwise, conducting polymer nanofilaments such as polyaniline (PANI) can be electropolymerized in a controlled way through the nanochannels of VMSF using the silica membrane as a hard template.[199] The obtained mesoporous silica/PANI composite exhibits electrocatalytic properties usable for the anodic detection of ascorbic acid and can be also exploited for pH sensing.[158] When additional Pt nanoparticles are generated in the composite, thanks to the favorable interactions between $PtCl_6^{2-}$ and PANI, the resulting electrode is a good electrochemical sensor for hydrogen peroxide over a wide concentration range (µM – mM).[169] Of related interest are Prussian Blue nanowires electrochemically grown through VMSF and also applied to the electrocatalytic detection of hydrogen peroxide.[140]

3.2.6. Composites made of ordered silica films and other nanomaterials

This last category relates to more heterogeneous deposits prepared either by taking advantage of the possibility to combine the EASA method with the entrapment of clay or organoclay particles in VMSF on electrode,[132, 135] or by generating silica-based nanochannels in the interlayer spacings of swelling clays to form so-called porous clay heterostructures as thin films on an electrode surface.[117] The interest of such composites is to combine the recognition/accumulation properties of the (organo)clays with the fast mass transport ensured by the ordered mesoporous silica matrix. They have been applied to the preconcentration electroanalysis of metal ions (Hg^{2+},[117] Cu^{2+}[132]) or nonsteroidal anti-inflammatory drug (diclofenac[135]).

4. Electrochemical biosensors

Silica films obtained by the sol-gel method are widely used for the encapsulation of biomolecules and their immobilization onto electrode surfaces; they hold a good position among electrodes modified with other nanomaterials.[200-204] The encapsulation of biomolecules (*i.e.*, enzymes) inside silica thin films helps to place them as close as possible to the conductive surface of the electrode. The polymeric framework prevents the biomolecules from leaching and contributes to protect them from the influence of aggressive surrounding environments. At the same time, the quaternary structure and conformational mobility of proteins entrapped inside silica film remain intact. Contrary to biosensors based on organic polymers, those based on biologically modified silica materials possess a porous three-dimensional rigid structure which makes proteins encapsulated inside the film accessible to the substrate. Bioelectrochemical sensors based on composite silica films are characterized by high catalytic activity and long-term stability. Both three-dimensional and planar electrodes are used as supports for bio-silica films as the sensitive elements of

biosensors. Among them, devices involving the use of planar printed electrodes are becoming widespread in recent times as disposable sensors for measurements outside the laboratory.[205, 206] They are significantly cheaper than three-dimensional sensors and usually easier to modify. They are compatible with the analysis of small sample volumes (5-10 µl) in biochemical and medical monitoring, suitable for quality control of food products, and attractive for on-site characterization of environmental media, etc. Planar electrodes can be connected to a smartphone, which plays the role of transducer.[206] The modification of planar screen-printed electrodes (Fig 5A) with silica-based biocomposite thin films is thus a perspective way for the development of disposable sol-gel biosensors.

There are a lot of reviews dealing with electrochemical sensors based on biomolecules encapsulated in silica materials,[7-10, 13, 200, 201, 207-209] some of them considering also the uniform silica-based biocomposite films.[13, 200, 201] Most often, protein molecules are mixed with the silica sol before being applied to the surface of the electrodes, the biomolecule being physically entrapped during gelation. Among the methods of depositing biocomposite films onto electrode surfaces (Table 4), one can highlight those based on evaporation (*i.e.*, spin-coating (rotation), dip-coating (immersion), drop casting or spraying), layer-by-layer (LbL) growth, and electrochemically-assisted deposition (EAD). The two first give the possibility to work mainly with smooth and flat electrode surfaces (evaporation) or involve time consuming procedures (LbL), whereas the third one (EAD) offers the advantage of being easily applied to the modification of electrodes with complicated geometry including macroporous electrodes,[34, 210] carbon nanotube assemblies,[37, 211] or screen-printed electrodes[212, 213] (an illustration of the EAD process on a screen-printed electrode is shown in Fig. 5B). It permits to bring proteins as close as possible to the conductive electrode surface, which helps to detect electrochemically the active center of the encapsulated enzymes during the biocatalytic cycle.[37, 214] As mentioned

above (section 3.2.4), it also enables the generation of ordered silica films supporting covalently-attached genes, antibodies or aptamers.[126, 131, 136, 143, 150-152, 161] By offering an easy way to immobilize biomolecules by weak (encapsulation) or strong (covalent) bonding, the sol-gel process opens up wide possibilities to create the sensitive elements of third-generation mediatorless biosensors.

Several examples of electrochemical biosensors integrating electrodes modified with silica-based biocomposite thin films are given in Table 4; they are discussed below by distinguishing the various families of materials.

4.1. Bioelectrodes based on sol-gel bioencapsulation

A straightforward way to confine proteins in silica films deposited onto electrode surfaces is their direct entrapment during the silica polycondensation by the so-called sol-gel bioencapsulation for biosensors.[22] As pioneers, Nadzhafova *et al.*[40] and Jia *et al.*[41] reported the one-step immobilization of glucose oxidase and/or haemoglobin by electrochemically induced sol-gel bioencapsulation. The encapsulated biomolecules (Fig 5C) were electrochemically accessible (*i.e.*, redox-active[34]) and they kept their biological activity (*e.g.*, possibility to detect glucose[40, 41]). Similar bioceramic thin films can be prepared by spin-coating or dip-coating on electrodes and exploited as electrochemical biosensors.[215] Both sol-gel bioencapsulation methods are compatible with the co-entrapment of nanoparticles (Fig 5D) to improve the bioceramic properties (notably its electrical conductivity). Atomic force microscopy can be used to evidence the formed bioceramic films (Fig 5E). However, such simple approaches might result in non-efficient bioencapsulation and poor electrochemical or biocatalytic responses,[210] requiring the use of suitable additives (polymers, surfactants, nanoparticles) or functionalization strategies

(with charge transfer cofactors) to get biosensors with enhanced performance, as described hereafter.

4.2. Silica-polymer biocomposite films

A way to improving the analytical characteristics of the electrodes modified with biocomposite films is to introduce conductive polymers, polyelectrolytes or polysaccharides into the starting silica sol, which are intended to form interpenetrated organic-inorganic networks (see right part (b) in Fig. 1B). It helps to fix the proteins more firmly inside the composite film due to electrostatic and hydrophobic interactions and it may also enhance the electrical conductivity (in case of conducting polymers) and plasticity of the bioceramic films. Various kinds of (macro)molecules are used for such purpose. Among them one can mention: polyaniline,[216] poly(ethyleneimine),[217] poly(vinyl alcohol),[77] poly(styrene sulfonic acid) or polydimethyldiallylammonium chloride,[37], or even ionic liquids.[218, 219] The biosensors based on such films are usually characterized by better stability and sensitivity due to increased amount of protein molecules firmly fixed in an active form and accessible for the substrate. For example, the natural polysaccharide Chitosan has good affinity to protein molecules, thus improving the plasticity of the films when used as additive to silica biocomposites.[51] Enzyme immobilization within sol–gel silica and poly(vinyl alcohol) on screen-printed electrodes according to a one-step process was even reported to achieve direct electrochemistry of glucose oxidase,[77] the observed electrochemical response being however most probably due to the prosthetic flavin adenine dinucleotide moieties, which may have dissociated away from the immobilized enzyme or else coming from impurities.[220] Direct electron transfer was further demonstrated for a smaller redox protein, hemoglobin (Hb), immobilized in a PANI–SiO_2 film also containing a surfactant (dodecyltrimethylammonium bromide, DTAB).[216] When deposited onto the surface of a

carbon paste electrode (CPE), the resulting Hb/PANI–SiO_2/DTAB/CPE biocomposite electrode demonstrated fast electron transfer processes for Hb, with an electron transfer rate constant of about 0.94 s^{-1}. This system was used as a highly sensitive biosensor for hydrogen peroxide thanks to the excellent electrocatalytic activity of Hb for the reduction of H_2O_2. The conductivity of PANI and the protective action of DTAB can provide a favourable microenvironment for redox proteins and enzymes, opening the door to other potential applications in direct electrochemistry biosensors and bioelectrocatalysis. In a different domain, a biocomposite film made of silica gel, an ionic liquid (1-amyl-2,3-dimethylimidazolium hexafluorophosphate) and a non-ionic surfactant (Triton X-100) on glassy carbon electrode was used for the immunosensing of aflatoxin B1 (AFB1).[218] The ionic liquid offered a biocompatible microenvironment for AFB1 antibody while Triton X-100 ensured the formation of a crack-free film. The resulting label-free immunosensor operated based on electrochemical impedance measurements and presented better sensitivity (2-fold) and much longer stability (190- fold) than the corresponding undoped silica gel immunosensor.

4.3. Biocomposite films based on silica-surfactant or functionalized silica materials

The surfactants are widely used in the formation of biocomposite films as they can behave either as structure directing agents (leading to porous and often ordered materials with enhanced accessibility, as those described in section 3.2), or as stabilizers for the biomolecules in the composite layer, or as both of them. For example, the cationic surfactant CTAB at its critical micellar concentration level helps distribute the proteins more uniformly in the biocomposite film via a better solubilisation in the silica sol. This leads to increasing amounts of the electroactive proteins (*e.g.*, Hb) encapsulated inside the biocomposite film, which remain accessible for the substrate, thus resulting in enhanced

sensitivity and long-term operational stability the developed biosensors.[212] This is also demonstrated for enzymes, such as choline oxidase entrapped in a biocomposite film on gold screen-printed electrode by electrochemically assisted sol-gel deposition, giving rise to a mediator-free choline biosensor with enhanced stability (over 3 weeks) when using the cationic surfactant CTAB in the electrodeposition medium.[221] Of related interest is the immobilization of other biological materials such as aptamers or antibodies onto the surface of ordered mesoporous silica films prepared with surfactant templates and the exploitation of their modulated permeability to redox probes upon hybridization as transduction mode in electrochemical aptasensors and immunosensors. Actually, silica-based electrochemical immunosensors recently gained much importance for detecting antigens and biomarkers responsible for cancer diagnosis and the determination of some biological molecules.[208] This has been mentioned above (see section 3.2.4) for aptamers and antibodies covalently grafted to the surface of vertically oriented silica nanochannels,[126, 131, 136, 143, 150-152, 161] but a softer attachment approach can be also used. This has been notably demonstrated for the label-free electrochemiluminescence (ECL) aptasensing of lysozyme, adenosine and potassium cations.[222] The principle (Fig 6A) implies the use of an amine-functionalized vertically oriented mesoporous silica film on a transparent ITO electrode filled with luminescence reagents $Ru(bpy)_3^{2+}$ and covered with the aptamer (Fig $6A_1$) interacting with the amino groups via non-covalent electrostatic interactions. In the presence of the target analyte, the mesopores became uncapped due to the specific aptamer-target binding and the release of $Ru(bpy)_3^{2+}$ species resulted in a decrease in the ECA signal (Fig $6A_2$), proportionally to the target analyte concentration. This is a quite versatile approach enabling the determination of enzymes, small molecules, and ions, based on a simple competitive procedure and probably easily transferable to the detection of other analytes by altering the

aptamer sequence without any need for its chemical modification (contrary to those grafted covalently).

An additional interest of silica-based materials is their ability to be functionalized in a covalent way by exploiting the rich chemistry of organosilane reagents, and this is of particular interest in bioelectrochemistry. An illustration (Fig 6B) is given for reagentless biosensors for D-glucose, D-sorbitol and D-lactic acid elaborated by coating glassy carbon electrodes with biocompatible composite films made of sol-gel silica and ferrocene-functionalized poly(ethyleneimine), encapsulating a bienzymatic system (the appropriate dehydrogenase enzyme and a diaphorase), and attaching the NAD^+ cofactor to the silica matrix using a suitable organosilane reagent (*i.e.*, glycidopropyltrimethoxysilane, GPS) (Fig $6B_1$). Such strategy allowed the durable immobilization of the cofactor while its 'simple' entrapment led to its rapid leaching out of the biocomposite film.[217] The resulting reagentless device offered good long-term operational stability (more than 12 h of continuous use under potentiostatic conditions in stirred medium whereas very fast deactivation was observed without GPS, see Fig $6B_2$ for the particular case of D-sorbitol detection). This constitutes an illustration of the interest of sol-gel-derived biocomposites integrating all components (enzymes, cofactors, redox mediator) in a durably immobilized form to fabricate reagentless biosensors with good stability. A similar methodology has been applied to wrap carbon nanotubes assemblies with biocomposites by electro-assisted deposition for co-immobilizing D-sorbitol dehydrogenase, an osmium-complex modified polymer or poly(methylene green) as mediator, and NAD-GPS as cofactor, which were applied to the amperometric biosensing of D-sorbitol.[211, 223]

4.4. Silica-nanoparticles biocomposite films

Second-generation biosensors using electron mediators, as well as third-generation mediatorless biosensors are of particular interest nowadays. To this end, it is promising to introduce on the electrode surface composites made of biosilica films with encapsulated nanomaterials likely to improve the electrical conductivity of the film and/or to act as electrocatalysts.[201] Examples of nanomaterials used for that purpose are: nanostructured carbon,[37, 217, 224, 225] metal nanoparticles,[51, 200, 212, 221, 226, 227] metal oxide particles,[203, 213, 214] or their combination [51, 219, 224]. The nanostructured conductive materials can serve as nanoconductors and/or electron mediators between the encapsulated protein and the surface of the electrode, thus increasing the number of electrochemically accessible protein molecules. Overall, they contribute at increasing the sensitivity of the analyte determination, enhancing the signal-to-noise ratio, and improving the long-term stability of such biosensors.

The co-immobilization of nanoparticles within/on silica biocomposite films on electrodes can be realised in several ways (Fig 6C): (a) one-step modification when all film components are mixed with the silica precursors and applied to the electrode;[77, 212, 214, 226] (b) two-step modification involving the formation of a porous silica layer and its subsequent functionalization with the nano-objects;[136, 143, 152, 218, 222] (c) the layer-by-layer (LbL) deposition in which the electrode surface is first coated with a layer of nanoparticles (NP) or nanostructured materials and then covered with the silica biocomposite film.[37, 51, 213, 217, 219, 224] Hereafter, we will essentially focus on the first (one-step) and the third (LbL) methods mainly used for the construction of enzymatic biosensors while the second one was mainly carried out for the development of the apta- and immunosensors already presented above.

Gold nanoparticles (Au-NPs) are widely used among the metal nanoparticles for such purpose because of the good affinity to proteins and high electrocatalytic activity.[202, 219, 224, 226] On the basis of an electrogenerated silica film entrapping hemoglobin (Hb) and glucose oxidase (GOx) on carbon and gold electrodes, with or without Au-NPs, it was demonstrated that the stability of the analytical response of the resulting bioelectrodes was significantly improved when Au-NPs (20 nm in diameter) were present.[212, 226] Electrochemical biosensing was possible in real media, as pointed out for glucose determination in porcine blood serum using a SiO_2–Hb–GOx–Au-NPs biocomposite film on a gold electrode.[226] On the other hand, electrodes modified with Hb were used for the determination of antiviral drugs that inhibit the ability of Hb to bind to oxygen.[212] The bioelectrochemical devices have been prepared by Hb encapsulation in silica sol–gel films, which were generated by EAD method onto pyrolytic graphite electrodes (PGEs). The stability and electrocatalytic activity of Hb entrapped into SiO_2 network was substantially enhanced in the presence of cationic surfactant (CTAB) and Au-NPs. The electrocatalytic current of dissolved oxygen decreased in the presence of the antivirus drug (rimantadine, an amino derivative of adamantane) which opens the way to the determination of this drug.[212] Another example is the determination of hydrogen peroxide and nitrite using a bioelectrode made of silica-coated gold nanorods (GNRs@SiO_2) and room-temperature ionic liquid (RTIL) 1-butyl-3-methylimidazolium tetrafluoroborate ([bmim][BF_4]) entrapping the redox protein myoglobin (Mb).[219] As illustrated in Fig 6D, GNRs@SiO_2 provides a favourable microenvironment for the direct electrochemistry of Mb and its electrocatalytic response to H_2O_2, while at the same time ensuring good hosting capability to prevent RTIL from leaking from the electrode surface. The biosensor exhibited high selectivity, good reproducibility, and long-term stability.

Beside gold, platinum nanoparticles (Pt-NPs) are promising modifiers of biosilica composite films, notably because Pt-NPs exhibit catalytic activity in relation to hydrogen peroxide, a product of many enzymatic reactions. Platinization gold electrodes modified with 3-aminopropyltriethoxysilane-chitosan (APTES–CS) hybrid gel film and *in situ* immobilized glucose oxidase (GOx), with or without Pt-NPs, were used for sensitive glucose sensing.[51] The presence of Pt-NPs in the biocomposite films made it possible to reduce the oxidation overpotential of the enzymatically generated H_2O_2 by *ca.* 200 mV. It resulted in both better sensitivity to glucose over a wider linear concentration range, and lower detection limit than the bioelectrode prepared without Pt-NPs. Following the same idea, systems that are even more sophisticated can be prepared, such as the biocomposite film made of GOx encapsulated in a bifunctional silane-ionic liquid reagent and chitosan generated in one-step by electro-assisted deposition on gold electrodes previously modified with reduced graphene oxide and Pt-NPs.[228]

Nanostructured metal oxide materials, including transition metal oxide nanoparticles, also possess good catalytic activity to hydrogen peroxide and other products of enzymatic reactions. They are quite easy to obtain and rather compatible with silica matrices and ITO electrodes because of their similar oxide nature.[203] Such modifiers are thus attractive for the development of biosensors made of silica-based biocomposite films. Several examples have been reported. Screen-printed electrodes (SPE) modified with oxides of transition metals (MnO_2 or CuO) and bienzymatic composite films were applied to the determination of disaccharides (maltose and sucrose).[213, 214] The indicator reaction was the catalytic current of hydrogen peroxide, a product of bienzymatic reactions, at SPE/metal oxide. The use of metal oxide has improved the selectivity of sensors, avoiding the interference of ascorbic acid, urea, and other reducing substances. SPE modified with MnO_2 particles and bienzymatic silica film with encapsulated GOx and invertase, prepared by

EAD technique, was applied to sucrose biosensing in food.[213] The determination of maltose in beverage products was achieved using an SPE modified with CuO/GOx/maltase/SiO_2 biocomposite film.[214] In another work, horseradish peroxidase (HRP) immobilized on glassy carbon electrode (GCE) with the aid of a silica–hydroxyapatite (HAp) hybrid film was applied to as H_2O_2 biosensing.[229] The silica/HRP–HAp/GCE was characterized by fast electron transfer rates and good electrocatalytic properties for the mediatorless reduction of H_2O_2, thanks to the cooperative effect of HAp nanoparticles with silica to provide a biocompatible microenvironment for HRP.

The use of carbon nanomaterials in the modification of electrodes allows increasing considerably the active surface area and electrocatalytic properties of the electrode, thus improving its sensitivity for analytical determinations. Beside that, carbon nanomaterials have a good affinity to biomolecules.[217, 225] Carbon nanotubes (CNTs) are suitable catalysts for the oxidation of the NADH coenzyme in NAD^+-dependent enzymatic reactions, an effect that is even greater for CNTs functionalized with a redox mediator such as ferrocene.[225] Electrophoretically-deposited CNTs were used as a porous support onto which silica layers encapsulating enzymes from the dehydrogenases group and a cationic polyelectrolyte were generated by EAD, and the resulting biocomposite was reported to be attractive for the amperometric biosensing of D-sorbitol.[37] Carbon nanodots (CND) and graphene oxide (GO) have demonstrated an excellent affinity to biopolymers and high catalytic activity to the products of several enzymatic reactions happening at electrode surfaces.[200, 201, 230] An illustrative example is the combination of Au-NPs in silica matrix, along with reduced GO (RGO) and β-cyclodextrins (CD), to generate a composite electrode with enhanced electroactive surface area, which was then exploited to immobilize HRP enzymes to get a bioelectrode sensitive to H_2O_2.[224] The silica support reduces the crumpled and wrinkled sheet structures of RGO-CD, hence a flatter platform was obtained. Au-NPs acted as tiny

nanoelectrodes thereby increasing electrical communication as well as interfacial interaction with RGO-CD. The obtained electrode demonstrated its affinity to enzyme conjugate HRP-adamantane carboxylic acid (ADA) via supramolecular association between CDs and HRP-ADA. Overall, these multiple components exhibited synergistic effects that favored H_2O_2 reduction in the presence of hydroquinone, in a more efficient way than the individual electrocatalytic effects known for Au-NPs and RGO-CD, respectively.[224] This strategy could find the way to combine metal nanostructures and RGO in silica-based biocomposites to develop novel solid supports for biosensor assembly.

5. Electrochemiluminescence detection and other sensors

5.1. Sensors based on electrochemiluminescence detection

Electrochemiluminescence (ECL) constitutes a combination of an electro-induced reaction and the visualization of luminescence.[231] It can become a quantitative measurement when applying a potential to an electrode surface that can generate species in an excited state resulting in the emission of light from luminophores, in proportion to the concentration of a target analyte involved in the process. Two categories of ECL mechanisms are generally reported:[231] annihilation ECL (in which only the luminophore participates in light emission) and coreactant ECL. The most efficient ECL systems are based on $Ru(bpy)_3^{2+}$/TPrA (where TPrA is tri-*n*-propylamine coreactant) and luminol derivatives/H_2O_2. The well-known mechanism involving $Ru(bpy)_3^{2+}$ luminophore and TPrA coreactant (see illustration in Fig. 7A) is based on two electrochemical oxidations and the redox reaction between the coreactant radical intermediate and the oxidized $Ru(bpy)_3^{2+}$ species to give the excited form of the luminophore, which subsequently emits light upon returning to the ground state during energetic electron transfer reaction, but several novel

systems have been reported for ECL sensing.[232, 233] The combination of ECL method within silica-modified electrodes is a quite old story, which has been reviewed for solid-state ECL sensors based on tris(2,2'-bipyridyl) ruthenium complexes,[234] involving mainly the use of $Ru(bpy)_3^{2+}$-doped silica nanoparticles. Here, we will focus only on the more recent developments of composite materials made of continuous sol-gel-derived silica films. Such porous matrices contribute to improving the stability of luminophores and coreactants immobilised in the film and facilitate the mass transport of electroactive species through the film, increasing the probability of contact between the analytes in solution and the active sites of the support, thus enhancing dramatically the sensitivity of the electrochemical sensors (see examples in Tables 1-3).[129, 145, 162, 165, 169-172, 179, 180, 235-242] ECL can be also used as a readout signal for the biosensors, providing a high sensitive and selective method of detection of substrates in enzymatic electrochemical biosensors as well as immuno- and aptasensors (see examples in Tables 3&4).[126, 127, 151, 161, 222, 243-247] They are mostly based on the two commonly used luminophores luminol and $Ru(bpy)_3^{2+}$, this latter offering the advantage to be regenerable unlike luminol which is consumed.

Solid-state ECL sensors obtained through immobilizing $Ru(bpy)_3^{2+}$ on the electrode surface could significantly reduce the consumption of reagents and improve the sensitivity of the detection. $Ru(bpy)_3^{2+}$ can be accumulated in either ordered or non-ordered silica matrices via favourable electrostatic interactions,[129, 145, 165, 1671, 172, 179, 180, 235, 236] or even through covalent bonding.[237] When applied to tri-*n*-propylamine detection, the ECL sensor fabricated by the sol-gel method (non-ordered silica film) led to a detection limit of 5 nM (*i.e.*, three orders of magnitude lower than that from pure Nafion-modified electrodes), with good stability (92% of the signal remaining after being 35 days storage in air).[235] By comparison, even much better performance can be achieved with a vertically-ordered thin film, with a detection limit 30 times lower (0.17 nM).[180] Similar ECL sensor platforms

based on ordered silica films were developed for the determination of various drugs and biologically-relevant molecules (Table 3) acting as coreactants, with detection limits at the nanomolar level.[129, 145, 165, 171, 172] Attaching the luminophore by covalent bonding to the silica material (using a tetrasilylated ruthenium tris-bipyridyl chloride complex) enabled to enhance significantly the sensor stability (*i.e.*, 90% response obtained after 8 hours of continuous use or 6 month storage), but at the expense of lower sensitivity (1 µM detection limit) due to restricted mass/charge transport processes, as reported for non-ordered films.[237] Finally, one has to mention that composite films made of silica in mixture with cation-exchange polymers (such as poly(styrene sulfonate) or Nafion bearing the $Ru(bpy)_3^{2+}$ luminophore) can be also used as ECL sensors,[238-240] yet exhibiting lower analytical performance compared to the pure silica thin films (Table 1) probably due to slower transport properties. This can be improved somehow by using conducting polymers and/or nanoparticles as additives. A first example is the ECL sensor for codeine phosphate obtained on the basis of a gold electrode modified with a conducting adhesive and a silica film doped with $Ru(bpy)_3^{2+}$, for which the sensitivity and stability was significantly improved by introducing nanoTiO_2-ZnO into the film.[241] Another one is the ECL sensing of H_2O_2 based on VMSF with immobilized luminol, for which the use of trimethylammonium-functionalized silica mesopores modified with AuNP helps to enhance sensitivity towards H_2O_2 for more than two orders of magnitude compared to a corresponding unfunctionalized film.[169, 170]

So far, the combination of ECL detection with molecular fingerprint recognition remains rare (Table 2). A recent example is the development of an electrochemiluminescent response molecularly imprinted composite film with high affinity for Ochratoxin A (OTA) and good sensitivity owing to the use of suitable additives (Fig. 7B).[242] For this purpose, a mesoporous SiO_2 film was drop-casted as nanosheets on the surface of graphene oxide (GO)

and used as support to load graphene quantum dot (NGQDs) and $CsPbBr_3$ perovskite nanocrystals (PNCs) (see part B_1 in Fig. 7B). Such special architecture made possible to achieve an efficient self-enhanced ECL reaction between NGQDs and PNCs inside the nanocomposite film (see part B_2 in Fig. 7B), leading to very high sensitivity for OTA sensing with a detection limit as low as 0.2 pg/mL. Moreover, depositing a molecularly imprinted polymer with OTA on top of the composite film, acting as both a protective barrier and a selective recognition layer, made possible the determination of the target OTA analyte with good selectivity over other typical mycotoxins (zearalenone, vomitoxin, and aflatoxins B1 and B2).[242]

A last category is that of ECL biosensors involving usually two critical components: a recognition biomolecule and a luminophore, which are selected for their ability to significantly improve selectivity and sensitivity of detection of the target substrate. Several examples have been reported (Table 4). A screen-printed carbon electrode covered with a first layer of polyluminol (likely to detect H_2O_2 by ECL) and a silica-Nafion overlayer encapsulating choline oxidase was applied to choline biosensing.[247] The detection principle is the ECL determination of the product of enzymatic transformation of choline (*i.e.*, H_2O_2), the porous structure of the film enabling choline diffusion to the encapsulated enzyme molecules, and the bilayer configuration preventing form luminol leaching.[248] Other polymer-silica composite films entrapping alcohol dehydrogenase along with $Ru(bpy)_3^{2+}$ luminophore were applied to ECL sensing of ethanol in the μM concentration range.[244, 245] In both cases, the silica network offered a good microenvironment for keeping the biological activity of the entrapped enzymes and the negatively-charged organic polymers improved the binding ability for immobilization of $Ru(bpy)_3^{2+}$ species. A glucose ECL flow-injection biosensor was otherwise developed on the basis of $Ru(bpy)_3^{2+}$-doped mesoporous silica (obtained in the presence of PEG-400 template) and glucose dehydrogenase (GDH)

immobilized in polymer Resydrol, as a thin biocomposite film deposited onto a transparent ITO electrode.[243] NADH, which is produced by the reaction of co-enzyme NAD^+ and glucose catalyzed by GDH, reacted with immobilized $Ru(bpy)_3^{2+}$ to generate ECL emission.

Nanomaterials-based luminophores are a perspective way to enhance sensitivity and selectivity of ECL sensors because they provide excellent signal transduction pathways. They play a significant role in ECL research by essentially functioning as emitters, accelerators, carriers, and multifunctional nanocomponents.[241-243, 246, 249] This is notably the case of noble metal nanoclusters exhibiting enhanced ECL emission due to the formation of a rigid shell through a host–guest interaction on the metal surface, or other nanomaterials acting as nanocarriers of luminophores for signal amplification (*e.g.*, Au and Ag NPs, magnetic nanoparticles, quantum dots, 2D nanomaterials (such as GO, MXene, and metal–organic layers), nanofibers, nanorods, and silica NPs).[249] They were also used in ECL biosensors, as exemplified for the ultrasensitive detection of NADH and ethanol using a gold disk electrode modified with partially sulfonated (3-mercaptopropyl)-trimethoxysilane sol–gel bearing $Ru(bpy)_3^{2+}$ species and Au NPs, alone or with the enzyme alcohol dehydrogenase.[246] The presence of Au NPs enhanced the electron transfer between $Ru(bpy)_3^{2+}$ and the electrode, resulting in the possible determination of these analytes at very low concentration (detection limits of 1 nM for NADH and 12 nM for ethanol).

Finally, beside the ECL aptasensor described in section 4.3 involving $Ru(bpy)_3^{2+}$-doped VMSF with adsorbed aptamers (Fig 6A),[222] a series of geno- and immuno-sensors with ECL detection have been reported (Table 4). In a first example, a glassy carbon electrode modified with a bilayer of mesoporous silica and chitosan bearing luminol, functionalized with human epidermal growth factor receptor 2 (HER-2) antibody, was used for ECL cyto-immunosensing of metastatic breast cancer cells (SKBR-3), which was quite

selective in the presence of other interfering cells (such as MCF-7 and MDA-MB-231).[250] Another recent example is the highly sensitive (femtomolar range) ECL biosensing of a leukaemia marker (BCR/ABL fusion gene detection) using a silica-luminol thin film modified with Au NPs and a ferrocene-labelled molecular beacon (Fc-MB).[251] Fc-MB served as a catalyst for the luminol ECL reaction which was enhanced by the presence of Au NPs. Upon hybridization with target DNA, ferrocene moieties departed from the nanocomposite electrode surface by stem opening of the Fc-MB reagent, resulting in a decrease in ECL intensity proportional to the probe concentration.

5.2. Other sensors

Beside their use in amperometric/voltammetric devices, silica thin films are considered as prospective membranes for potentiometric sensors or ion-selective field-effect transistors (ISFET) exhibiting high sensitivity and requiring small sample volume. Among the potentiometric sensors, one can cite a carbon paste electrode modified with diazo-thiophenol-functionalized silica for the detection of Ag(I) (with LOD at 9.5×10^{-7} M),[252] or the selective potentiometric detection of chloride ions using an ultra-thin (300 nm thick) nanostructured film of porous silica grafted with amino-groups and gold nanoparticles.[253] A potentiometric biosensor for urea has been fabricated by immobilizing urease in a composite film made of silica and MWCNTs on ITO electrode, exhibiting a fast response time (10–25 s) with a sensitivity of 23 mV/decade in the concentration range extending from 0.02 to 1 mM.[254] Knowing that sol-gel films can be patterned on ISFETs by photo-assisted electrodeposition,[255] or deposited as ultrathin layers on p-type and n-type organic field effect transistors (OFETs) by spin-coating,[256] and that such films can be generated in the form of composites with organic compounds or polymers,[257-259] has opened the door to silica-based ISFET and OFET sensors. To name but a few, there are the

Si/SiO_2-based ISFETs functionalized with either thiacalix[4]arene for the detection of copper(II) ions[260] or butyrylcholinesterase for sensing organophosphorus pesticides,[261] or OFETs silanized with various organosilanes and applied to gas sensing.[262]

Other gas sensors have been developed on the basis of composite silica films, but the silica material acted mostly as a support for the active components and/or as a way to enhance mass transport properties and therefore improving the response time and sensitivity of the devices. Detection was mainly performed by optical methods, quartz crystal microbalance measurements, or resistance monitoring. As this review is devoted to electrochemical sensors, we will only consider the resistive-type gas sensors. Examples are available for hydrogen sensing in the 50-100 ppm concentration range with using Pd-silica thin films exhibiting fast resistance changes (10-30 s),[263] the room-temperature detection of ammonia gas at ppb level with an Ag-doped γ-Fe_2O_3/SiO_2 composite film,[264] or gaseous hydrogen sulphide sensing via resistance monitoring of TiO_2/SiO_2 composite aerogel deposited onto gold interdigitated electrodes offering a detection limit of 0.5 ppm at 250°C (with 53 s response time and 74 s recovery time).[265]

Finally, one can also cite the use of Au@SiO_2 core-shell nanoparticles for improving the performance of either electrochemical surface plasmon resonance (SPR) studies[266] or the detection of molecular species by surface-enhanced Raman spectroscopy (SERS).[267] Clad-based fiber SPR or local surface plasmon resonance (LSPR) sensors with an additional layer of oxide material including SiO_2 had demonstrated enhanced sensing performance in terms of reliability, sensitivity and long-term stability.[268, 269] This is because the oxide overlayer enlarged the evanescent field towards the sensing region and protected metal surface from degradation. Silica layer can also act as a linker for modification of such sensors, and the use of these materials is perspective for biosensing.[268] To date, however,

there are only few 'real' electrochemical (bio)sensors' applications based on these systems. One related example is the use of a composite film made of Au NPs, SiO_2 NPs, and graphene oxide, for the electrochemical SPR biosensing of NADH, for which detection can be achieved by both differential pulse voltammetry (DPV) and SPR, yet with an SPR response less sensitive than the DPV one.[270]

6. Conclusion and outlook

Composite materials made of sol-gel-derived silica, being either nanostructrured around soft templates, or functionalized with organic moieties, or doped with suitable reagents, macromolecules or nanomaterials, are attractive electrode modifiers for applications in electrochemical sensing and biosensing. This review focused especially on the recent advances made with these composite materials deposited as continuous thin films on electrode surfaces, in relation to their use as promising platforms for electrochemical sensing devices. The versatility of the sol-gel process makes it possible to generate thin films with a wide range of composition and nanoscale organization, including the physical entrapment of conductive or catalytic nano-objects and/or biologically active materials. They can be obtained by evaporation-induced polycondensation or electrochemically assisted deposition. So far, the main electrochemical sensing applications are in the fields of preconcentration electroanalysis, electrocatalytic detection, selective recognition by complexation or molecular imprinting, permselective accumulation/rejection of analytes/interferences, electrochemical enzymatic sensors, geno/apta/immunosensors, and detection by electrogenerated chemiluminescence. A major attractiveness of the silica network relies on its rigidity, imparting a mechanical stability to the porous film, thus enabling easy and fast diffusion of analytes (and reagents) to the electrode surface. This becomes overwhelming for silica frameworks produced in an organized form with

mesopore channels of monodisperse diameter all oriented vertically relative to the underlying electrode support, resulting in dramatic increases in sensitivity of the sensors. One can also play with the composite composition and structure to ensure proper selectivity to the sensors. Another major interest is the possibility to immobilize redox proteins and enzymes by sol-gel bioencapsulation while keeping their biological activity and the accessibility to their substrates and cofactors, leading to good performance electrochemical biosensing. A drawback of silica materials when used for electrochemical purposes is their insulating properties, but this can be solved somehow by associating metal nanoparticles, conducting polymers or nanocarbons, or by attaching redox moieties likely to enable charge transfer by electron hopping. These additives can otherwise contribute to induce more effective electrocatalytic properties. However, a major practical constraint of silica gel is its rather poor chemical stability in solution, especially when rising pH, which may lead to limited long-term operational stability of silica-based electrochemical sensors and biosensors.

Among the first prospects in this field, it is therefore not surprising to affirm the need to improve the chemical stability of composite films in order to increase the long-term operational use of electrochemical devices integrating composite silica-based thin films. A possible direction would be the formation of silica-based mixed oxide films (*e.g.*, mesoporous silica films prepared with 10% or less ZrO_2 or Al_2O_3 undergo much less degradation than pure silica materials under biologically relevant conditions[271]) for which significant improvement in chemical stability under electrochemical cycling can be observed.[272] Even more stable oxide films can be obtained (*e.g.*, IrO_x nanostructures prepared using VMSF as hard template and used for pH sensing at human skin surface,[273] yet after dissolution of the silica membrane), but they are losing one key advantage of silica-based materials: the possibility to be derivatized with organo-functional groups. And such

functionalization to get organic-inorganic composite films constitutes another attractive perspective in the field, not only to improve their chemical stability,[274, 275] but also to create novel properties and additional reactivity towards the target analytes. In particular, the possibility of obtaining multifunctional mesoporous thin films by combining several selective click reactions,[63] or by functionalization strategies likely to achieve a spatial surface modification or selective deposition of guest species within multimodal and hierarchical ordered mesoporous materials.[276] The achievement of multiple functionalization and extending the possibilities of host-guest interactions in designing silica-based composite thin films should also contribute to explore new horizons and to bring real synergetic (and not only additional) effects expected to improve the analytical performance of the electrochemical (bio)sensors in terms or enhanced sensitivity, selectivity and stability. Finally, the emergence 3D-printing technologies starts to benefit to electrochemistry,[277] in particular for manufacturing electrochemical sensors,[278, 279] but this has not yet been exploited in connection to composite silica-based thin films. Considering that 3D-printed conductive materials can be produced as porous electrodes of complex geometry,[280] such new generation electrodes could be easily modified with silica-based thin films prepared by electrochemically assisted deposition, in the same way as that applied to uniformly coat the inner surface of macroporous metal electrodes with sol-gel biocomposites[34] or to generate vertically aligned mesoporous silica films on 3D graphene-carbon nanotube assemblies,[149] for instance. Another strategy could be the direct additive manufacturing of composite electrodes made of a conductive matrix (carbon, metal) and silica with a mesoporous structure (the 3D-printing of ordered mesoporous silica monoliths has been developed,[281] and it could be extended to the production of conductive nanocomposites). This would offer novel nanofabrication opportunities especially attractive for miniaturization of the composite silica-based electrochemical sensors.

7. References

[1] J. Fraden, *Handbook of Modern Sensors*, Springer, Cham. **2016**, pp. 645-697.

[2] H Ju, J. Li (eds), *Biochemical Sensors, vol. 1 Fundament and Development*, World Scientific Series (From Biomaterials Towards Medical Devices, vol. 4), Singapore, **2021**.

[3] D. Yang, in: B. S. R. Reddy (ed), *Advances in Nanocomposites – Synthesis, Characterization and Industrial Applications*, InTech Open, Rijeka, Croatia, **2011**, chap. 37, pp. 857–882.

[4] V. P. Elanjeitsenni, K. S. Vadivu, B. M. Prasanth, *Mater. Res. Express* **2022**, *9*, 022001.

[5] T. Ribeiro, C. Baleizão, J. P. S. Farinha, *Materials* **2014**, *7*, 3881–3900.

[6] B. Barsan, G. Gauglitz, A. Oprea, E. Ostertag, G. Proll, K. Rebner, K. Schierbaum, Chemical and Biochemical Sensors, 1. Fundamentals, Wiley-VCH, Weinheim, **2016**.

[7] J. Wang, *Anal. Chim. Acta* **1999**, *399*, 21–27.

[8] A. Walcarius, *Chem. Mater.* **2001**, *13*, 3351–3372.

[9] L. Rabinovich, O. Lev, *Electroanalysis* **2001**, *13*, 265–275.

[10] A. Walcarius, *Electroanalysis* **2001**, *13*, 701–718.

[11] Y. Gushikem, S. S. Rosatto, *J. Braz. Chem. Soc.* **2001**, *12*, 695–705.

[12] S. V. Aurobind, K. P. Amirthalingam, H. Gomathi, *Adv. Colloid Interface Sci.* **2006**, *121*, 1–7.

[13] K. Miecznikowski, J. A. Cox, *J. Solid State Electrochem.* **2020**, *24*, 2617–2631.

[14] A. Walcarius, D. Mandler, J. Cox, M. M. Collinson, O. Lev, *J. Mater. Chem.* **2005**, *15*, 3663–3689.

[15] A. Walcarius, A. Kuhn, *Trends Anal. Chem.* **2008**, *27*, 593–603.

[16] A. Walcarius, *Electroanalysis* **2015**, *27*, 1303–1340.

[17] O. Lev, Z. Wu, S. Bharathi, V. Glezer, A. Modestov, J. Gun, L. Rabinovich, S. Sampath, *Chem. Mater.* **1997**, *9*, 2354–2375.

[18] J. Wen, G. L. Wilkes, *Chem. Mater.* **1996**, *8*, 1667–1681.

[19] C. Sanchez, F. Ribot, B. Lebeau, *J. Mater. Chem.* **1999**, *9*, 35–44.

[20] O. Lev, D. Rizkov, S. Mizrahi, I. Ekeltchik, Z. G. Kipervaser, V. Gitis, A. Goifman, D. Tessema, A. Kamyshny Jr., A. Modestov, J. Gun, in: L. Klein, M. Aparicio, A. Jitianu (eds), *Handbook of Sol-Gel Science and Technology*, Springer, Cham, **2018**, pp. 2663–2694.

[21] M. Faustini, L. Nicole, E. Ruiz-Hitzky, C. Sanchez, *Adv. Funct. Mater.* **2018**, *28*, 1704158.

[22] S. N. Tan, W. Wang, L. Ge, in: P. Ducheyne (ed.), *Comprehensive Biomaterials II*, Elsevier, Oxford, 2017, vol. 3, p. 657–689.

[23] P. Innocenzi, *Chem. Sci.* **2022**, *13*, 13264–13279.

[24] M. Etienne, A. Quach, D. Grosso, L. Nicole, C. Sanchez, A. Walcarius, *Chem. Mater.* **2007**, *19*, 844–856.

[25] A. Walcarius, *Chem. Soc. Rev.* **2013**, *42*, 4098–4140.

[26] A. Walcarius, *Acc. Chem. Res.* **2021**, *54*, 3563–3575.

[27] P. Zhou, L. Yao, K. Chen, B. Su, *Crit. Rev. Anal. Chem.* **2020**, *50*, 424–444.

[28] A. Walcarius, *Electroanalysis* **2008**, *20*, 711–738.

[29] A. Walcarius, P. Audebert, in: P. Gomez-Romero, C. Sanchez (eds.), *Functional Hybrid Materials*, Wiley-VCH, Weinheim, **2004**, Chap. 6, pp. 172–209.

[30] C.J. Brinker, G.W. Scherer, *Sol-Gel Science*, Academic Press, San Diego, **1990**.

[31] C.J. Brinker, A.J. Hurd, P.R. Schunk, G.C. Frye, C.S. Ashley, *J. Non-Cryst. Solids* **1992**, *147-148*, 424–436.

[32] M.M. Collinson, *Acc. Chem. Res.* **2007**, *40*, 777–783.

[33] L. Liu, D. Mandler, in: L. Klein, M. Aparicio, A. Jitianu (eds.), *Handbook of Sol-Gel Science and Technology*, Springer, Cham, **2018**, pp. 531-568.

[34] F. Qu, R. Nasraoui, M. Etienne, Y. Bon Saint Come, A. Kuhn, J. Lenz, J. Gajdzik, R. Hempelmann, A. Walcarius, *Electrochem. Commun.* **2011**, *13*, 138–142.

[35] I. Mazurenko, M. Etienne, R. Ostermann, B. M. Smarsly, O. Tananaiko, V. Zaitsev, A. Walcarius, *Langmuir* **2011**, *27*, 7140–7147.

[36] J. Wang, N. Vilà, A. Walcarius, *Electrochim. Acta* **2021**, *366*, 137407.

[37] I. Mazurenko, M. Etienne, O. Tananaiko, V. Zaitsev, A. Walcarius, *Electrochim. Acta* **2012**, *83*, 359–366.

[38] E. Sibottier, S. Sayen, F. Gaboriaud, A. Walcarius, *Langmuir* **2006**, *22*, 8366–8373.

[39] X. Wang, N. Ben Ahmed, G. S. Alvarez, M. V. Tuttolomondo, C. Hélary, M. F. Desimone, T. Coradin, *Curr. Top. Med. Chem.* **2015**, *15*, 223–244.

[40] O. Nadzhafova, M. Etienne, A. Walcarius, *Electrochem. Commun.* **2007**, *9*, 1189–1195.

[41] W.-Z. Jia, K. Wang, Z.-J. Zhu, H.-T. Song, X.-H. Xia, *Langmuir* **2007**, *23*, 11896–11900.

[42] W. Ghach, M. Etienne, P. Billard, F. Jorand, A. Walcarius, *J. Mater. Chem. B* **2013**, *1*, 1052–1059.

[43] W. Boumya, S. Charafi, M. Achak, H. Bessbousse, A. Elhalil, M. Abdennouri, N. Barka, *Res. Chem.* **2022**, *4*, 100623.

[44] X. Liu, B. Li, X. Wang, C. Li, *Microchim. Acta* **2010**, *171*, 399–405.

[45] G. Arken, G. Li, X. Zheng, X. Liu, *Anal. Lett.* **2014**, *47*, 2522–2536.

[46] A. Kovalyk, O. Tananaiko, A. Borets, M. Etienne, A. Walcarius, *Electrochim. Acta* **2019**, *306*, 680–687.

[47] L. Fang, Q.-Q. He, M.-J., Zhou, J.-P. Zhao, *Electrochem. Commun.* **2019**, *109*, 106609.

[48] X. Q. Du, Y. W. Liu, D. C. Chen, Z. Zhang, Y. Chen, *Surf. Coat. Technol.* **2022**, *436*, 128279.

[49] D. Ravi Shankaran, N. Ueheara, T. Kato, *Biosens. Bioelectron.* **2003**, *18*, 721–728.

[50] M. Yang, Y. Yang, Y. Liu, G. Shen, R. Yu, *Biosens. Bioelectron.* **2006**, *21*, 1125–1131.

[51] L. Lei, Z. Cao, Q. Xie, Y. Fu, Y. Tan, M. Ma, S. Ya, *Sens. Actuat. B* **2011**, *157*, 282–289.

[52] M. Raveh, L. Liu, D. Mandler, *Phys. Chem. Chem. Phys.* **2013**, *15*, 10876–10884.

[53] T.-C. Wei, H. W. Hillhouse, *Langmuir* **2007**, *23*, 5689–5699.

[54] M. Etienne, Y. Guillemin, D. Grosso, A. Walcarius, *Anal. Bioanal. Chem.* **2013**, *405*, 1497–1512.

[55] L. Rimoldi, V. Pifferi, D. Meroni, G. Soliveri, S. Ardizzone, L. Falciola, *Electrochim. Acta* **2018**, *291*, 73–83.

[56] S. Sayen, M. Etienne, J. Bessière, A. Walcarius, *Electroanalysis* **2002**, *14*, 1521–1525.

[57] M. Etienne, A. Walcarius, *Electrochem. Commun.* **2005**, *7*, 1449–1456.

[58] C. Sanchez, C. Boissière, D. Grosso, C; Laberty, L. Nicole, *Chem. Mater.* **2008**, *20*, 682–737.

[59] D. Feng, J. Wei, M. Wang, Q. Yue, Y. Deng, A.M. Asiri, D. Zhao, *Adv. Porous Mater.* **2013**, *1*, 164–186.

[60] A. Walcarius, E. Sibottier, M. Etienne, J. Ghanbaja, *Nature Mater.* **2007**, *6*, 602–608.

[61] A. Goux, M. Etienne, E. Aubert, C. Lecomte, J. Ghanbaja, A. Walcarius, *Chem. Mater.* **2009**, *21*, 731–741.

[62] G. E. Moehl, T. Nasir, Y. Han, Y. J. Noori, R. Huang, R. Beanland, P. N. Bartlett, A. L. Hector, *Nanoscale* **2022**, *14*, 5404–5411.

[63] N. Vilà, J. Ghanbaja, E. Aubert, A. Walcarius, *Angew. Chem. Int. Ed.* **2014**, *53*, 2945–2950.

[64] N. Vilà, J. Ghanbaja, A. Walcarius, *Adv. Mater. Interfaces* **2016**, *3*, 1500440.

[65] N. Vilà, A. Walcarius, *Electrochim. Acta* **2015**, *179*, 304–314.

[66] Z. Teng, G. Zheng, Y. Dou, W. Li, C.-Y. Mou, X. Zhang, A. M. Asiri, D. Zhao, *Angew. Chem. Int. Ed.* **2012**, *51*, 2173−2177.

[67] M.-A. Pizzoccaro-Zilamy, C. Huiskes, E. G. Keim, S. N. Sluijter, H. van Veen, A. Nijmeijer, L. Winnubst, and M. W. J. Luiten-Olieman, *ACS Appl. Mater. Interfaces* **2019**, *11*, 18528−18539.

[68] X. Lin, Q. Yang, L. Ding, B. Su, *ACS Nano* **2015**, *9*, 11266−11277.

[69] C. Karman, N. Vilà, A. Walcarius, *ChemElectroChem* 2016, 3, 2130−2137.

[70] N. Vilà, E. André, R. Ciganda, J. Ruiz, D. Astruc, A. Walcarius, Chem. Mater. 2016, 28, 2511−2514.

[71] W. Yantasee, B. Charnhattakorn, G. E. Fryxell, Y. Lin, C. Timchalk, R. S. Addleman, *Anal. Chim. Acta* **2008**, *620*, 55–63.

[72] I. Sebarchievici, B.-O. Taranu, S.F. Rus, E. Fagadar-Cosma, *J. Electroanal. Chem*. **2020**, *865*, 114127.

[73] A. Kornii, V. V. Lisnyak, L. Grishchenko, O. Tananaiko, *Electrochim. Acta* **2022**, *409*, 139938.

[74] N. Shaabani, N. W. C. Chan, A. B. Jemere, *Nanomaterials* **2021**, *11*, 631.

[75] O. Yu. Nadzhafova, T. S. Rozhanchuk, V. N. Zaitsev, V. V. Shevchenko, *Ukr. Chim. Zhurn*. **2008**, *74*, 59–64.

[76] P.-G. Su, W.-L. Shiu, M.-S. Tsai, *Sens. Actuat. B* **2015**, *216*, 467–475.

[77] S. Zuo, Y. Teng, H. Yuan, M. Lan, *Sens. Actuat. B* **2008**, *133*, 555–560.

[78] C. T. Canevari, P. A. Raymundo-Pereira, R. Landers, E. V. Benvenutti, S. A. S. Machado, *Talanta* **2013**, *116*, 726–735.

[79] K. M.Wiaderek, J. A. Cox, *Electrochim. Acta* **2011**, *56*, 3537–3542.

[80] G. Maduraiveeran, P. Manivasakan, R. Ramaraj, *Int. J. Nanotechnol,* **2011**, *8*, 925–934.

[81] P.Yang, H. Cai, S. Liu, Q. Wan, X. Wang, N. Yang, *Electrochim. Acta* **2011**, *56*, 7097–7103.

[82] P. L. Almeida Jr., C. H. S. Mendes, I. A. F. S. Lima, M. F. Belian, S. C. B. Oliveira, C. M. A. Brett, V. B. Nascimento, *Anal. Lett*. **2018**, *51*, 496–511.

[83] S. Bharathi, M. Nogami, O. Lev, *Langmuir* **2001**, *17*, 2602–2609.

[84] A. Celebanska, M. Opallo, *ChemElectroChem* **2016**, *3*, 1629–1634.

[85] G. Maduraiveeran, R. Ramaraj, *J. Electroanal. Chem*. **2007**, *608*, 52–58.

[86] X. Liu, L. Xie, H. Li, *J. Electroanal. Chem*. **2012**, *682*, 158–163.

[87] A. Taheri, M. Noroozifar, M. Khorasani-Motlagh, *J. Electroanal. Chem*. **2009**, *628*, 48–54.

[88] I. Sadok, K. Tyszczuk-Rotko, *J. Electroanal. Chem*. **2018**, *808*, 204–210.

[89] Y. Battie, O. Ducloux, L. Patout, P. Thobois, A. Loiseau, *Sens. Actuat. B* **2012**, *163*, 121–127.

[90] A. Hassan Oghli, A. Soleymanpour, *Microchem. J.* **2022**, *173*, 107034.

[91] S. Kozhukharova, Z. Nenova, T. Nenov, N. Nedev, M.Machkova, *Sens. Actuat. B* **2015**, *210*, 676–684.

[92] E. L. Holthoff, F. V. Bright, *Anal. Chim. Acta* **2007**, *594*, 147–161.

[93] C. G. Xie, B. H. Liu, Z. Y. Wang, D. M. Gao, G. J. Guan, Z. P. Zhang, *Anal. Chem.* **2008**, *80*, 437–443.

[94] B. B. Prasad, R. Madhuri, M. P. Tiwari, P. S. Sharma. *Biosens. Bioelectron*. **2010**, *25*, 2140–2148.

[95] J. Zhang, Y. Q. Wang, R. H. Lv, L. Xu, *Electrochim. Acta* **2010**, *55*, 4039–4044.

[96] T. Sikolenko, E. Bou-Maroun, T. Karbowiak, *Curr. Opin. Electrochem.* **2022**, *36*, 101151.

[97] R. Makote, M.M. Collinson, *Chem. Mater.* **1998**, *10*, 2440–2445.

[98] N. F. Atta, A. M. Abdel-Mageed, *Talanta* **2009**, *80*, 511–518.

[99] T. Rozhanchuk, M. Velychko, M. Titov, O. Tananaiko, *Electroanalysis* **2013**, *25*, 2045–2053.

[100] J. Luo, J. Cong, R. Fang, X. Fei, X. Liu, *Microchim. Acta* **2014**, *181,*1257–1266.

[101] Z. Zhang, Y. Hu, H. Zhang, L. Luo, S. Yao, *Biosens. Bioelectron.* **2010**, *26*, 696–702.

[102] W. de J. R. Santos, M. Santhiago, I. V. P. Yoshida, L. T. Kubota, *Anal. Chim. Acta* **2011**, *695*, 44–50.

[103] W. J. R. Santos, M. Santhiago, I. V. P. Yoshida, L. T. Kubota, *Sens. Actuat. B* **2012**, *166–167*, 739–745.

[104] Y. Hu, J. Li, Z. Zhang, H. Zhang, L. Luo, S. Yao, *Anal. Chim. Acta* **2011**, *698*, 61–68.

[105] J. Huang, X. Zhang, Q.Lin, X.He, X. Xing, H. Huai, W. Lian, H. Zhu, *Food Control* **2011**, *22*, 786-791.

[106] Y.-F. Hu, Z.-H. Zhang, H.-B. Zhang, L.-J. Luo, S.-Z. Yao, *Talanta* **2011**, *84*, 305–313.

[107] Z. Zhang, Y. Hu, H. Zhang, L. Luo, S. Yao, *J. Electroanal. Chem.* **2010**, *644*, 7–12.

[108] C. Lafarge, M. Bitar, L. El Hosry, P. Cayot, E. Bou-Maroun, *Mater. Today Commun*. **2020**, *24*, 101157.

[109] X .Tan, B. Li, K. Y. Liew, C. Li, *Biosens. Bioelectron*. **2010**, *26*, 868–871.

[110] S. Fireman-Shoresh, I. Turyan, D. Mandler, S. Marx, *Langmuir* **2005**, *21*, 7842–7847.

[111] J. Zou, G.-Q. Zhao, G.-L. Zhao, J.-G. Yu, *Coord. Chem. Rev.* **2022**, *471*, 214732.

[112] S. Zhu, X. Lin, Q. Wang, Q. Xia, P. Ran, Y. Fu, *Electroanalysis* **2017**, *29*, 466–471.

[113] I. Sulym, A. Cetinkaya, M. Yence, M. E. Çorman, L. Uzun, S. A. Ozkan, *Electrochim. Acta* **2022**, *430*, 141102.

[114] S. Li, D. Du, J. Huang, H. Tu, Y. Yang, A. Zhang, *Analyst* **2013**, *138*, 2761–2768.

[115] H. Zhou, Y. Ding, R. Su, D. Lu, H. Tang, F. Xi, *Front. Chem.* **2022**, *9*, 812086.

[116] M. Etienne, J. Cortot, A. Walcarius, *Electroanalysis* **2007**, *19*, 129–138.

[117] A. Jieumboué Tchinda, E. Ngameni, A. Walcarius, *Sens. Actuat. B* **2007**, *121*, 113–123.

[118] A. Sanchez, A. Walcarius, *Electrochim. Acta* **2010**, *55*, 4201–4207.

[119] W. Yantasee, Y. Lin, X. Li, G. E. Fryxell, T. S. Zemanian, V. V. Viswanathan, *Analyst* **2003**, *128*, 899-904.

[120] Z. Li, H. Xu, D. Wu, J. Zhang, X. Liu, S. Gao, Y. Kong, *ACS Appl. Mater. Interfaces* **2019**, *11*, 2840–2848.

[121] F. Xi, L. Xuan, L. Lu, J. Huang, F. Yan, J. Liu, X. Dong, P. Chen, *Sens. Actuat. B* **2019**, *288*, 133–140.

[122] M. Saadaoui, I. Fernández, A. Sánchez, P. Díez, S. Campuzano, N. Raouafi, J. M. Pingarrón, R. Villalonga, *Electrochem. Commun.* **2015**, *58*, 57–61.

[123] F. Yan, M. Wang, Q. Jin, H. Zhou, L. Xi, H. Tang, J. Liu, *J. Electroanal. Chem.* **2021**, *881*, 114969.

[124] Y. Zou, X. Zhou, L. Xie, H. Tang, F. Yan, *Front. Chem.* **2022**, *10*, 939510.

[125] F. Yan, T. Luo; Q. Jin, H. Zhou, A. Sailjoi, G. Dong, J. Liu, W. Tang, *J. Hazard. Mater.* **2021**, *410*, 124636.

[126] J. Huang, T. Zhang, Y. Zheng, J. Liu, *Biosensors* **2023**, *13*, 317.

[127] J. Gong, T. Zhang, P. Chen, F. Yan, J. Liu, *Sens. Actuat. B* **2022**, *368*, 132086.

[128] Q. Han, T. Zhang, M. Wang, F. Yan, J. Liu, *Molecules* **2022**, *27*, 8200.

[129] X. Wei, X. Luo, S. Xu, F. Xi, T. Zhao, *Front. Chem.* **2022**, *10*, 872582.

[130] K. Wang, L. Yang, H. Huang, N. Lv, J. Liu, Y. Liu, *Molecules* **2022**, *27*, 2739.

[131] N. Ma, X. Luo, W. Wu, J. Liu, *Nanomater.* **2022**, *12*, 3981.

[132] A. Maghear, M. Etienne, M. Tertiş, R. Sandulescu, A. Walcarius, *Electrochim. Acta* **2013**, *112*, 333–341.

[133] M. Etienne, A. Goux, E. Sibottier, A. Walcarius, *J. Nanosci. Nanotechnol.* **2009**, *9*, 2398–2406.

[134] H. Maheshwari, N. Vilà, G. Herzog, A. Walcarius, *ChemElectroChem* **2020**, *7*, 2095–2101.

[135] S. L. Z. Jiokeng, I. K. Tonlé, A. Walcarius, *Sens. Actuat. B* **2019**, *287*, 296–305.

[136] M. Saadaoui, I. Fernández, G. Luna, P. Díez, S. Campuzano, N. Raouafi, A. Sánchez, J. M. Pingarrón, R. Villalonga, *Anal. Bioanal. Chem.* **2016**, *408*, 7321–7327.

[137] W. Li, L. Ding, Q. Wang, B. Su, *Analyst* **2014**, *139*, 3926–3931.

[138] F. Yan, J. Chen, Q. Jin, H. Zhou, A. Sailjoi, J. Liu, W. Tang, *J. Mater. Chem. C* **2020**, *8*, 7113–7119.

[139] L. Yang, T. Zhang, H. Zhou, F. Yan, Y. Liu, *Front. Nutr.* **2022**, *9*, 987442.

[140] A. Goux, J. Ghanbaja, A. Walcarius, *J. Mater. Sci.* **2009**, *44*, 6601–6607.

[141] S. Ahoulou, N. Vilà, S. Pillet, D. Schaniel, A. Walcarius, *Electroanalysis* **2020**, 32, 690–697.

[142] J. Guo, X. Liu, A. Wang, X. Yu, L. Ding, *Microchem. J.* **2022**, *183*, 107964.

[143] F. Asadpour, M. Mazloum-Ardakani, F. Hoseynidokht, S. M. Moshtaghioun, *Biosens. Bioelectron.* **2021**, *180*, 113124.

[144] T. Nasir, A. Gamero-Quijano, C. Despas, M. Dossot, G. Herzog, A. Walcarius, *Talanta* **2020**, *220*, 121347.

[145] R. Liang, J. Jiang, Y. Zheng, A. Sailjoi, J. Chen, J. Liu, H. Li, *RSC Adv.* **2021**, *11*, 34669–34675.

[146] X. Deng, X. Lin, H. Zhou, J. Liu, H. Tang, *Nanomater.* **2023**, *13*, 239.

[147] C. Karman, N. Vilà, C. Despas, A. Walcarius, *Electrochim. Acta* **2017**, *228*, 659–666.

[148] T. Nasir, G. Herzog, L. Liu, M. Hébrant, C. Despas, A. Walcarius, *ACS Sensors* **2018**, *3*, 484–493.

[149] W. Zheng, R. Su, G. Yu, L. Liu, F. Yan, *Nanomater.* **2022**, *12*, 3632.

[150] L. Yan, S. Xu, F. Xi, *Nanomater.* **2022**, *12*, 3810.

[151] K. Ma, Y. Zheng, L. An, J. Liu, *Front. Chem.* **2022**, *10*, 851178.

[152] W. Argoubi, A. Sánchez, C. Parrado, N. Raouafia, R. Villalonga, *Sens. Actuat. B* **2018**, *255*, 309–315.

[153] Y. Ma, W. Liao, H. Zhou, Y. Tong, J. Liu, F. Yan, H. Tang, J. Liu, *J. Mater. Chem. B* **2020**, *8*, 10630–10636.

[154] H. Zhu, X. Ma, A. Sailjoi, Y. Zou, X. Lin, F. Yan, B. Su, J. Liu, *Sens. Actuat. B* **2022**, *353*, 131101.

[155] W. Zheng, R. Su, X. Lin, J. Liu, *Front. Chem.* **2022**, *10*, 954802.

[156] X. Zhu, L. Xuan, J. Gong, J. Liu, X. Wang, F. Xi, *Talanta* **2022**, *238*, 123027.

[157] K. Ma, L. Yang, J. Liu, J. Liu, *Nanomater.* **2022**, *12*, 1157.

[158] L. Ding, W. Li, Q. Wang, Q. Sun, S. He, B. Su, *Chem. Eur. J.* **2014**, *20*, 1829–1833.

[159] L. Ding, W. Li, Q. Sun, S. He, B. Su, *Chem. Eur. J.* **2014**, *20*, 12777–12780.

[160] J. Wang, J. Yu, Y. Yu, Z. Luo, G. Li, X. Lin, *Food Chem.* **2023**, *405*, 134806.

[161] X. Mi, H. Li, R. Tan, Y. Tu, *Anal. Chem.* **2020**, *92*, 14640–14647.

[162] S. Chen, Y. Lei, J. Xu, Y. Yang, Y. Dong, Y. Li, H. Yi, Y. Liao, L. Chen, Y. Xiao, *RSC Adv.* **2022**, *12*, 17330–17336.

[163] Q. Sun, F. Yan, L. Yao, B. Su, *Anal. Chem.* **2016**, *88*, 8364–8368.

[164] W. Zheng, B. Su, *J. Electroanal. Chem.* **2016**, *781*, 383–388.

[165] L. Zhu, W. Fu, J. Chen, S. Li, X. Xie, Z. Zhang, J. Liu, L. Zhou, B. Su, X. Chen, *Sens. Actuat. B* **2022**, *366*, 131972.

[166] F. Yan, X. Ma, Q. Jin, Y. Tong, H. Tang, X. Lin, J. Liu, *Microchim. Acta* **2020**, *187*, 470.

[167] J. Ding, X. Li, L. Zhou, R. Yang, F. Yan, B. Su, *J. Mater. Chem. B* **2020**, *8*, 3616–3622.

[168] L. Ding, B. Su, *J. Electroanal. Chem.* **2015**, *736*, 83–87.

[169] J. Zhang, H. Ding, L. Zhu, S. Zhao, D. Jiang, H.-Y. Chen, *Electrochem. Commun.* **2019**, *98*, 38–42.

[170] Z.-M. Lyu, X.-L. Zhou, X.-N. Wang, P. Li, L. Xu, E.-H. Liu, *Sens. Actuat. B* **2019**, *284*, 437–443.

[171] Y. Xiao, L. Xu, P. Li, X.-C. Tang, L.-W. Qi, *Anal. Chim. Acta* **2017**, *983*, 96–102.

[172] Y. Xiao, S. Chen, G. Zhang, Z. Li, H. Xiao, C. Chen, C. He, R. Zhang, X. Yang, *Analyst* **2020**, *145*, 4806–4814.

[173] L. Yao, F. Yan, B. Su, *Analyst* **2016**, *141*, 2303-2307.

[174] X. Lin, B. Zhang, Q. Yang, F. Yan, X. Hua, B. Su, *Anal. Chem.* **2016**, *88*, 7821–7827.

[175] F. Yan, H. He, L. Ding, B. Su, *Anal. Chem.* **2015**, *87*, 4436–4441.

[176] L. Shi, F. Cao, L. Zhang, Y. Tian, *Anal. Chem.* **2020**, *92*, 4535–4540.

[177] F. Yan, B. Su, *Anal. Chem.* **2016**, *88*, 11001–11006.

[178] Q. Sun, F. Yan, B. Su, *Biosens. Bioelectron.* **2018**, *105*, 129–136.

[179] S. Li, D. Zhang, J. Liu, C. Cheng, L. Zhu, C. Li, Y. Lu, S. S. Low, B. Su, Q. Liu, *Biosens. Bioelectron.* **2019**, *129*, 284–291.

[180] Z. Zhou, W. Guo, L. Xu, Q. Yang, B. Su, *Anal. Chim. Acta* **2015**, *886*, 48–55.

[181] L. Lu, L. Zhou, J. Chen, F. Yan, J. Liu, X. Dong, F. Xi, P. Chen, *ACS Nano* **2018**, *12*, 12673–12681.

[182] X. Li, L. Zhou, J. Ding, L. Sun, B. Su, *ChemElectroChem* **2020**, *7*, 2081–2086.

[183] S. Ahoulou, N. Vilà, S. Pillet, D. Schaniel, A. Walcarius, *Chem. Mater.* **2019**, 31, 5796–5807.

[184] F. Yan, X. Lin, B. Su, *Analyst* **2016**, *141*, 3482–3495.

[185] N. Vilà, P. de Oliveira, A. Walcarius, I. M. Mbomekallé, *Electrochim. Acta* **2019**, *309*, 209–218.

[186] T. Nasir, L. Zhang, N. Vila, G. Herzog, A. Walcarius, *Langmuir* **2016**, *32*, 4323–4332.

[187] W. Ullah, G. Herzog, N. Vilà, M. Brites-Helu, A. Walcarius, *ChemElectroChem* **2021**, *8*, 142–150.

[188] L. Xuan, W. Liao, M. Wang, H. Zhou, Y. Ding, F. Yan, J. Liu, H. Tang, F. Xi, *Talanta* **2021**, *225*, 122066.

[189] M. B. Serrano, C. Despas, G. Herzog, A. Walcarius, *Electrochem. Commun.* **2015**, *53*, 34–36.

[190] J. Liu, H. Cheng, D. He, X. He, K. Wang, Q. Liu, S. Zhao, X. Yang, *Anal. Chem.* **2017**, *89*, 9062–9068.

[191] A. Walcarius, M. Etienne, B. Lebeau, *Chem. Mater.* **2003**, *15*, 2161–2173.

[192] A. Walcarius, C. Delacôte, *Chem. Mater.* **2003**, *15*, 4181–4192.

[193] A. Walcarius, M. Etienne, S. Sayen, B. Lebeau, *Electroanalysis* **2003**, *15*, 414–421.

[194] N. Vilà, A. Walcarius, *Front. Chem.* **2020**, *8*, 830.

[195] S. Ahoulou, N. Vilà, S. Pillet, C. Carteret, D. Schaniel A. Walcarius, *ChemPhysChem* **2021**, *22*, 2464–2477.

[196] P. Audebert, N. Vilà, C. Allain, F. Maisonneuve, A. Walcarius, P. Hapiot, *ChemElectroChem* **2015**, *2*, 1695–1698.

[197] M. Etienne, L. Zhang, N. Vilà, A. Walcarius, *Electroanalysis* **2015**, *27*, 2028–2054.

[198] W. Ullah, G. Herzog, N. Vilà, A. Walcarius, *Electrochem. Commun.* **2021**, *122*, 106896.

[199] A. Gamero-Quijano, C. Karman, N. Vilà, G. Herzog, A. Walcarius, Langmuir 33 (2017) 4224–4234.

[200] A. Walcarius, *Curr. Opin. Electrochem.* **2018**, *10*, 88–97.

[201] E. Casero, M. D. Petit-Domínguez, L. Vázquez, Enzymatic Sol–Gel Biosensors. In: Klein, L., Aparicio, M., Jitianu, A. (eds), Handbookof sol-gel science and technology.- 2016.- Springer: Cham. pp. 1-39.

[202] J. Wang, *Microchim. Acta* **2012**, *177*, 245–270.

[203] M. U. Anu Prathap, B. Kaur, R. Srivastava, *Chem. Rec*. **2019**, *19*, 883–907.

[204] Y. Xian, Y. Xian, L. Zhou, F. Wu, Y. Ling, L. Jin, *Electrochem. Commun*. **2007**, *9*, 142–148.

[205] F. Arduini, L. Micheli, D. Moscone, D. Palleschi, S. Piermarini, F. Ricci, G. Volpe, *Trends Anal. Chem.* **2016**, *79*, 114–126.

[206] X. Huang, D. Xu, J. Chen, J. Liu, Y. Li, J. Song, X. Ma, J. Guo, *Analyst* **2018**, *143*, 5339–5351.

[207] A. Walcarius, M. M. Collinson, *Annu. Rev. Anal. Chem.* **2009**, *2*, 121–143.

[208] M. Hasanzadeh, N. Shadjou, M. Eskandani, M. de la Guardia, *Trends Anal. Chem.* **2012**, *40*, 106–118.

[209] H. Kholafazad Kordasht, M. Pazhuhi, P. Pashazadeh-Panahi, M. Hasanzadeh, N. Shadjou, *Trends Anal. Chem.* **2020**, *124*, 115778.

[210] Z. Wang, M. Etienne, G.-W. Kohring, Y. Bon Saint Côme, A. Kuhn, A. Walcarius, *Electrochim. Acta* **2011**, *56*, 9032-9040.

[211] Z. Wang, M. Etienne, S. Pöller, W. Schuhmann, G.-W. Kohring, V. Mamane, A. Walcarius, *Electroanalysis* **2012**, *24*, 376–385.

[212] T. Rozhanchuk, O. Tananaiko, I. Mazurenko, M. Etienne, A. Walcarius, V. Zaitsev, *J. Electroanal. Chem.* **2009***, 625*, 33–39.

[213] A. A. Kornii, A. S. Borets, O. Yu. Tananaiko, *Methods Objects Chem. Anal.* **2021**, *16*, 61–70.

[214] A. Kornii, V. Saska, V. V. Lisnyak, O. Tananaiko, *Electroanalysis*, **2020**, *32*, 1468–1479.

[215] O. Lev, D. Rizkov, S. Mizrahi, I. Ekeltchik, Z. G. Kipervaser, V. Gitis, A. Goifman, D. Tessema, A. Kamyshny Jr., A. D. Modestov, J. Gun, in: L. Klein, M. Aparicio, A. Jitianu (eds.), Handbook of Sol-Gel Science and Technology, Springer, Cham, 2018, pp. 2663–2694.

[216] B. Chen, H. Wang, H. Zhang, Z. He, S. Zhang, T. Liu, Y. Zhou, *J. Mol. Liq.* **2012**, *171*, 23–28.

[217] Z. Wang, M. Etienne, F. Quilès, G.-W. Kohring, A. Walcarius, *Biosens. Bioelectron.* **2012**, *32*, 111–117.

[218] L. Zaijun, W. Zhongyun, S. Xiulan, F. Yinjun, C. Peipei, *Talanta* **2010**, *80*, 1632–1637.

[219] W.-L. Zhu, Y. Zhou, J.-R. Zhang, *Talanta* **2009**, *80*, 224–230.

[220] P. N. Bartlett, F. A. Al-Lolage, *J. Electroanal. Chem.* **2018**, *819*, 26–37.

[221] I. Mazurenko, O. Tananaiko, O. Biloivan, M. Zhybak, I. Pelyak, V. Zaitsev, M. Etienne, A. Walcarius, *Electroanalysis* **2015**, *27*, 1685–1692.

[222] J. Liu, D. He, Q. Liu, X. He, K. Wang, X. Yang, J. Shangguan, J. Tang, Y. Mao, *Anal. Chem.* **2016**, *88*, 11707–11713.

[223]. Wang, M. Etienne, V. Urbanova, G.-W. Kohring, A. Walcarius, *Anal. Bioanal. Chem.* **2013**, *405*, 3899–3906.

[224] S. Manivannan, K. Kim, *Electroanalysis* **2016**, 28, 1608–1616.

[225] N. Allali, V. Urbanova, M. Etienne, X. Devaux, M. Mallet, B. Vigolo, J.-J. Adjizian, C. P. Ewels, S. Oberg, A. V. Soldatov, E. McRae, Y. Fort, M. Dossot, V. Mamane, *Beilstein J. Nanotechnol*. **2018**, *9*, 2750–2762.

[226] Yu. V. Iminova, O. Yu. Tananaiko, T. S. Rozhanchuk, T. G. Gruzina, L. S. Reznichenko, L. Malysheva, Z. R. Ulberg. *J. Anal. Chem. (Russia)* ***2015***, *70*, 1247–1253.

[227] S. Sladkevich, J. Gun, P. Prikhodchenko, D. Rizkov, R. Shelkov, N. Kyi, V.Gutkin, O. Lev, Selected Contemporary Topics in Sol-Gel Electro-Chemistry. In: Sol-Gel Methods for Materials Processing. NATO Science for Peace and Security Series C: Environmental Security. Eds: Innocenzi P., Zub Y.L., Kessler V.G.– 2008 Springer: Dordrecht. pp. 155-186.

[228] F. Wu, T. Huang, Y. Hu, X. Yang, Q. Xie, *J. Electroanal. Chem.* **2016**, *781*, 296–303.

[229] B. Wang, J.-J. Zhang, Z.-Y. Pan, X.-Q. Tao, H.-S. Wang, *Biosens. Bioelectron.* **2009***, 24*, 1141–1145.

[230] A. Walcarius, *Trends Anal. Chem.* **2012**, *38*, 79–97.

[231] M. M. Richter, *Chem. Rev.* **2004**, *104*, 3003−3036.

[232] C. Ma, Y. Cao, X. Gou, J.-J. Zhu, *Anal. Chem.* **2020**, *92*, 431−454.

[233] X. Ma, W. Gao, F. Du, F. Yuan, J. Yu, Y. Guan, N. Sojic, G. Xu, *Acc. Chem. Res.* **2021**, *54*, 2936−2945.

[234] H. Wei, E. Wang, *Trends Anal. Chem.* **2008**, *27*, 447−459.

[235] L. Qian, X. Yang, *Anal. Chim. Acta* **2008**, *609*, 210–214.

[236] L. Armelao, R. Bertoncello, S. Gross, D. Badocco, P. Pastore, *Electroanalysis* **2003**, *15*, 803–811.

[237] J.-K. Lee, S.-H. Lee, M. Kim, H. Kim, D.-H. Kim, W.-Y. Lee, *Chem. Commun.* **2003**, 1602–1603.

[238] H. Wang, G. Xu, S. Dong, *Analyst* **2001**, *126*, 1095–1099.

[239] C. Yi, Y. Tao, B. Wang, X. Chen, *Anal. Chim. Acta* **2005**, *541*, 73–81.

[240] B. Qiu, X. Chen, H.-L. Chen, G.-N. Chen, *Luminescence* **2007**, *22*, 189–194.

[241] L. Yang, L. Li, Y. Luo, R.-R. Zhang, Y. Cui, F. H. Cui, K. Sun, Y.-O. Li, *Chin. J. Anal. Chem*. **2015**, *43*, 547–552.

[242] J. Wei, L. Chen, X. Cai, W. Lai, X. Chen, Z. Cai, *Biosens. Bioelectron*. **2022**, *216*, 114664.

[243] R. Lei, X. Wang, S. Zhu, N. Li, *Sens. Actuat. B* **2011**, *158*, 124–129.

[244] Z. Xu, Z. Guo, S. Dong, *Biosens. Bioelectron.* **2005**, *21*, 455–461.

[245] L. Zhang, Z. Xu, S. Dong, *Anal. Chim. Acta* **2006**, *575*, 52–56.

[246] L. Deng, L. Zhang, L. Shang, S. Guo, D. Wen, F. Wang, S. Dong, *Biosens. Bioelectron*. **2009**, *24*, 2273–2276.

[247] A. Sassolas, L. J. Blum, B. D. Leca-Bouvier, *Sens. Actuat. B* **2009**, *139*, 214–221.

[248] B. D. Leca-Bouvier, A. Sassolas, L. J. Blum, *Anal. Bioanal. Chem.* **2014**, *406*, 5657–5667.

[249] J. Zhou, X. Lv, J. Jia, Z. Din, S. Cai, J. He, F. Xie, J. Cai, *Biosensors* **2022**, *12*, 1046.

[250] H. Nasrollahpour, M. Mahdipour, I. Isildak, M.-R. Rashidi, A. Naseri, B. Khalilzadeh, *Biosens. Bioelectron.* **2021**, *178*, 113023.

[251] Y. Li, Z. Ding, Y. Bao, K. Han, G. Li, *Anal. Lett.* **2022**, *55*, 203–214.

[252] T. Zhang, Y. Chai, R. Yuan, J. Guo, *Mater. Sci. Eng. C* **2012**, *32*, 1179–1183.

[253] A. Ruiz-Gonzalez, J. Huang, C. Xun, R. Chhabra, R. Lee, H. Yizhong, A. Davenport, B. Li, R. Palgrave, K. L. Choy*, Appl. Mater. Today* **2022***, 29*, 101600.

[254] T. Ahuja, D. Kumar, N. Singh, A. M. Biradar, Rajesh, *Mater. Sci. Eng. C* **2011**, *31*, 90–94.

[255] J.-H. Zhou, L.-L. Jiang, L.-K. Wu, J.-M. Hu, *Electrochem. Comm*. **2015**, *61*, 40–44.

[256] S. Guo, Z. Wang, Z. Xu, S. Wang, K. Wu, S. Chen, Z. Zhang, C. Xu, W. Qiu, L. Li, *Chin. Chem. Lett*. **2017**, *28*, 2143–2146.

[257] Y. Bai, X. Liu, L. Chen, K.-u. Haq, M. A. Khan, W. Q. Zhu, X. Y. Jiang Z. L. Zhang. *Microelectron. J.* **2007**, *38*, 1185–1190.

[258] M. D. Morales-Acosta, M. A. Quevedo-López, R. Ramírez-Bon, *Mater. Chem. Phys*. **2014**, *146*, 380–388.

[259] J. Hu, W. Que, H. Liu. *Mater. Lett*. **2020**, *317*, 132120.

[260] M. B. Ali, A. Abdelghani, H. B. Ouada, N. Jaffrezic-Renault, R. Lamartine, *Mater. Sci. Eng. C* **2002**, *21*, 29–34.

[261] F. Abdelmalek, M. Shadaram, H. Boushriha, *Sens. Actuat. B* **2001**, *72*, 208–213.

[262] T. Mori, Y. Kikuzawa, K. Noda, *Jpn. J. Appl. Phys.* **2013**, *52*, 05DC02.

[263] C. Lo, S.-W. Tan, C.-Y. Wei, J.-H. Tsai, W.-S. Lour, *Int. J. Hydrogen Energy* **2013**, *38*, 313–318.

[264] Y. Tang, Z. Li, X. Zu, J. Ma, L. Wang, J. Yang, B. Du, Q. Yu, *J. Hazard. Mater.* **2015**, *298*, 154–161.

[265] F. Yang, J. Zhu, X. Zou, X. Pang, R. Yang, S. Chen, Y. Fang, T. Shao, X. Luo, L. Zhang, *Ceram. Int.* **2018**, *44*, 1078–1085.

[266] S. Szunerits, R. Boukherroub, *Electrochem. Commun.* **2006**, *8*, 439–444.

[267] Y.-F. Huang, C.-Y. Li, I. Broadwell, J.-F. Li, D.-Y. Wu, B. Ren, Z.-Q. Tian, *Electrochim. Acta* **2011**, *56*, 10652–10657.

[268] M. Chauhan, V. K. Singh, *Opt. Fiber Technol*. **2021**, 64, 102580.

[269] S. Singh, S. K. Mishra, B. D. Gupta, *Sens. Actuat. A* **2013**, 193, 136–140.

[270] J. Breczko, E. Regulska, A. Basa, M. Baran, K. Winkler, M. E. Plonska-Brzezinska, *ECS J. Solid State Sci. Technol.* **2016**, *5*, M3018–M3025.

[271] J. D. Bass, D. Grosso, C. Boissière, E. Belamie, T. Coradin, C. Sanchez, *Chem. Mater.* **2007**, *19*, 4349–4356.

[272] S. Alberti, P. Y. Steinberg, G. Giménez, H. Amenitsch, G. Ybarra, O. Azzaroni, P. C. Angelomé, G. J. A. A. Soler-Illia, *Langmuir* **2019**, *35*, 6279−6287.

[273] L. Zhou, C. Cheng, X. Li, J. Ding, Q. Liu, B. Su, *Anal. Chem*. **2020**, *92*, 3844−3851.

[274] T. Fontecave, C. Sanchez, T. Azaïs, C. Boissière, *Chem. Mater.* **2012**, *24*, 4326–4336.

[275] M. Etienne, S. Goubert-Renaudin, Y. Rousselin, C. Marichal, F. Denat, B. Lebeau, A. Walcarius, *Langmuir* **2009**, *25*, 3137–3145.

[276] M. Tiemann, C. Weinberger, *Adv. Mater. Interfaces* **2021**, *8*, 2001153.

[277] A. Ambrosi, M. Pumera, *Chem. Soc. Rev.* **2016**, *45*, 2740–2755.

[278] R. M. Cardoso, C. Kalinke, R. G. Rocha, P. L. dos Santos, D. P. Rocha, P. R. Oliveira, B. C. Janegitz, J. A. Bonacin, E. M. Richter, R. A. A. Munoz, *Anal. Chim. Acta* **2020**, *1118*, 73–91.

[279] A. Abdalla, B. A. Patel, *Curr. Opin. Electrochem.* **2020**, *20*, 78–81.

[280] M. H. Omar, K. A. Razak, M. N. Ab Wahab, H. H. Hamzah, *RSC Adv.* **2021**, *11*, 16557–16571.

[281] E. S. Farrell, Y. Schilt, M. Y. Moshkovitz, Y. Levi-Kalisman, U. Raviv, S. Magdassi, *Nano Lett.* **2020**, *20*, 6598–6605.

List of Tables

Table 1. Electrochemical sensors based on composite electrodes elaborated from continuous non-ordered silica thin films modified with organic polymers, analytical reagents, and/or nanomaterials.

Analyte [a]	Film type [b]	Electrode configuration [c]	Detection method		Analytical performance		Stability (%) [f]		Refs.
			Procedure [d]	Technique [e]	Concentration range	Det. limit	Operational	Storage	
Ag^{+}in water	Spin-coating	GCE/SH-SiO_2/PbNP	Acc. – Det.	SWV	9.3×10^{-12} – 1.85×10^{-9} M	1.2×10^{-12} M	10 me. (RSD = 3.1%)		88
Ascorbic acid (in human plasma)	PLD	CE/MnTTP/SiO_2	EC	SWV	0.082 – 33 mM	0.04 mM			72
Bromate Methionine	EAD	GCE/APTES/AuNP-Rh_2PMo_{11}	EC	FIA	5×10^{-6} – 10×10^{-5} M 5×10^{-6} – 50×10^{-6} M	4.0×10^{-8} M 2.5×10^{-7} M	100 inject.	1 day	79
Cd^{2+} Cu^{2+} Pb^{2+} (in natural water)	SAM and spin-coating	GCE/SH-SAMMS-Nafion	Acc. – Det.	SWV	2.5–100 ppb 0–1.5 ppb	2.5 ppb 2.5 ppb 0.5 ppb	8 me. (95%)	4 days, 120 me (91%)	71
Codeine Morphine	Drop-casting	GCE/DiMeDiMOS-TMOS-PSS-Ru(bpy)$_3^{2+}$	Direct det.	ECL	2×10^{-8} – 5×10^{-5} M 1×10^{-7} – 3×10^{-3} M	5×10^{-9} M 3×10^{-8} M	10 me. (RSD = 4.8 & 4.2%)	5 days, 250 me (96.8%)	240
Codeine phosphate	Dip-coating	Au/SiO_2,-NanoTiO_2-ZnO-CA-Ru(bpy)$_3^{2+}$	Direct det.	ECL	1.0×10^{-7} – 1.0×10^{-4} M	2.5×10^{-8} M	10 me. (92.6%)		241
Cyanide	Soaking	GE/SiO_2/AgNP	Acc. – Det.	CV	1.5×10^{-6} – 2.1×10^{-4} M	1.4×10^{-8} M	7 me. (RSD = 1.7%)	60 days (96.7%)	87
DNP (in environment)	Spin-coating	GCE/V_2O_5–CeO_2–SBA-15–poly(vitamin B1)	Acc. – Det.	CV	$(3.0–30)\times10^{-6}$ M	0.5×10^{-6} M	10 me. (97%)	30 days (95%)	81
Dopamine Acetaminophen	EAD	nanoSPCE/Fe_2O_3/nanoC/(NH_2-SiO_2+CTAB)	Acc. – Det. & EC	DPV	2×10^{-6} – 1.0×10^{-5} M 2×10^{-6} – 1.0×10^{-5} M	6×10^{-7}M 4×10^{-7}M	20 me. (~90%)	1 month (80%)	73
Dopamine Uric acid (in urine)	Drop-casting	rGO–AuNP–CS–APTES	EC	DPV	1.0×10^{-6} – 2.0×10^{-4} M 1.0×10^{-6} – 3.0×10^{-4} M	0.3×10^{-6}M 0.7×10^{-6}M	5 me. (RSD = 3.9%)	1 month (92%)	86
Dopamine Acetaminophen Uric acid (in urine)	Drop-casting	GCE/MWCNT/SiO_2/Nafion	EC	DPV	5.0×10^{-7} – 6.0×10^{-6} M 5.0×10^{-7} – 5.0×10^{-6} M 5.0×10^{-7} – 1.0×10^{-5} M	0.014×10^{-6}M 0.098×10^{-6}M 0.068×10^{-6}M	10 me. (RSD = 5%)		78

Table 1. Continued.

Analyte [a]	Film type [b]	Electrode configuration [c]	Detection method		Analytical performance		Stability (%) [f]		Refs.
			Procedure [d]	Technique [e]	Concentration range	Det. limit	Operational	Storage	
Humidity (RH)	Dropping	AuSPE/MPTMS-SiO_2 /AuNP/GO	Direct det.	EIS	22 - 90%				76
Humidity (RH)	Dip-coating	Ag-Pd/TiO_2-SiO_2/Ce	Direct det.	EIS	15 – 90%				91
H_2O, NH_3, NO_2	Dip-coating	Pt/SWCNT/SiO_2	Direct det.	Res.	200 ppm				89
H_2O_2	Drop-casting	GCE/SiO_2-AuNP	EC	A	2.5×10^{-6} – 45.0×10^{-6} M	3.15×10^{-9} M			85
Methamphetamine	Drop-casting	GCE/DiMeDiMOS-TMOS-PSS-Ru(bpy)$_3^{2+}$	Direct det.	ECL	5.0×10^{-7} – 1.0×10^{-5} M	2.0×10^{-7} M	6 me. (RSD = 1.1%)	10 days, (95%)	239
$Mo^{(VI)}$ (in vitamins)	Drop-casting	PGE/(SiO_2+PDMDA)/LG	Acc. – Det.	CV	2.0×10^{-6} - 10.0×10^{-5} M	1.0×10^{-6} M	5 me. (RSD = 3-5 %)	1 month (80%)	75
Nitrite	Drop-casting	GCE/SH-SiO_2/AgNP	EC	A	4×10^{-6} – 48×10^{-6} M	4×10^{-6} M			80
Nitrite (in water)	EAD	Au/MPTMS-TEOS-AEPTMS/$K_4Fe(CN)_6$	EC	FIA	1.0 – 40.0 µmol L^{-1}	0.53 µmol L^{-1}			82
Oxalic acid	Dip-coating	FTO/Ru(bpy)$_3$$Cl_2$-$SiO_2$	Direct det.	ECL-FIA	2×10^{-6} – 3×10^{-4} M	1×10^{-6} M			236
Pb^{2+} (in urine and drinking water)	EAD	PGE/rGO/PWA/SiO_2	Acc. – Det.	DPASV	5.0×10^{-10} – 5.0×10^{-7} M	2.2×10^{-11}M	5 me. (RSD = 8.2%)	15 days	90
Tri-*n*-propylamine	Drop-casting	GCE/Ru(bpy)$_3$$Cl_2$-$SiO_2$	Direct det.	ECL	5.8×10^{-8} – 2.4×10^{-4} M	5.0×10^{-9} M	8 me. (RSD = 2.6%)	35 days (92%)	235
Tri-*n*-propylamine	Spin-coating	ITO/Tetrasil-Ru(bpy')$_3$$Cl_2$	Direct det.	ECL	1×10^{-6} – 1×10^{-3} M	1.0×10^{-6} M	8 hours (~90%)	6 months (90%)	237
Tri-*n*-propylamine Oxalate NADH	Drop-casting	GCE/(SiO_2-Triton X-100)+(PSS-Ru(bpy)$_3^{2+}$)	Direct det.	ECL-FIA	1×10^{-3} – 1 M 1×10^{-3} – 1 M 1×10^{-3} – 1 M	1×10^{-4} M 1×10^{-4} M 5×10^{-4} M	5 me. (RSD 0.9 to 3.9 %)	1 week (98%)	238

Table 1. Continued.

[a] Abbreviation: DNP, 2,4-dinitrophenol; RH, relative humidity.

[b] Abbreviations for silica film preparation procedures: PLD, laser ablation deposition technique; EAD, electro-assisted deposition; SAM, self-asembled monolayer.

[c] Abbreviations: GCE, glassy carbon electrode; SH-SiO_2, thiol-functionalized silica; PbNP, lead nanoparticles; CE, carbon electrode; MnTTP 5,10,15,20-tetra(4-tolyl)porphyrinato manganese(III) chloride; APTES, 3-aminopropyltriethoxysilane; AuNP, gold nanoparticles; Rh_2PMo_{11}, dirhodium(II) phosphomolybdate; SH-SAMMS, thiol self-assembled monolayers on mesoporous silica; DiMeDiMOS, dimethyldimethoxysilane; TMOS, tetramethoxysilane; PSS, poly(*p*-styrene sulfonate); CA, conductive adhesive; AgNP, silver nanoparticles; SBA, Santa Barbara Amorphous; nanoSPCE, carbon nanostructured screen-printed electrodes; nanoC, carbon nanoparticles with carboxyl and fluorine containing groups; NH_2-SiO_2, amine-functionalized silica; CTAB, cetyltrimethylammonium bromide; rGO, reduced graphene oxide; AuNP, gold nanoparticles; CS, chitosan; MWCNT, multiwall carbon nanotubes; Ag-Pd/TiO_2-SiO_2/Ce, silver-palladium planar electrodes modified with TiO_2-SiO_2 composite film doped with diammonium hexanitrocerate; AuSPE, gold screen-printed electrode; MPTMS, 3-mercaptopropyltrimethoxysilane; GO, graphene oxide; SWCNT, single wall carbon nanotubes; PGE, pyrolytic graphite electrode; PDMDA, polydimethyldiallylammonium; LG, lumogallion; MPTMS, 3-mercaptopropyltrimethoxysilane; TEOS, tetraethoxysilane; AEPTMS, 3-[2-(2-aminoethylamino)ethylamino]propyltrimethoxysilane; FTO, fluorine-doped tin oxide; PWA, phosphotungstic acid; Tetrasil-Ru(bpy')$_3Cl_2$, tetrasilylated ruthenium trisbipyridyl chloride complex.

[d] Abbreviations: Acc., accumulation; Det., detection; EC, electrocatalytic detection.

[e] Abbreviations: SWV, square wave voltammetry; FIA, flow injection analysis; ECL, electrochemiluminescence; CV, cyclic voltammetry; DPV, differential pulse voltammetry; EIS, electrochemical impedance spectroscopy; Res., resistance measurement; A, amperometry; DPASW, differential pulse anodic stripping voltammetry.

[f] Expressed as % of remaining response (in parentheses) after a number of measurements (me.) or injections (inject.) or as RSD (relative standard deviation) for operational stability, or the given period of storage.

Table 2. Electrochemical sensors based on composite electrodes elaborated from molecularly imprinted silica-based thin films.

Analyte [a]	Film type [b]	Electrode configuration [c] (+ MIS composition)	Detection method		Analytical performance		Stability (%) [f]		Refs.
			Procedure [d]	Technique [e]	Concentration range	Det. limit	Operational	Storage	
Adenine Guanine	Drop casting	GCE/MIS(TEOS,polyelectrolytes(PSS+PVS or PDDA))	Acc. – Det.	CV	2.0×10^{-5} – 5.0×10^{-4} M 2.0×10^{-5} – 4.0×10^{-4} M	1.5×10^{-5} M	3 me. (RSD = 4%)	2 month (90%)	99
Benzylpenicillin (in blood plasma)	EAD	CE/Fe_3O_4@SiO_2–MWCNT–CS/MIS(TEOS,PTMOS,MTMOS)	Acc. – Det.	DPV	5.0×10^{-8} – 1.0×10^{-3} M	1.5×10^{-9} M	60 me. (96,2%)	30 days	104
Bisphenol A (in honey, tap water, grape juice)	EAD	Au/MWCNT–AuNPs/MIS(TEOS,APTES)	Acc. – Det.	A	1.13×10^{-7} – 8.2×10^{-3} M	3.6×10^{-9} M	5 me. (RSD = 4.8%)		105
Caffeine (in coffee and energy drink)	Spin-coating	GCE/MWCNT–VTMOS/MIS(TEOS,MTMOS,APTES)	Acc. – Det.	DPV	0.75 – 40 µM	0.22 µM	50 me. (RSD = 2.7%)	1 month	103
Chlorogenic acid (in food)	Spin-coating	Au/MPTMS/MIS(TEOS,PTEOS,APTES)	Acc. – Det.	DPV	0.5×10^{-6} – 1.4×10^{-5} M	1.5×10^{-7} M	50 me. (RSD = 2.3%)	3 month	102
Dopamine	Spin-coating	GCE/MIS(TMOS,PTMOS,MTMOS)	Acc. – Det.	CV	0 – 0.5mM		48 hr	7 days	97
Dopamine Tyramine	Spin-coating	GCE/MIS(TEOS,PTEOS)	Acc. – Det.	SWV	1.0×10^{-5} – 1.0×10^{-4} M	1.0×10^{-5} M	3 me. (RSD = 7.4%)	2 weeks (78%)	98
L-Histidine (in human blood serum)	LbL-EAD	ITO/APTES/MWCNT/MIS(TEOS,PTMOS,MTMOS)	Acc. – Det.	DPV	2.0×10^{-6} – 1.0×10^{-3} M	5.8×10^{-9} M	9 me. (RSD = 3.4%)		101
Methyl parathion	EAD	GCE/MIS(TEOS,VTES)	Acc. – Det.	SWV	1.0×10^{-8} – 1.0×10^{-5} M	9.0×10^{-9} M	50 me. (RSD < 5%)		109
Naloxone (in urine)	EAD	ITO/MWCNT/PPy@MIS(TEOS,PTEOS)	Acc. – Det.	DPV	0.0 – 12 µM	0.02 µM	4 sensors (RSD = 9.3%)	14 days (92%)	74
Ochratoxin A (in wheat flour)	Drop casting	MIS/PNCs-NGQDs/2D mSiO_2-G	Direct det.	ECL	10^{-5} – 1.0 ng/mL	0.2 pg/mL	15 me (RSD = 1.63%)		242

Table 2. Continued.

Analyte [a]	Film type [b]	Electrode configuration [c] (+ MIS composition)	Detection method		Analytical performance		Stability (%) [f]		Refs.
			Procedure [d]	Technique [e]	Concentration range	Det. limit	Operational	Storage	
p-Nitrophenol	EAD	GCE/CS/PTMOS/AuNPs	Acc. – Det.	DPV	3.0×10^{-8} – 3.5×10^{-4} M	5.0×10^{-9} M	10 me. (RSD = 2- 3%)	10 days (96 %)	114
Paracetamol (in tablets and urine)	Drop-casting	GCE/GO/MIS(TEOS,PTEOS)	Acc. – Det.	DPV	0.1×10^{-6} – 8.0×10^{-5} M	2.0×10^{-8} M	5 me. (RSD = 8.2%)	1 week (93%)	100
L-Phenylalanine (in blood plasma)	LbL-EAD	CE/PANI/β-CD–MWCNT/MIS(TEOS,PTMOS,MTMOS)	Acc. – Det.	DPV	1×10^{-7} – 1.0×10^{-4} M	1.0×10^{-9} M	5 sensors (RSD = 4.1%)	1 month (92,3%)	106
Tetracycline (in water & serum)	Drop-casting	GCE/L-His–MWCNT@PDMS-5/MIS(TEOS,CTAB)	Acc – Det.	DPV	1×10^{-11} – 1×10^{-10} M	2.64×10^{-12} M (in water) & 2.20×10^{-12} M (in serum)			113
Thymidine (in tablets)	LbL-EAD	CE/MWCNT/MIS(TEOS,VTMOS,MTMOS)	Acc. – Det.	DPV	2.0×10^{-6} – 2.2×10^{-5} M	1.6×10^{-9} M	8 me. (RSD = 2.7%)		107

[a] In parentheses are real media used for recovery measurements performed after spiking (but, unless stated otherwise, the analytical performance is given for the analysis of aquous solutions).

[b] Abbreviations for silica film preparation procedures: EAD, electro-assisted deposition; LbL, layer-by-layer.

[c] Abbreviations: MIS, molecularly imprinted silica (in parenthesis, the acronyms of sol-gel precursors used for their synthesis); GCE, glassy carbon electrode; TEOS, tetraethoxysilane; PSS, poly(styrene sulfonate); PVS, poly(vinyl sulfonate); PDDA, poly(diallyldimethyl ammonium); CE, carbon electrode; $Fe_3O_4@SiO_2$, core-shell Fe_3O_4-SiO_2 nanoparticles; MWCNT, multiwall carbon nanotubes; CS, chitosan; PTMOS, phenyltrimethoxysilane; MTMOS, methyltrimethoxysilane; AuNPs, gold nanoparticles; APTES, 3-aminopropyltriethoxysilane; VTMOS, vinyltrimethoxysilane; MPTMS, 3-mercaptopropyltrimethoxysilane; PTEOS, phenyltriethoxysilane; TMOS, tetramethoxysilane; ITO, indium-tin oxide; VTES, vinyltriethoxysilane; PPy, polypyrrole; PNCs, perovskite nanocrystals; NGQDs, N-doped graphene quantum dots; 2D $mSiO_2$-G, graphene supported two-dimensional mesoporous SiO_2 nanosheets; GO, graphene oxide; PANI, polyaniline; β-CD, β-cyclodextrin; L-His, L-Histidine; PDMS, poly(dimethyl siloxane); CTAB, cetyltrimethylammonium bromide.

[d] Abbreviations: Acc., accumulation; Det., detection.

[e] Abbreviations: CV, cyclic voltammetry; DPV, differential pulse voltammetry; A, amperometry; SWV, square wave voltammetry; ECL, electrochemiluminescence.

[f] Expressed as % of remaining response (in parentheses) after a number of measurements (me.) or as RSD (relative standard deviation) for operational stability, or the given period of storage.

Table 3. Electrochemical sensors based on composite electrodes elaborated from continuous ordered mesoporous silica thin films.

Analyte [a]	Film type [b]	Electrode configuration [c]	Detection method		Analytical performance		Stability (%) [f]		Refs.
			Procedure [d]	Technique [e]	Concentration range	Det. limit	Operational	Storage	
Acetaminophen	EISA	AuF/CDG/OMSF	Direct det.	DPV	2×10^{-7} – 5.0×10^{-5} M	1.4×10^{-8} M	10 me. (80%)		115
Acetaminophen Norepinephrine Tryptophan	EASA	GCE/rGO/VMSF	Acc. – Det.	DPV	2×10^{-7} – 1.0×10^{-4} M 1×10^{-7} – 3.0×10^{-5} M 8×10^{-7} – 2.0×10^{-4} M	9.7×10^{-9} M 1.4×10^{-8} M 3.6×10^{-8} M		10 days (98.4%)	121
Ag^{+}	EISA	GCE/(OMSF-SH)	Acc. – Det.	ASDPV	2×10^{-7} – 1.0×10^{-5} M	6×10^{-9} M			116
Ascorbic acid	Stöber	ITO/(VMSF-PANI)	EC	CV	1×10^{-4} – 1.0×10^{-2} M	-			158
Ascorbic acid	Stöber	ITO/(VMSF-NH_2/AuNPs)	EC	DPV	5×10^{-5} – 1.0×10^{-2} M	-			159
Ascorbic acid Cu^{2+}	EASA	Au/(VMSF-GPS-DNAzyme)	Indirect det.	SWV	1.0×10^{-6} – 1.2×10^{-4} M 310 ppb – 4.5 ppm	7.0×10^{-7} M 250 ppb			122
Bisphenol A	Stöber	ITO/(VMSF-PDMS)	Acc. – Det.	DPV	1.0×10^{-6} – 2.0×10^{-5} M & 2.0×10^{-5} M – 1.0×10^{-4} M	2.3×10^{-7} M	10 h - 6 me. (~90%)	5 days (100%)	160
tert-butylhydroquinone	EASA	GCE/ErGO/VMSF	Acc. – Det.	DPV	1×10^{-9} – 5×10^{-7} M & 5×10^{-7} – 1.2×10^{-4} M	2.3×10^{-10} M	20 min (real media)		123
Carbendazim	EASA	GCE/BN-rGO/VMSF	Acc. – Det.	DPV	5×10^{-9} – 7×10^{-6} M	2.3×10^{-9} M			124
Cardiac Troponin I	Stöber	ITO/(VMSF-NH_2-Tro4 Apt)	Aptasensing	EIS	0.05 pg mL^{-1} – 1 ng mL^{-1}	0.05 pg mL^{-1}		7 days (89.4%)	161
				ECL	0.05 pg mL^{-1} – 10 ng mL^{-1}	0.02 pg mL^{-1}		7 days (90.3%)	
Catechol	Stöber	Patterned ITO/(VMSF-$Ru(bpy)_3^{2+}$, DBAE)	Direct det.	ECL	1.0×10^{-5} – 1.0×10^{-3} M	9.52×10^{-6} M			162
Catechol	EASA	AuE/ErGO/(VMSF-CTAB)	Acc. – Det.	DPV	1×10^{-6} – 2.0×10^{-5} M & 2.0×10^{-5} – 6.0×10^{-5} M	1.7×10^{-8} M	12 min (90%)		125
Hydroquinone		AuE/ErGO/VMSF			1×10^{-6} – 6.0×10^{-5} M	1.5×10^{-8} M			
CA15-3	EASA	ITO/(VMSF-GPS-Ab, $Ru(bpy)_3^{2+}$)	Immunosensing	ECL DPV	0.0001 – 100 U mL^{-1} 0.01 – 100 U mL^{-1}	9 µU mL^{-1} 5.4 mU mL^{-1}		15 days (95%)	126

Table 3. Continued.

Analyte [a]	Film type [b]	Electrode configuration [c]	Detection method		Analytical performance		Stability (%) [f]		Refs.
			Procedure [d]	Technique [e]	Concentration range	Det. limit	Operational	Storage	
CEA CA15-3	EASA	ITO/(VMSF-Ru(bpy)$_3^{2+}$)/(VMSF-NH_2)/GluA-Ab	Immunosensing	ECL DPV	0.0001 – 50 ng mL^{-1} 0.005 – 500 U mL^{-1}	0.06 pg mL^{-1} 2.3 mU mL^{-1}			127
Chloramphenicol	Stöber	ITO/(VMSF-CTAB)	Acc. – Det.	DPV	0.1 – 3.7 ppm & 3.7 – 15.0 ppm	37.7 ppb			163
Chloramphenicol	Stöber	ITO/(VMSF-CTAB)	Acc. – Det.	DPV	0.3 – 5.8 ppm & 5.8 – 40 ppm (honey) 0.3 – 5.8 ppm & 5.8 – 32 ppm (milk)	148.4 ppb (honey) 80.6 ppb (milk)			164
Chlorpromazine	EASA	SPCE/ErGO/VMSF	Acc. – Det.	DPV	3×10^{-7} – 2.3×10^{-5} M & 1×10^{-6} – 1×10^{-5} M (blood)	6.1×10^{-9} M 1.6×10^{-8} M			128
Clindamycin	EASA	PET-ITO/(VMSF-Ru(bpy)$_3^{2+}$)	Direct det.	ECL	10 nM – 25 µM & 25 – 70 µM	4 nM			129
Clozapine	EASA	p-SPCE/VMSF	Acc. – Det.	DPV	50 nM – 20 µM	2.8×10^{-8} M			130
C-reactive protein	EASA	SPCE/ErGO/(VMSF-NH_2)/GluA-Ab	Immunosensing	DPV	10 pg mL^{-1} – 100 ng mL^{-1}	8 pg mL^{-1}		7 days (91%)	131
Cu^{2+}	EASA	GCE/(clay + VMSF)	Acc. – Det.	SWV	1×10^{-7} – 1.0×10^{-6} M	-			132
Cu^{2+}	EASA	GCE/(VMSF-NH_2)	Acc. – Det.	ASDPV	1×10^{-8} – 1.0×10^{-6} M	3×10^{-9} M			133
Cysteine	EASA	ITO/(VMSF-Fc)	Mediated EC	A, FIA	3×10^{-6} – 1.0×10^{-4} M	-			134
Diclofenac	EASA	GCE/APTES/(Amino-AT + VMSF)	Acc. – Det.	SWV	3×10^{-7} – 2.0×10^{-5} M	5.3×10^{-8} M	3 me. (95%)		135
DNA	EASA	Au/(VMSF-GPS-DNA ab)	Genosensing	CV	5×10^{-9} – 7.0×10^{-7} M	2.5×10^{-9} M		1 month (93%)	136
Dopamine	Stöber	ITO/(VMSF-Ru(bpy)$_3^{2+}$)	Direct det.	ECL	5 nM – 20 µM	3.5×10^{-9} M		7 days	165
Dopamine Ascorbic acid	EASA	GCE/(VMSF-NMe_3^+)	Acc. – Det.	DPV	2.0×10^{-5} – 2.26×10^{-4} M 4.9×10^{-5} – 2.65×10^{-3} M	9×10^{-6} M 1.1×10^{-5} M			137

Table 3. Continued.

Analyte [a]	Film type [b]	Electrode configuration [c]	Detection method		Analytical performance		Stability (%) [f]		Refs.
			Procedure [d]	Technique [e]	Concentration range	Det. limit	Operational	Storage	
Doxorubicin	EASA	GCE/ErGO/VMSF	Acc. – Det.	DPV	1×10^{-9} – 2.0×10^{-5} M	7.7×10^{-10} M	24 min (97%)		138
F^-	Stöber	ITO/(VMSF-PBA)	Indirect det.	DPV	1×10^{-9} – 2.3×10^{-2} M	8.3×10^{-10} M	2 h	2 months	166
Glucose	Stöber	FTO/(VMSF-NiO(OH))	EC	A	1.0×10^{-5} – 1.2×10^{-2} M	4.4×10^{-7} M			167
Guanine	EASA	ITO/(VMSF-$Ru(bpy)_3^{2+}$)	EC	CV	2×10^{-7} – 5.0×10^{-4} M	5.8×10^{-8} M			139
Hg^{2+}	IA-MS-clay	GCE/(PCH-SH)	Acc. – Det.	ASSWV	5×10^{-8} – 1.0×10^{-6} M	2.4×10^{-8} M			117
Hg^{2+}	EISA	GCE/(OMSF-MTTZ)	Acc. – Det.	ASSWV	5×10^{-8} – 1.0×10^{-6} M	2.4×10^{-8} M			118
Hg^{2+}	Stöber	ITO/(VMSF-GQDs)	Acc. – Det.	ASDPV	10 pM – 1.0 nM & 1.0 nM – 0.5 µM	9.8 pM			181
Cu^{2+}				ASDPV	10 pM – 1.0 nM & 1.0 nM – 1.5 µM	8.3 pM			
Cd^{2+}				ASDPV	20 nM – 1.0 µM & 1.0 µM – 20 µM	4.3 nM			
Dopamine	EASA	AuE/(VMSF-GQDs)		DPV	200 nM – 20 µM & 20 – 100 µM	120 nM			
Hydrogen peroxide	EASA	ITO/(VMSF-PB wires)	Mediated EC	CV	1×10^{-4} – 1×10^{-2} M				140
Hydrogen peroxide	EASA	ITO/(VMSF-$Fe(Htrz)_3$)	Mediated EC	A, FIA	5×10^{-6} – 3.0×10^{-4} M	2×10^{-6} M			141
Hydrogen peroxide	Stöber	ITO/(VMSF-PANI/PtNPs)	EC	A	1.0×10^{-6} – 2.0×10^{-3} M	2.4×10^{-7} M			168
Hydrogen peroxide	Stöber	ITO/(VMSF, luminol)	Direct det.	ECL	5×10^{-6} – 1×10^{-3} M	5×10^{-6} M			169
Hydrogen peroxide	Stöber	ITO/(VMSF-NMe_3^+-AuNPS, luminol)	Direct det.	ECL	1×10^{-7} – 2.0×10^{-4} M	2.53×10^{-8} M			170
Hydrogen peroxide	Stöber	ITO/(VMSF-PtNS)	EC	A	1×10^{-5} – 5.0×10^{-3} M	-	50 min (100%)		182
	EASA	CFME/(VMSF-PtNS)			5×10^{-4} – 2.0×10^{-3} M	-	90 min (in brain)		

Table 3. Continued.

Analyte [a]	Film type [b]	Electrode configuration [c]	Detection method		Analytical performance		Stability (%) [f]		Refs.
			Procedure [d]	Technique [e]	Concentration range	Det. limit	Operational	Storage	
Imidacloprid	EASA	GCE/ErGO/VMSF	Acc. – Det.	CV	1.0 μg mL^{-1} – 50 μg mL^{-1} & 50 μg mL^{-1} – 400 μg mL^{-1}	0.3 μg mL^{-1}		5 days (94%)	142
Insulin	EASA	GCE/APTES/(VMSF-NH_2)/GluA-cDNA-Apt.	Aptasensing	DPV	1.0×10^{-8} – 3.5×10^{-7} M	3.0×10^{-9} M	5 me.		143
Isoproturon	EASA	GCE/APTES/VMSF	EO amplif.	SWV	1.0×10^{-5} – 1.0×10^{-4} M	-			144
Lidocaine	EASA	FTO/(VMSF-Ru$(bpy)_3^{2+}$)	Direct det.	ECL	1.0×10^{-8} – 5.0×10^{-5} M	8×10^{-9} M			145
Matrine	Stöber	P-μchip/ITO/(VMSF-Ru$(bpy)_3^{2+}$)	Direct det.	ECL	1×10^{-7} – 5.0×10^{-5} M	4.02×10^{-9} M			171
Metoprolol					1×10^{-7} – 1.0×10^{-4} M	11.4×10^{-9} M			
Chlorphenamine					1×10^{-7} – 1.0×10^{-4} M	9.05×10^{-9} M			
Lincomycin					1×10^{-7} – 1.0×10^{-4} M	4.01×10^{-9} M			
Levosulpiride					1×10^{-7} – 2.5×10^{-5} M	3.04×10^{-9} M			
Sophoridine					1×10^{-7} – 4.0×10^{-5} M	1.80×10^{-9} M			
Sophocarpine					1×10^{-7} – 5.0×10^{-5} M	2.70×10^{-9} M			
Methidazine	EASA	3DG/VMSF	Acc. – EC Det.	DPV	5.0×10^{-8} – 1×10^{-5} M	3.0×10^{-8} M	5 me.		146
Nicotine	Stöber	ITO/(VMSF-Ru$(bpy)_3^{2+}$)	Direct det.	ECL	1×10^{-7} – 1.5×10^{-5} M	2.78×10^{-8} M			172
Nitrate	EASA	ITO/(VMSF-Fc)	Indirect det.	IC-A	2.0×10^{-5} – 1.0×10^{-4} M	1.6×10^{-5} M			147
Fluoride					5×10^{-6} – 5.0×10^{-5} M	3×10^{-6} M			
Chloride					5×10^{-6} – 5.0×10^{-5} M	4×10^{-6} M			
Bromide					1.0×10^{-5} – 7.5×10^{-5} M	1.0×10^{-5} M			
Phosphate					2.0×10^{-5} – 1.0×10^{-4} M	1.2×10^{-5} M			
Sulfate					1.5×10^{-5} – 1.0×10^{-4} M	1.0×10^{-5} M			
p-NCB	Stöber	ITO/(VMSF-CTAB)	Acc. – Det.	DPV	6 – 302 ppb & 302 – 1500 ppb	5.52 ppb			173
m-NCB					5 – 147 ppb & 147 – 1000 ppb	0.98 ppb			
p-NBB					8 – 136 ppb & 136 – 1000 ppb	3.55 ppb			
DNBB					6 – 259 ppb & 259 – 2000 ppb	4.23 ppb			

Table 3. Continued.

Analyte [a]	Film type [b]	Electrode configuration [c]	Detection method		Analytical performance		Stability (%) [f]		Refs.
			Procedure [d]	Technique [e]	Concentration range	Det. limit	Operational	Storage	
Paraoxon Methyl parathion Fenitrothion	Stöber	ITO/(VMSF-PDMS)	Acc. – Det.	DPV	5 – 1000 ppb 5 – 1000 ppb 50 – 600 & 600 – 2000 ppb	1.83 ppb 2.59 ppb 17.2 ppb			174
Paraoxon Methyl parathion Fenitrothion	Stöber	ITO/(VMSF-CTAB)	Acc. – Det.	DPV	5 – 385 ppb & 385 – 2000 ppb 5 – 136 ppb & 136 – 1000 ppb 400 – 7000 ppb	3.53 ppb 3.01 ppb 114.86 ppb			175
Paraquat	EASA	GCE/APTES/VMSF	Acc. – Det.	SWV	1.0×10^{-8} – 1.0×10^{-5} M	4×10^{-9} M			148
Paraquat	EASA	GCE/3DG-CNT/VMSF	Acc. – Det.	DPV	2×10^{-9} – 1.0×10^{-8} M & 1.0×10^{-8} – 1.0×10^{-5} M	1.17×10^{-9} M		5 days (93%)	149
Pb^{2+}	Spin-coating	Au/(OMSF-SH)	Acc. – Det.	SWV	250 – 5000 ppb & 25 – 100 ppb	250 ppb & 25 ppb			119
pH	Stöber	ITO/(VMSF-i-motif DNA)	Direct det.	DPV	pH 5 – 8	-			176
PSA	EASA	ITO/(VMSF-NH_2)/GluA-Ab)	Immunosensing	DPV	10 pg mL^{-1} – 1 µg mL^{-1}	8.1 pg mL^{-1}		6 days (91.5%)	150
PSA	EASA	ITO/VMSF/GPS-Ab	Immunosensing	ECL	1 pg mL^{-1} – 100 ng mL^{-1}	0.1 pg mL^{-1}		15 days (97.2%)	151
PSA	EASA	Au/(VMSF-GPS-PSA Apt.)	Aptasensing	DPV	1 – 300 ng mL^{-1}	0.28 ng mL^{-1}		30 days (97%)	152
Retinol Trolox	Stöber	ITO/(VMSF-CTAB)	Acc. – Det.	DPV	1×10^{-6} – 6.0×10^{-5} M 1×10^{-6} – 1.0×10^{-4} M	6.5×10^{-7} M 2.9×10^{-7} M			177
Rutin	EASA	GCE/ErGO/VMSF	Acc. – Det.	DPV	3×10^{-7} – 2×10^{-6} M & 2×10^{-6} – 4.0×10^{-5} M	2.3×10^{-9} M	10 min (95%)		153

Table 3. Continued.

Analyte [a]	Film type [b]	Electrode configuration [c]	Detection method		Analytical performance		Stability (%) [f]		Refs.
			Procedure [d]	Technique [e]	Concentration range	Det. limit	Operational	Storage	
Serotonin	EASA	ITO/ErGO-CNT/VMSF	Direct det.	DPV	1×10^{-7} – 1.0×10^{-5} M 1.0×10^{-5} – 3.0×10^{-5} M	5.4×10^{-9} M			164
Melatonin					1×10^{-6} – 2.0×10^{-5} M 2.0×10^{-5} – 1.0×10^{-4} M	1.41×10^{-8} M			
TMB	Stöber	ITO/(VMSF-CTAB)	Direct det.	DPV	1×10^{-7} – 1.0×10^{-5} M	1.7×10^{-8} M	'pretty good'		178
K^+	Stöber	ITO/(VMSF-CTAB) (+TMB and G4zyme in solution)	Indirect det. (TMB responsive)	DPV	10^{-6} – 10^{-5} M & 10^{-5} – 10^{-3} M	9.3×10^{-7} M			178
ATP					10^{-5} – 1.5×10^{-3} M	9.6×10^{-6} M			
Thrombin					10^{-7} – 10^{-6} M	9.8×10^{-8} M			
DNA					5×10^{-10} – 5×10^{-8} M	3.98×10^{-10} M			
TNT	Stöber	ITO/(VMSF-Ru(bpy)$_3^{2+}$)	Direct det.	ECL	10^{-7} – 10^{-3} mg/mL	2.3×10^{-9} mg/mL			179
TNT	Stöber	ITO/(VMSF-CTAB)	Acc. – Det.	DPV	10 – 1000 ppb	4.97 ppb			175
DNT					10 – 1000 ppb	5.87 ppb			
TNP					2 – 80 ppb	1.46 ppb			
NP					40 – 2000 ppb	12.90 ppb			
NB					10 – 3000 ppb	14.28 ppb			
2,4,6-trichlorophenol	EASA	3DG/VMSF	Acc. – EC Det.	DPV	1.0×10^{-8} – 1×10^{-7} M & 1×10^{-7} – 1.5×10^{-5} M	2.4×10^{-9} M	5 me.		155
Tri-*n*-propylamine	Stöber	ITO/(VMSF-Ru(bpy)$_3^{2+}$)	Direct det.	ECL	0.5 nM – 15.8 µM & 15.8 – 150 µM	0.17 nM			180
Nicotine					0.565 – 75.1 µM & 75.1 – 500 µM	565 nM			
Atropine					0.2 – 82.9 µM & 82.9 – 500 µM	85 nM			
L-Tryptophan	EISA	ITO/(Trp-MI-OMSF-NH_2)	Acc. – Det.	DPV	2×10^{-4} – 4.0×10^{-3} M	1.06×10^{-4} M			120
D-Tryptophan					2×10^{-4} – 4.0×10^{-3} M	1.27×10^{-4} M			

Table 3. Continued.

Analyte [a]	Film type [b]	Electrode configuration [c]	Detection method		Analytical performance		Stability (%) [f]		Refs.
			Procedure [d]	Technique [e]	Concentration range	Det. limit	Operational	Storage	
Uric acid	EASA	pl-3DG/VMSF	Direct det.	DPV	100 nM – 30 μM & 30 – 150 μM	2.3×10^{-8} M			156
Uric acid	EASA	SPCE/ErGO/(VMSF-NH_2)	Direct det.	DPV	5×10^{-7} – 1.80×10^{-4} M	1.29×10^{-7} M		7 days (97.1%)	157

[a] Abbreviations: CA15-3, cancer antigen 15-3; CEA, carcino-embryonic antigen; DNA, deoxyribonucleic acid; *p*-NCB, 1-chloro-4-nitrobenzene; *m*-NCB, 1-chloro-3-nitrobenzene; *p*-NBB, 1-bromo-4-nitrobenzene; DNBB, 2,4-dinitrobromobenzene; PSA, prostate specific antigen; TMB, 3,3',5,5'-tetramethylbenzidine; ATP, adenosine 5'-triphosphate; TNT, 2,4,6-trinitrotuluene; DNT, 2,6-dinitrotuluene; TNP, 2,4,6-trinitrophenol; NP, 3-nitrophenol; NB, nitrobenzene.

[b] Abbreviations for ordered mesoporous film preparation procedures: EISA, evaporation-induced self-assembly; EASA, electrochemically assisted self-assembly; Stöber, Stöber growth method; IA-MS-clay, intragallery assembly of mesoporous organosilica in smectite clay.

[c] Abbreviations: AuF, gold film; CDG, β-cyclodextrin-graphene; OMSF, ordered mesoporous silica film; VMSF, vertically-oriented mesoporous silica film; GCE, glassy carbon electrode; rGO, reduced graphene oxide; VMSF-SH, thiol-functionalized vertically-oriented mesoporous silica film; ITO, indium-tin oxide; PANI, polyaniline; VMSF-NH_2, amine-functionalized vertically-oriented mesoporous silica film; AuNPs, gold nanoparticles; GPS, (3-glycidopropyl) trimethoxysilane; DNAzyme, deoxyribozyme; PDMS, polydimethylsiloxane; ErGO, electrochemically reduced graphene oxide; BN-rGO, boron nitride-reduced graphene oxide; Tro4 Apt, aminated troponin aptamer; $Ru(bpy)_3^{2+}$, tris(2,2'-bipyridyl)ruthenium(II); DBAE, *N*,*N*-dibutylethanolamine; AuE, gold electrode; CTAB, cetyltrimethylammonium bromide; Ab, antibody; GluA, glutaraldehyde; SPCE, screen-printed carbon electrode; PET-ITO, polyethyleneterephthalate coated with indium-tin oxide; p-SPCE, electrochemically pretreated screen-printed electrode; Fc, ferrocene; APTES, aminopropyl-triethoxysilane; Amino-AT, amino-attapulgite; VMSF-NMe_3^+, trimethylammonium-functionalized vertically-oriented mesoporous silica film; PBA, phenylboronic acid; FTO, fluorine-doped tin oxide; PCH-SH, thiol-functionalized porous clay heterostructure; MTTZ, 5-mercapto-1-methyl-1-H-tetrazole; PB, Prussian Blue; $Fe(Htrz)_3$, iron-triazole coordination polymer (Htrz=1,2,4,- 1H-triazole); GQDs, graphene quantum dots; PtNPs, platinum nanoparticles; PtNS, platinum nanostructure; CFME, carbon fiber microelectrode; cDNA, complementary DNA oligonucleotide; Apt., aptamer; P-μchip, paper microchip; 3DG, 3D graphene; 3DG-CNT, 3D graphene-carbon nanotube assemblies; PSA Apt., prostate specific antigen aptamer; TMB, 3,3',5,5'-tetramethylbenzidine; G4zyme, G-quadruplex/hemin DNAzyme; Trp-MI, molecularly imprinted tryptophan; pl-3DG, plasma-treated 3D graphene.

[d] Abbreviations: Det., detection; Acc., accumulation; EC, electrocatalysis; EO amplif., electro-oligomerisation signal amplification.

[e] Abbreviations: DPV, differential pulse voltammetry; ASDPV, anodic stripping differential pulse voltammetry; CV, cyclic voltammetry; EIS, electrochemical impedance spectroscopy; ECL, electrochemiluminescence; SWV, square wave voltammetry; A, amperometry; FIA, Flow injection analysis; ASSWV, anodic stripping square wave voltammetry; IC-A, ion chromatography with amperometric detection.

[f] Expressed as % of remaining response (in parentheses) after a number of measurements (me.) or minutes/hours (min/h) of use (operational stability), or the given period of storage.

Table 4. Electrochemical sensors based on biocomposite electrodes elaborated from silica thin films and biomolecules.

Analyte [a]	Film type [b]	Electrode configuration [c]	Detection method		Analytical performance		Stability (%) [f]		Refs.
			Procedure [d]	Technique [e]	Concentration range	Det. limit	Operational	Storage	
AFB1 (in bee pollen)	Drop-casting	GCE/SiO_2-IL/AFB1 AB	Immunosensor Acc. – Det.	EIS	0.1 – 10 ng mL^{-1}	0.01 ng mL^{-1}	6 me. (RSD = 1.6%)	180 days (95%)	218
BCR/ABL (in human serum)	EAD	GE/SiO_2-luminol/AuNP/Fc-MB	Genosensor Acc. – Det.	ECL	1.0×10^{-15} – 1.0×10^{-9} M	4.6×10^{-16}	100 me. (RSD = 1.15%)		251
Choline (in food and blood serum)	EAD	SPCE/SiO_2-ChOx	EC	A	1.60 – 65.50 mg L^{-1}	1.0 mg L^{-1}		3 weeks (93%)	221
Choline	Drop-casting	SPCE/Polyluminol/SiO_2-Nafion-ChOx	EC	ECL	4×10^{-7} – 1.3×10^{-4} M				247
D-sorbitol (in food and cosmetics)	LbL-ED-EAD	SPCE/MWCNT/SiO_2-DSDH	EC	A	0.5×10^{-3} – 3.5×10^{-3} M	0.16×10^{-3} M		1 month (90%)	37
D-sorbitol	LbL-EAD	GCE/MWCNT-Os/SiO_2-PEI-DI-DSDH-NADGPS	EC	A	0.4 – 2.8 mM				211
D-sorbitol	LbL-EAD	GCE/(MWCNT+CS)-PMG/SiO_2-DSDH-NADGPS	EC	A	0.1 – 1.0 mM	0.11 mM			223
D-sorbitol D-glucose Lactic acid	Drop-casting	GCE/SiO_2-(DSDH+DI)-(PEI-Fc)-(NADGPS)	EC	CV, A			12 h		217
Ethanol	Drop-casting	GCE/SiO_2-PVA4VP-Nafion-$Ru(bpy)_3^{2+}$-ADH	Direct det.	ECL	2.5×10^{-5} – 5.0×10^{-2} M	1.0×10^{-5} M	15 me. (RSD < 5%)	1 week (70%)s	244
Ethanol	Drop-casting	GCE/SiO_2-CS-PSS-$Ru(bpy)_3^{2+}$-ADH	Direct det.	ECL	2.79×10^{-5} – 5.78×10^{-2} M	9.3×10^{-6} M	100 me. (RSD = 7%)	10 days	245
Ethanol	Immersion	Au/PSSG/AuNP/$Ru(bpy)_3^{2+}$/ADH	EC	ECL	5.0×10^{-6} – 5.2×10^{-3} M	12×10^{-9} M	10 me. (RSD = 0.6%)	1 week (85%)	246
NADH		Au/PSSG/AuNP/$Ru(bpy)_3^{2+}$			2.5×10^{-9} – 5.9×10^{-4} M	1×10^{-9} M			

Table 4. Continued.

Analyte [a]	Film type [b]	Electrode configuration [c]	Detection method		Analytical performance		Stability (%) [f]		Refs.
			Procedure [d]	Technique [e]	Concentration range	Det. limit	Operational	Storage	
Glucose	Spreading	CSPE/SiO_2-PVA/GOx	EC	A	$0 - 4.13\times10^{-3}$ M	9.8×10^{-6} M			77
Glucose	EAD	Au or (Ptnano/Au)/GOx-APTES-CS	EC	A	$0.2\times10^{-6} - 8.2\times10^{-3}$ M	0.2×10^{-6} M	10 me. (RSD = 2%)	6 month	51
Glucose (in juice, serum blood)	EAD	Au/SiO_2-Hb-GOx-AuNP	EC	CV	$1.5\times10^{-5} - 2.0\times10^{-4}$ M	8.0×10^{-6} M	10 me. (85%)	3 weeks (95%)	226
Glucose	Drop-casting and spreading	ITO/$Ru(bpy)_3^{2+}$/SiO_2/GDH/ Resydrol	Direct det.	ECL	$2.5\times10^{-5} - 2.0\times10^{-4}$ M	0.5×10^{-6}M			243
H_2O_2	Drop-casting	GCE/HAp/SiO_2/HRP	EC	A	$1\times10^{-6} - 1.0\times10^{-6}$ M	0.35×10^{-6} M	2 h (96%)	2 weeks (95%)	229
H_2O_2	LbL-drop-casting	ITO/AuNP+SiO_2/RGO-CD/HRP-ADA	EC	CV	0.25 – 1.0 mM				224
H_2O_2	Casting	CPE/DTAB/PANI-SiO_2/Hb	EC	CV	$0.09\times10^{-3} - 2.8\times10^{-3}$ M	0.03×10^{-3} M			216
H_2O_2	EAD	CE/SiO_2-Hb	EC	CV	0.034 – 0.14 mg L^{-1}	0.017 mg L^{-1}			40
H_2O_2 Nitrite	LbL-Spreading	GCE/RTIL-sol-gel/GNRs@SiO_2-Mb	EC	CV	$0.2\times10^{-6} - 1.8\times10^{-4}$ M $0.04\times10^{-3} - 5.0\times10^{-3}$ M	0.12×10^{-6} M 0.02×10^{-3}M		21 days (93%)	219
Lysozyme Adenosine K^+	Stöber and drop-casting	ITO/MSFs@Ru-Aptamer	Aptasensor Acc. – Det.	ECL	1 – 100 µM 1 nM – 10 µM 0.1 nM – 1 µM	0.06 nM 0.75 nM 0.5 µM	5 me. (RSD = 5.95%)		222
Maltose (in food)	EAD	SPCE/SiO_2+CuO/GOx+Malt	EC	CV	$1.0\times10^{-5} - 1.0\times10^{-4}$ M	5.0×10^{-6} M	15 me. (RSD = 2 %)		214
O_2 (in tap water) Rimantadine	EAD	PGE/SiO_2-AuNP/Hb	EC EC-Inh	CV	0.5 – 9.0 mg L^{-1} 0.5 – 2.0 mg L^{-1}	0.12 mg L^{-1} 0.30 mg L^{-1}	30 scans (85%)		212

Table 4. Continued.

Analyte [a]	Film type [b]	Electrode configuration [c]	Detection method		Analytical performance		Stability (%) [f]		Refs.
			Procedure [d]	Technique [e]	Concentration range	Det. limit	Operational	Storage	
SKBR-3 cells	EAD/dip-coating	GCE/mesop. SiO_2/CS-luminol/HER-2 AB	Immunosensor Acc. – Det.	ECL	20 – 2000 cells mL^{-1}	20 cells mL^{-1}	5 me. (RSD = 1.6%)		250
Sucrose (in food)	LbL-EAD	SPCE/MnO_2/SiO_2/GOx+Inv	EC	CV	0.017 – 0.342 mg mL^{-1}	0.006 mg mL^{-1}	4 me. (RSD = 4%)	1 month	213

[a] Abbreviations: AFB1, Aflatoxin B1; BCR/ABL, mutated breakpoint cluster region protein; SKBR-3 cells, metastasic breast cancer cells.

[b] Abbreviations for biocomposite silica-based film preparation procedures: EAD, electrochemically assisted electrodeposition; LbL, layer-by-layer; ED, electrophertic deposition; Stöber, Stöber growth method.

[c] Abbreviations: GCE, glassy carbon electrode; IL, ionic liquid; AFB1 AB, Aflatoxin B1 antibody; GE, graphite electrode; AuNP, gold nanoparticle; Fc-MB, ferrocene-labeled molecular beacon; SPCE, screen printed carbon electrode; ChOx, choline oxidase; MWCNT, multiwall carbon nanotubes; DSDH, D-sorbitol dehydrogenase; MWCNT-Os, multiwall carbon nanotubes wrapped with a Osmium polymer; PEI, poly(ethylene imine); DI, diaphorase; NADGPS, nicotinamide adenine dinucleotide covalently bonded to glycidopropyl-silane; CS, chitosan; PMG, poly(methylene green); PEI-Fc, ferrocene-functionalized poly(ethylene imine); PVA4VP, poly(vinyl alcohol – 4-vinylpyridine); ADH, alcohol dehydrogenase; PSS, poly(styrene sulfonate); PSSG, partial sulfonated (3-mercaptopropyl)-trimethoxysilane sol–gel; CSPE, carbon screen-printed electrode; PVA, poly(vinyl alcohol); GOx, glucose oxidase; APTES, 3-aminopropyltriethoxysilane; Hb, haemoglobin; ITO, indium tin oxide; GDH, glucose dehydrogenase; Hap, hydroxyapatite; HRP, horseradish peroxidase; RGO-CD, reduced graphene oxide nanosheets with cyclodextrine; ADA, adamantane carboxylic acid; CPE, carbon paste electrode; DTAB, dodecyltrimethylammonium bromide; PANI, polyanaline; CE, carbon electrode; RTIL, room temperature ionic liquid; GNRs@SiO_2, silica coated gold nanorods; Mb, myoglobin; MSFs@Ru-Aptamer, mesoporous silica film loaded with $Ru(bpy)_3^{2+}$ and caped with aptamer; Malt, maltase; mesop. SiO_2, mesoporous silica; HER-2 AB, human epidermal growth factor receptor 2 antobody; PGE, pyrolitic graphite electrode; Inv, invertase.

[d] Abbreviations: Acc., accumulation; Det., detection; EC, electrocatalysis; Inh, inhibition.

[e] Abbreviations: EIS, electrochemical impedance spectroscopy; ECL, electrochemiluminescence; A, amperometry; CV, cyclic voltammetry.

[f] Expressed as % of remaining response (in parentheses) after a number of measurements (me.) or minutes/hours (min/h) of use (operational stability) or as RSD (relative standard deviation), or the given period of storage.

Figure captions

Figure 1. (**A**) Schematic illustration of the various coating methods applied to deposit sol-gel-derived silica layers on electrode surfaces. (**B**) The various ways to modify these layers in the form of hybrids and composites: (a) co-condensation route to organic-inorganic hybrids; (b) entrapment of biomolecules, nano-objects, or as interpenetrated silica-organic polymer; (c) the template route to nanostructuration and functionalization of the mesoporous films.

Figure 2. (**A**) Vertically oriented mesoporous silica films prepared by electrochemically assisted self-assembly (EASA): (a) schematic illustration of the EASA process; (b) TEM images of the ordered and oriented mesoporous silica film (b_1 top view with electron diffraction pattern as inset; b_2 cross-section, *reproduced with permission from ref. [60], Copyright 2007 Nature Publishing Group*); (c) Typical GI-XD pattern confirming the hexagonal packing of vertically aligned mesopore channels (*reproduced from ref. [61], Copyright 2009, with permission from American Chemical Society*); (d) FE-SEM micrograph obtained for a film generated by EASA on ITO electrode (the inset is an enlargement of the cross-sectional view obtained after vertical cleaving of the sample, *reproduced from ref. [60], Copyright 2007, with permission from Nature Publishing Group*); (e) TEM micrographs of electrogenerated multilayer mesoporous thin films prepared by sequential EASA (bottom: cross-section views of a four-layer film: top: a magnified view at the intersection between two electrodeposited layers in which white dashed lines represent the interlayer domain and the red ones illustrate the pore orientation maintained in both sides of the interface; arrows indicate silica wall and channel, *reproduced from G. Giordano et al., Electrochim. Acta 2017, 237, 227-236, Copyright 2017, with permission from Elsevier*); (f) an illustration of the electron hopping charge

transfer mechanism in a ferrocene-functionalized silica nanochannel (*reproduced from ref. [36], Copyright 2021, with permission from Elsevier*). (**B**) Silica nanochannel membranes generated by the Stöber solution spontaneous growth method: (a) schematic illustration of the process; (b-e) TEM images of the films deposited on glass ((b,c) cross-sections, (d,e) top-views, with insets in (c) and (e) representing the structural models of the cross-section and surface of the mesoporous silica film, respectively, *reproduced from ref. [66], Copyright 2012, with permission from Wiley-VCH Verlag*).

Figure 3. (**A**) Illustration of the various ways to deposit molecularly imprinted silica (MIS) films on electrodes (*reproduced from ref. [96], Copyright 2022, with permission from Elsevier*). (**B**) Schematic representation of the molecularly imprinted electrochemical sensor constructed for the detection of chlorogenic acid (CGA) by deposition of a molecularly imprinted silica (MIS) film a gold electrode surface pre-treated with (3-mercaptopropyl)trimethoxysilane (MPTMS); MIS was obtained by the sol-gel process from a solution constituted by tetraethoxysilane (TEOS), phenyltriethoxysilane (PTEOS), 3-(aminopropyl)trimethoxysilane (APTMS) and CGA (*reproduced from ref. [102], Copyright 2011, with permission from Elsevier*). (**C**) Schematic representation of the preparation a MIS sensor for L-phenylalanine based on a carbon electrode covered with a polyaniline (PAN) layer subsequently modified with β-cyclodextrin (β-CD)-incorporated multi-walled carbon nanotube (MWNT), and overcoated with an imprinted silica sol-gel film entrapping the target analyte (*reproduced from ref. [106], Copyright 2011, with permission from Elsevier*). (**D**) Left: illustration the fabrication of a molecularly imprinting sol-gel hybrid film on glassy carbon electrode (GCE) by the one-step electrodeposition of chitosan (CS), phenyltrimethoxysilane (PTMS), *in situ* formed gold nanoparticles (AuNPs) and template *p*-nitrophenol (*p*-NP). Right: selectivity revealed by differential pulse voltammetry responses of four nitrophenols (*p*-NP, *o*-NP, *m*-NP, and 2,3-diF-*o*-NP), measured with the

imprinted (black bars) and non-imprinted (gray bars) hybrid film modified GCEs at the individual characteristic oxidation potentials in their reduced states (*Reprinted from ref. [114], Copyright (2013), with permission from The Royal Society of Chemistry*).

Figure 4. Illustration of the various electrochemical sensing applications involving composite electrodes elaborated from continuous ordered mesoporous silica thin films, respectively with filled pores, open pores and functionalized pores.

Figure 5. (**A**) Planar screen-printed electrode configuration (three-electrode cell) and (**B**) schematic view of its modification with a silica biocomposite film (*reproduced from ref. [221], Copyright 2012, with permission from Wiley-VCH Verlag*). (**C**, **D**) Schemes of biocomposite films on electrode, with either (**C**) only the protein (Enzyme) or (**D**) or both the protein and nanoparticles (NP) encapsulated inside the silica matrix. (**E**) AFM images of the surface of glassy carbon electrode, respectively (a) before and (b, c) after modification with (b) SiO_2 and (c) SiO_2-Hb (c) biocomposite film (*reproduced from ref. [40], Copyright 2007, with permission from Elsevier*).

Figure 6. (**A**) Schematic illustration of (A_1) the preparation of aptamer-capped $Ru(bpy)_3^{2+}$-loaded mesoporous silica films (MSFs) modified ITO electrode (Apt-Ru@MSFs/ITO) and (A_2) Apt-Ru@MSFs/ITO-assisted ECL aptasensor platform for target detection (*reproduced from ref. [222], Copyright 2016, with permission from American Chemical Society*). (**B**) Detection of the dehydrogenase enzymatic substrate: (B_1) illustration of the electrochemical pathway used for the co-immobilization of D-sorbitol dehydrogenase (DSDH) and diaphorase (DI) enzymes with ferrocene-functionalized poly(ethylene imine) (PEI-Fc) and the covalently attached cofactor NAD^+ with the aid of glycidopropyl trimethoxysilane (GPS); (B_2) Amperometric responses obtained at an applied potential of 0.4V using GCE/(TEOS+GPS)/(DSDH+DI)/NAD-GPS/PEI-Fc (*i.e.*, with GPS) and

GCE/(TEOS)/(DSDH+DI)/NAD^+/PEI-Fc (*i.e.*, without GPS); measurements have been performed for 14 h oxidation under convective conditions in 0.1 M Tris–HCl buffer (pH 9) containing 2 mM D-sorbitol (*reproduced from ref. [217], Copyright 2012, with permission from Elsevier*). (**C**) Illustration of the main approaches used for electrode modification with silica-based biocomposite films: (a) one-step entrapment of proteins and nanoparticles, (b) two-step modification by formation of a porous silica film and subsequent binding of biological nano-obects, and (c) electrodeposition of a first nanoparticles layer covered with silica biocomposite film. (**D**) Bioelectrocatalytic detection of H_2O_2 and nitrite: (D_1) scheme of GCE modification with silica-coated gold nanorods (GNRs@SiO_2), myoglobin and ionic liquid (RTIL); (D_2) CVs of the modified electrode in the presence of H_2O_2 at different concentration ((a) 0, (b) 113.1 μM, and (c) 346.5 μM); (D_3) linear plot of catalytic current (i_{cat}) *vs.* H_2O_2 concentration (*reproduced from ref. [219], Copyright 2009, with permission from Elsevier*).

Figure 7. (**A**) Schematic illustration of ECL oxidative-reduction mechanism of $Ru(bpy)_3^{2+}$ molecule and TPrA (*reproduced with permission from C. Venkateswara Raju, M. Sornambigai, S. Senthil Kumar, IntechOpen, 2022, doi:10.5772/intechopen.96819*). (**B**) Schematic illustration of (B_1) the fabrication and application of a MIP-ECL sensor for Ochratoxin A (OTA) and (B_2) the proposed self-enhanced ECL mechanism; the self-enhanced superstructures was constructed by successively loading N-doped graphene quantum dot (NGQDs) and $CsPbBr_3$ perovskite nanocrystals (PNCs) onto graphene supported two-dimensional mesoporous SiO_2 nanosheets (2D mSiO_2-G) prepared from TEOS and CTAB, and subsequently depositing a molecularly imprinted overlayer with high affinity for OTA (*reproduced from ref. [242], Copyright 2022, with permission from Elsevier).*

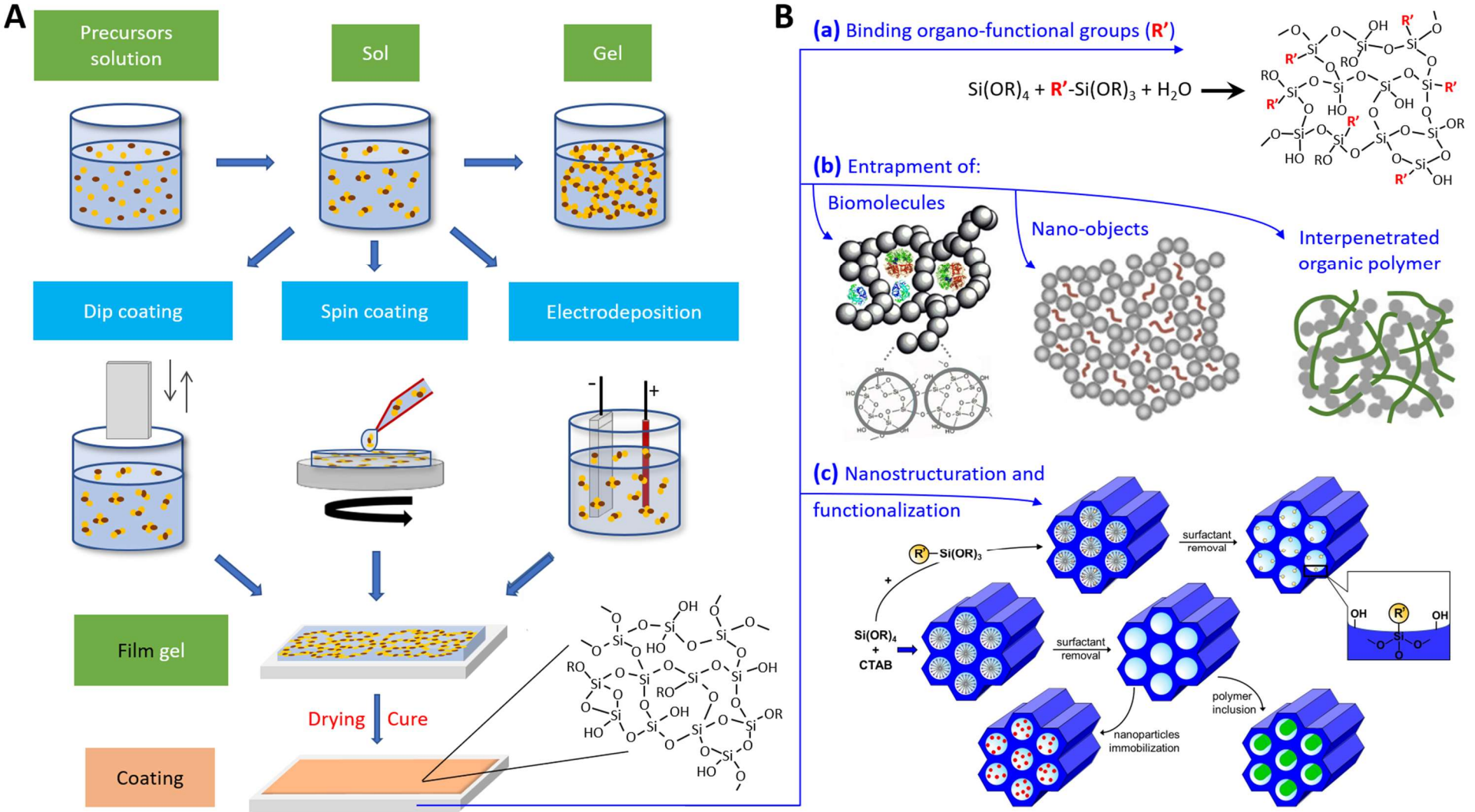
A
Precursors solution
Sol
Gel
Dip coating
Spin coating
Electrodeposition
Film gel
Drying
Cure
Coating
B
(a) Binding organo-functional groups (R')
Si(OR)4 + R'-Si(OR)3 + H2O
(b) Entrapment of:
Biomolecules
Nano-objects
Interpenetrated organic polymer
(c) Nanostructuration and functionalization
surfactant removal
Si(OR)4 + CTAB
polymer inclusion
nanoparticles immobilization

Figure 1

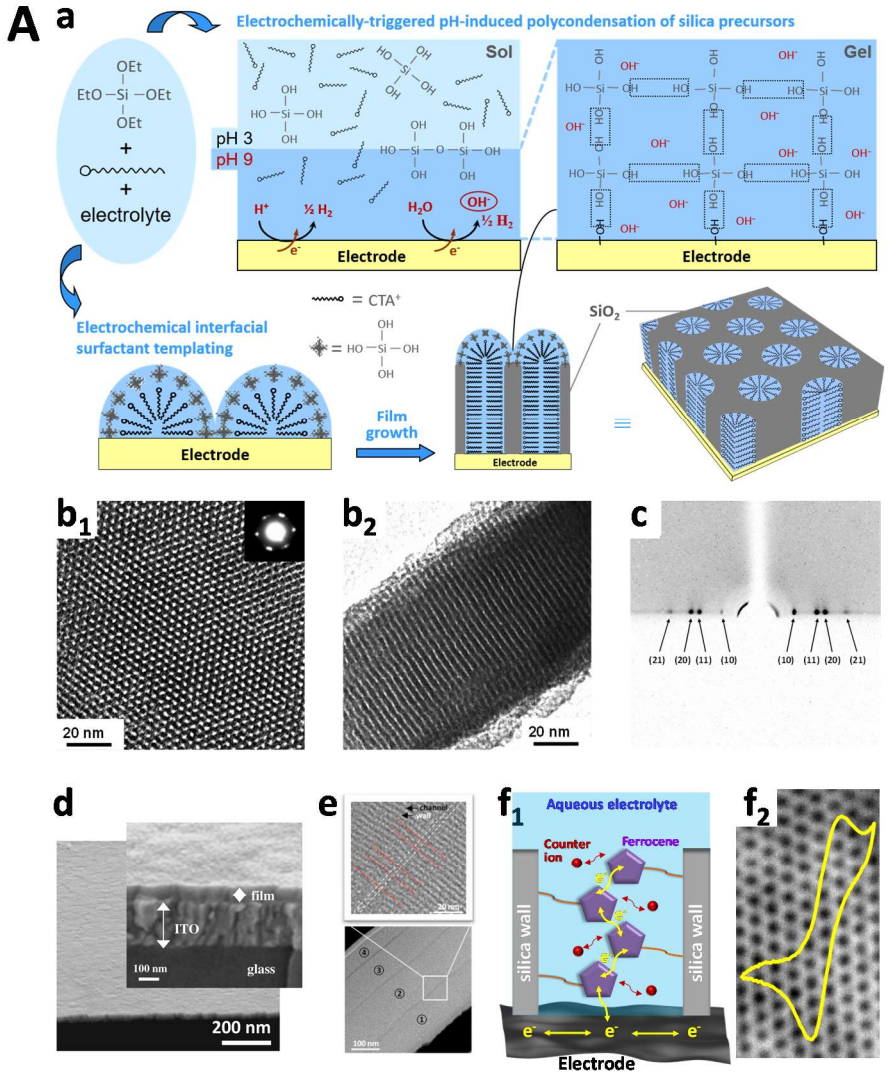
A
a
Electrochemically-triggered pH-induced polycondensation of silica precursors
Sol
Gel
pH 3
pH 9
electrolyte
Electrode
Electrochemical interfacial surfactant templating
Film growth
SiO2
b1
b2
c
20 nm
d
film
ITO
glass
100 nm
200 nm
e
f1
Aqueous electrolyte
Counter ion
Ferrocene
silica wall
f2

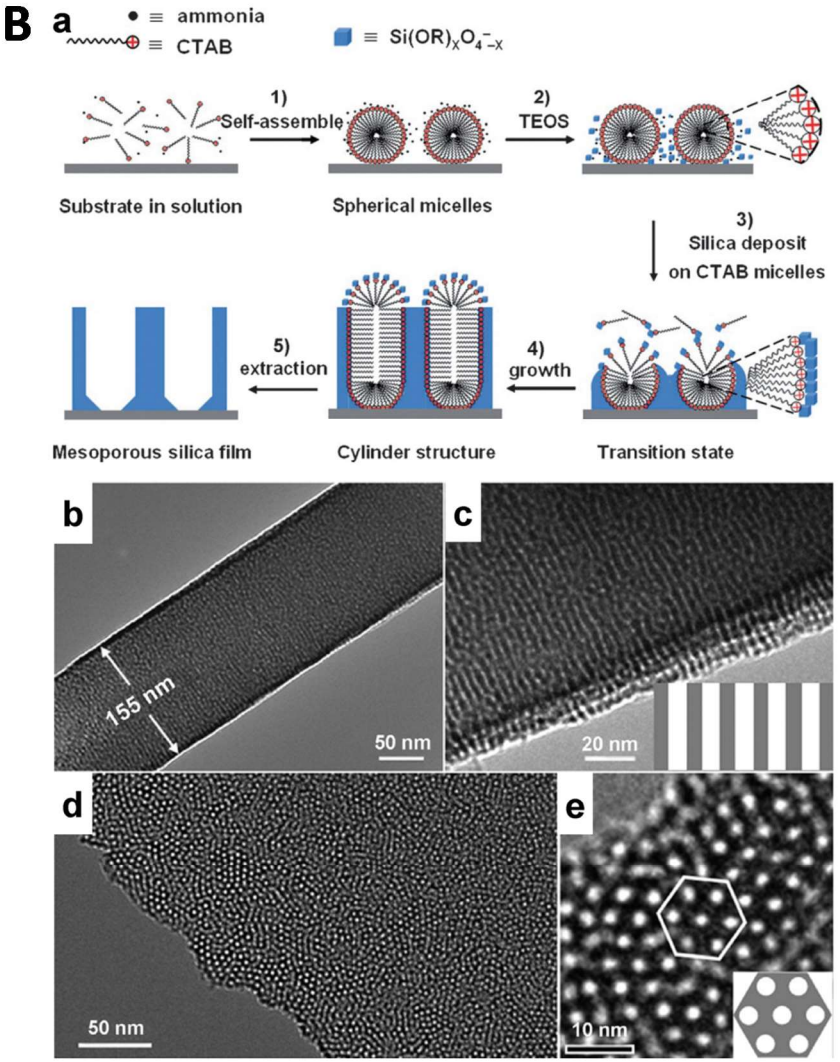
B
a
ammonia
CTAB
Si(OR)xO4-x
1) Self-assemble
2) TEOS
Substrate in solution
Spherical micelles
3) Silica deposit on CTAB micelles
4) growth
5) extraction
Mesoporous silica film
Cylinder structure
Transition state
b
155 nm
50 nm
c
20 nm
d
50 nm
e
10 nm

Figure 2

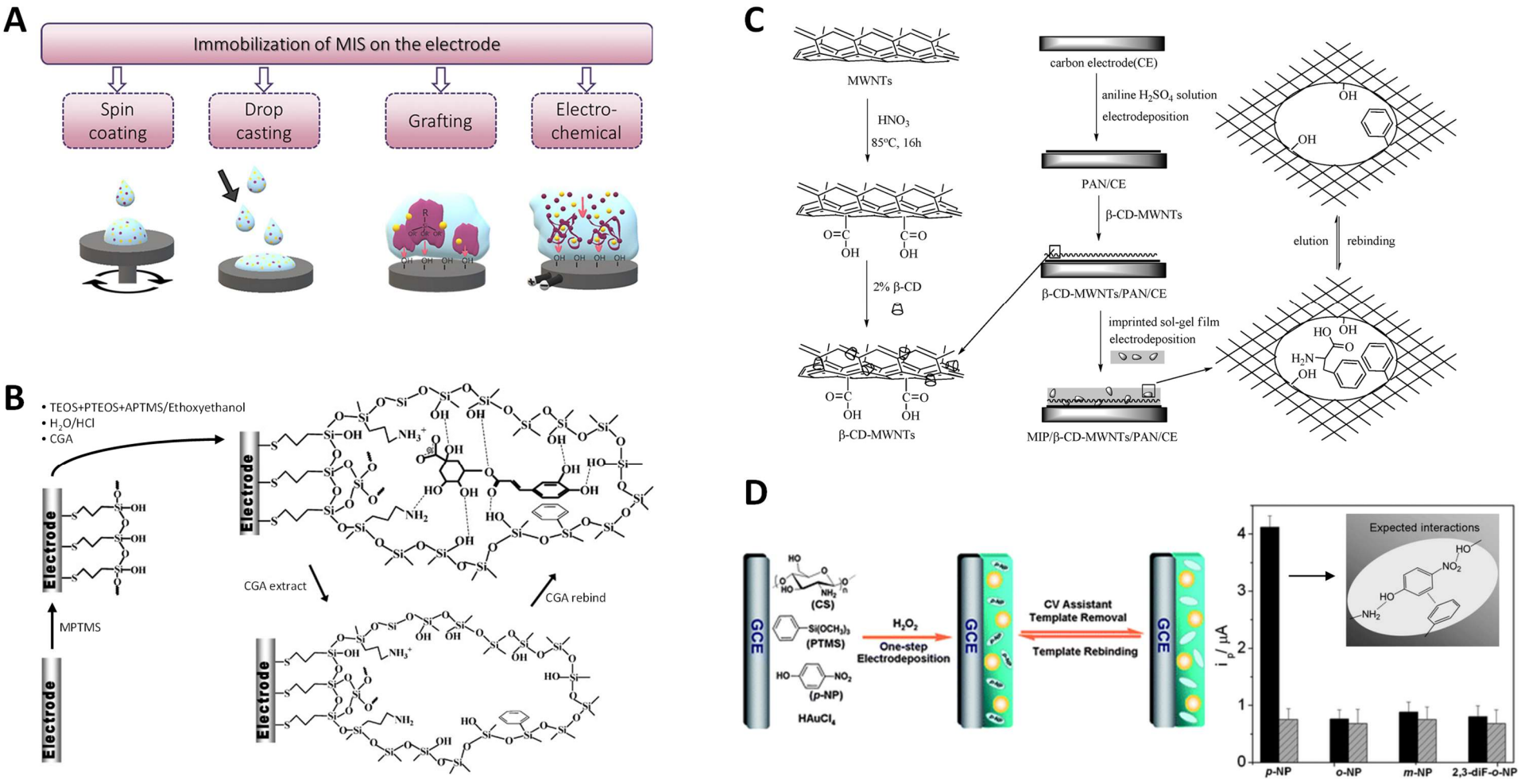
A
Immobilization of MIS on the electrode
Spin coating
Drop casting
Grafting
Electro-chemical
B
• TEOS+PTEOS+APTMS/Ethoxyethanol
• H2O/HCl
• CGA
Electrode
MPTMS
CGA extract
CGA rebind
C
MWNTs
HNO3
85°C, 16h
2% β-CD
β-CD-MWNTs
carbon electrode(CE)
aniline H2SO4 solution
electrodeposition
PAN/CE
β-CD-MWNTs
β-CD-MWNTs/PAN/CE
imprinted sol-gel film
electrodeposition
MIP/β-CD-MWNTs/PAN/CE
elution
rebinding
D
GCE
(CS)
(PTMS)
(p-NP)
HAuCl4
H2O2
One-step Electrodeposition
CV Assistant Template Removal
Template Rebinding
Expected interactions
i p / μA
p-NP
o-NP
m-NP
2,3-diF-o-NP

Figure 3

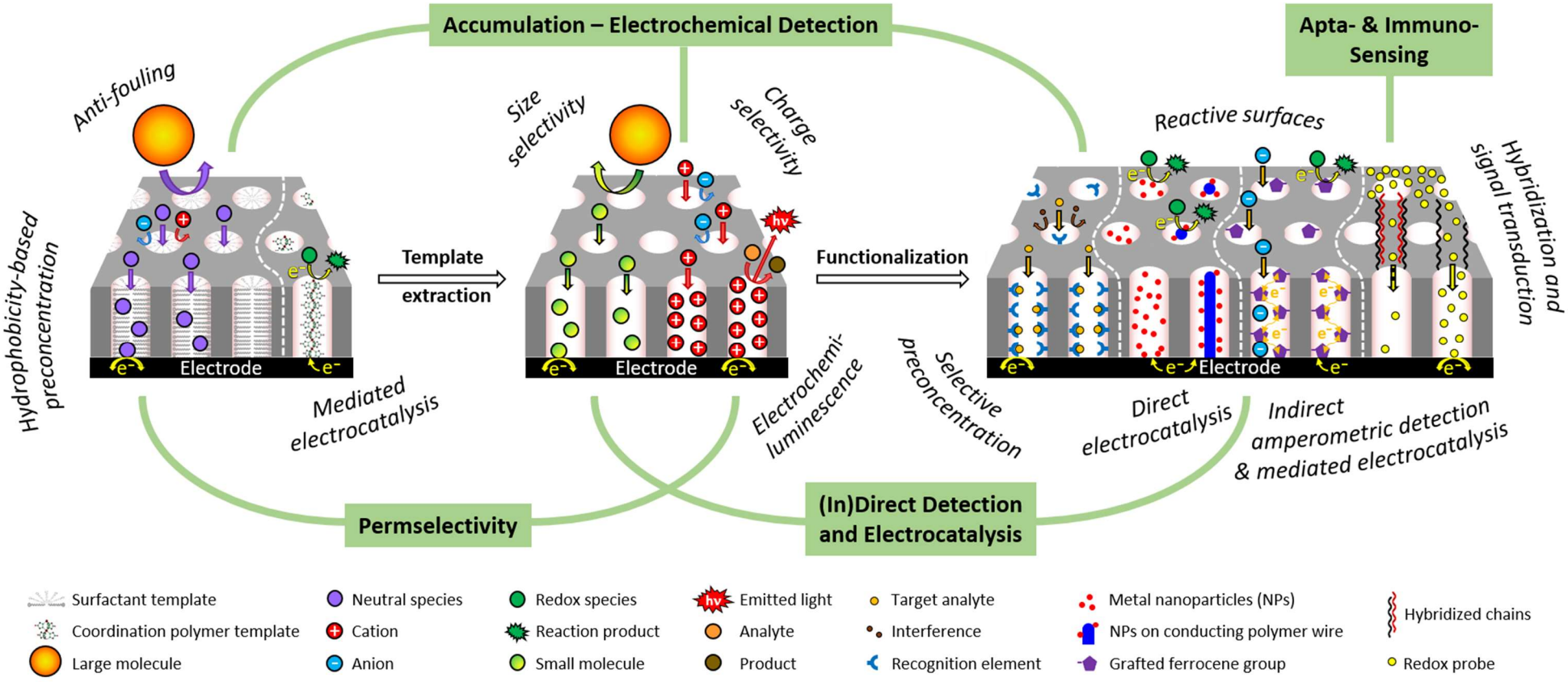
Accumulation – Electrochemical Detection
Apta- & Immuno-Sensing
Permselectivity
(In)Direct Detection and Electrocatalysis
Anti-fouling
Hydrophobicity-based preconcentration
Size selectivity
Charge selectivity
Reactive surfaces
Hybridization and signal transduction
Template extraction
Functionalization
Electrode
Mediated electrocatalysis
Electrochemi-luminescence
Selective preconcentration
Direct electrocatalysis
Indirect amperometric detection & mediated electrocatalysis
Surfactant template
Coordination polymer template
Large molecule
Neutral species
Cation
Anion
Redox species
Reaction product
Small molecule
Emitted light
Analyte
Product
Target analyte
Interference
Recognition element
Metal nanoparticles (NPs)
NPs on conducting polymer wire
Grafted ferrocene group
Hybridized chains
Redox probe

Figure 4

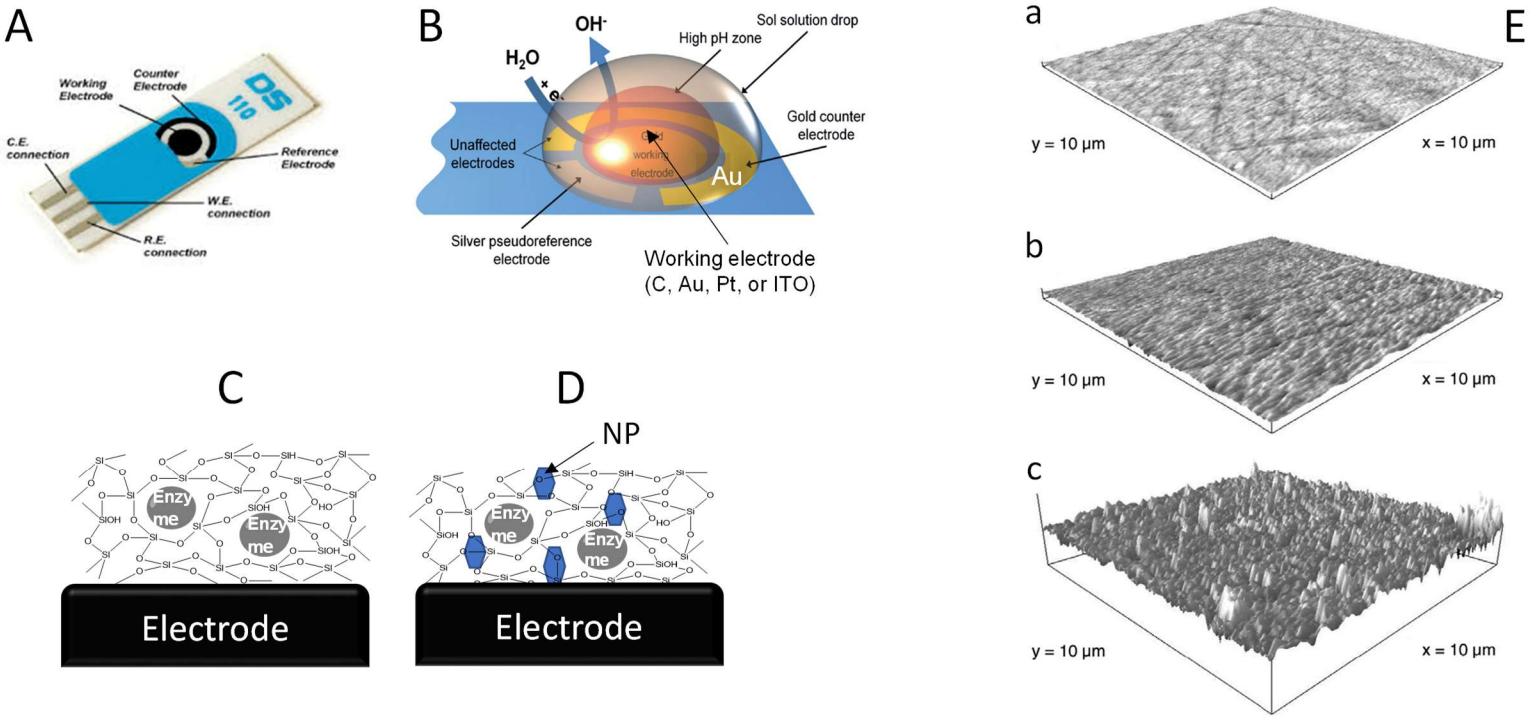
A
Working Electrode
Counter Electrode
DS 110
C.E. connection
Reference Electrode
W.E. connection
R.E. connection
B
OH-
H2O
Sol solution drop
High pH zone
Gold counter electrode
Unaffected electrodes
working electrode
Au
Silver pseudoreference electrode
Working electrode
(C, Au, Pt, or ITO)
C
Enzyme
Electrode
D
NP
Enzyme
Electrode
a
E
y = 10 µm
x = 10 µm
b
y = 10 µm
x = 10 µm
c
y = 10 µm
x = 10 µm

Figure 5

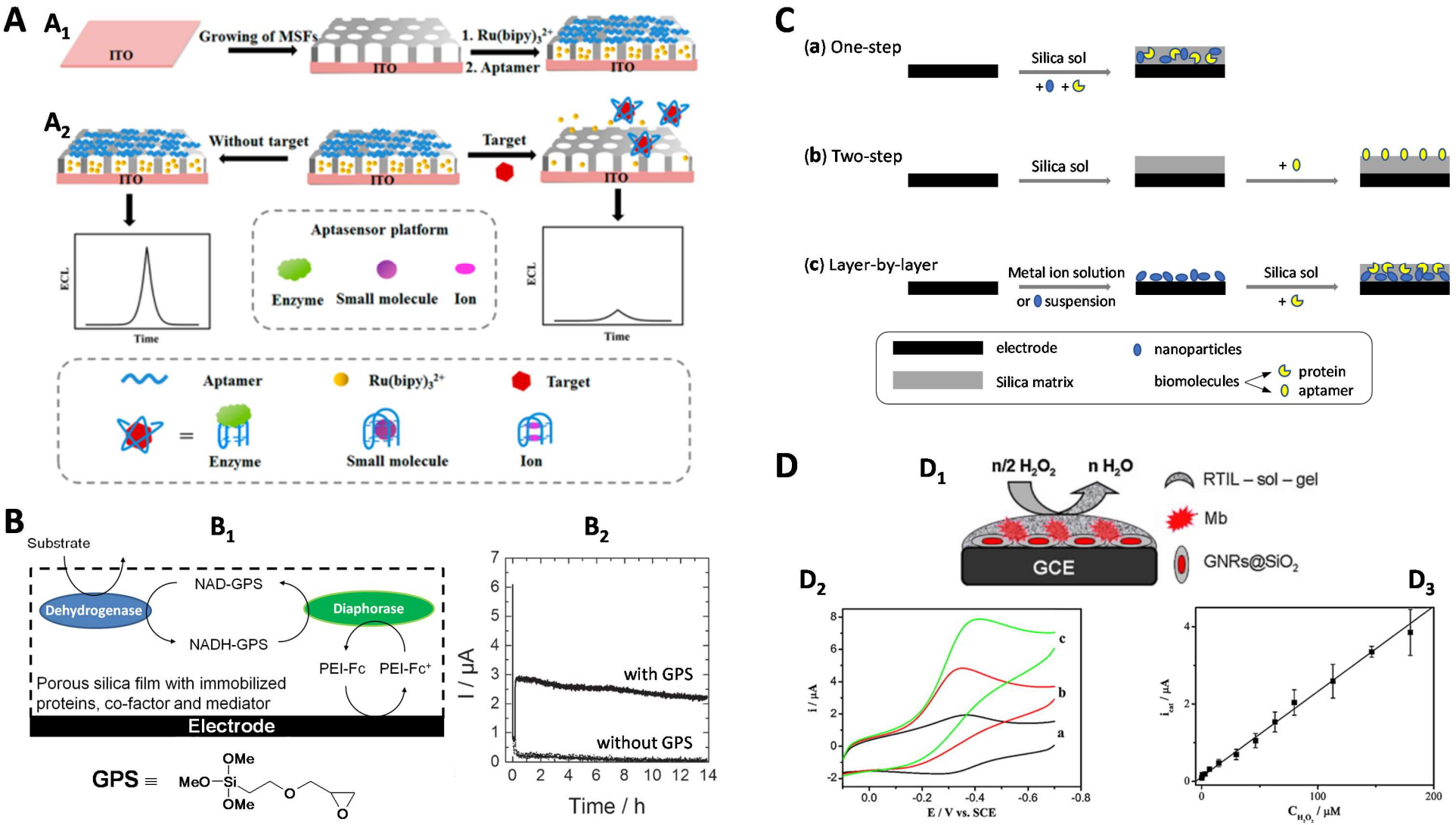
A
A1
ITO
Growing of MSFs
1. Ru(bipy)3 2+
2. Aptamer
A2
Without target
Target
Aptasensor platform
Enzyme
Small molecule
Ion
ECL
Time
Aptamer
Ru(bipy)3 2+
Target
B
B1
Substrate
NAD-GPS
NADH-GPS
Dehydrogenase
Diaphorase
PEI-Fc
PEI-Fc+
Porous silica film with immobilized proteins, co-factor and mediator
Electrode
GPS ≡
B2
with GPS
without GPS
I / μA
Time / h
C
(a) One-step
Silica sol
(b) Two-step
(c) Layer-by-layer
Metal ion solution
or suspension
electrode
Silica matrix
nanoparticles
biomolecules
protein
aptamer
D
D1
n/2 H2O2
n H2O
RTIL – sol – gel
Mb
GNRs@SiO2
GCE
D2
i / μA
E / V vs. SCE
D3
i cat / μA
C H2O2 / μM

Figure 6

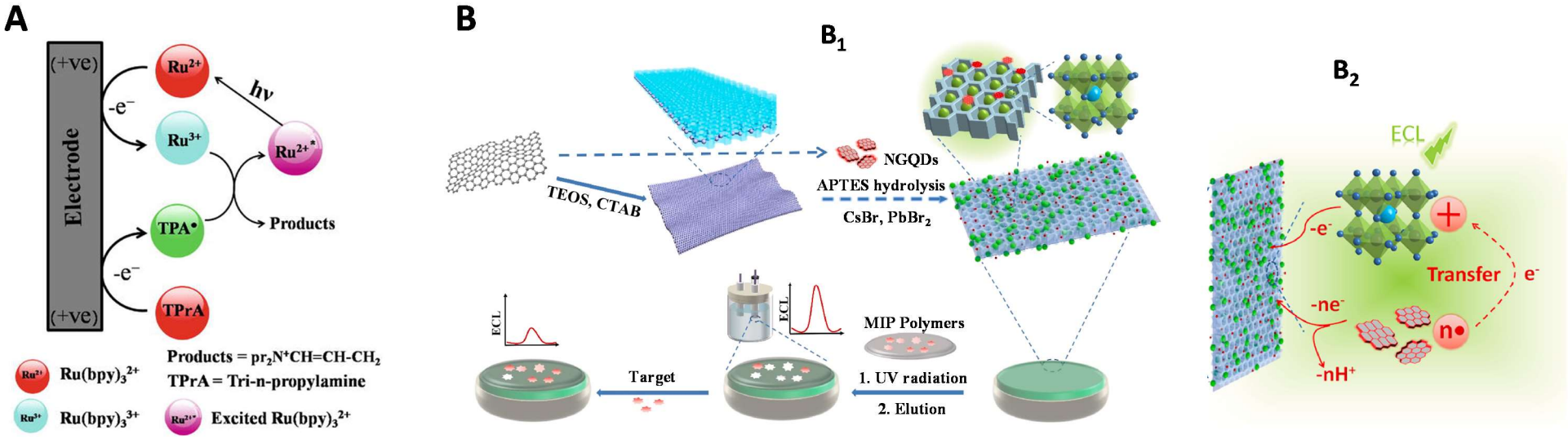
A
(+ve)
Electrode
(+ve)
-e⁻
-e⁻
Ru2+
Ru3+
TPA•
TPrA
hν
Ru2+*
Products
Products = pr2N+CH=CH-CH2
TPrA = Tri-n-propylamine
Ru(bpy)3 2+
Ru(bpy)3 3+
Excited Ru(bpy)3 2+
B
B1
TEOS, CTAB
NGQDs
APTES hydrolysis
CsBr, PbBr2
MIP Polymers
1. UV radiation
2. Elution
Target
ECL
ECL
B2
ECL
-e⁻
Transfer
e⁻
-ne⁻
n•
-nH+

Figure 7